AD-A190 245 ON THE PREDICTION OF HIGHLY VORTICAL FLOWS USING AN EULER EQUATION MODEL..(U) GRUMMAN CORP BETHPAGE NY CORPORATE RESEARCH CENTER F MARCONI 30 OCT 87 1/2

UNCLASSIFIED AFOSR-TR-87-1910 F49620-85-C-0115 F/G 20/4 NL

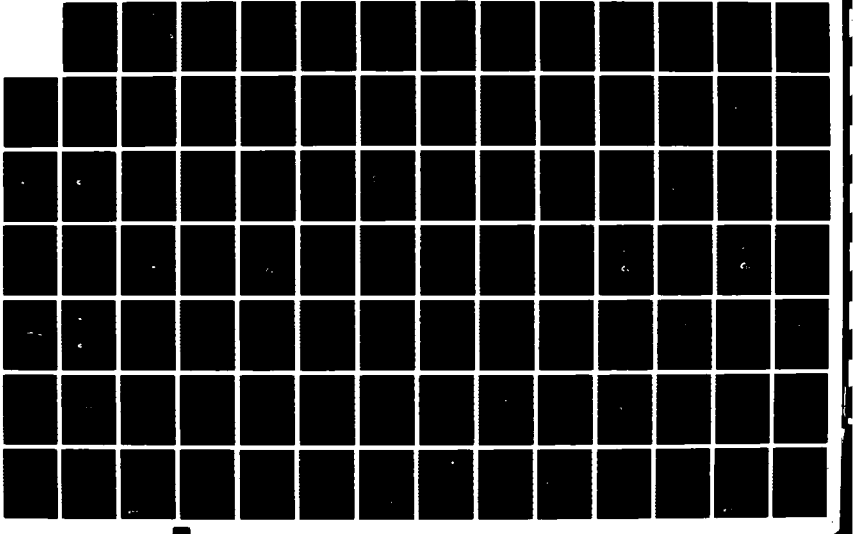

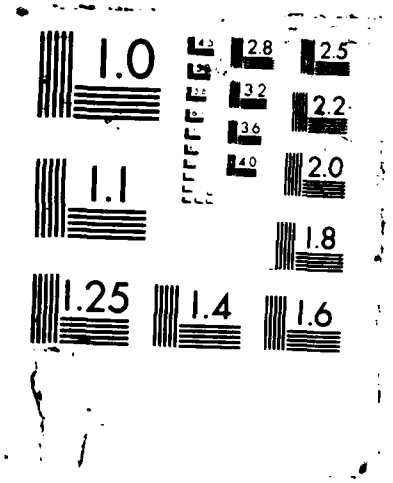
1.0
2.8
2.5
3.2
2.2
3.6
4.0
2.0
1.1
1.8
1.25
1.4
1.6

UNCLASSIFIED
SECURITY CLASSIFICATION OF THIS PAGE

(2)

REPORT DOCUMENTATION PAGE

DTIC FILE COPY

AD-A190 245

1b. RESTRICTIVE MARKINGS: NONE

3 DISTRIBUTION/AVAILABILITY OF REPORT: APPROVED FOR PUBLIC RELEASE; DISTRIBUTION UNLIMITED

4 PERFORMING ORGANIZATION REPORT NUMBER(S): RE-

5. MONITORING ORGANIZATION REPORT NUMBER(S): AFOSR-TR- 87-1910

6a. NAME OF PERFORMING ORGANIZATION	6b OFFICE SYMBOL (If applicable)	7a. NAME OF MONITORING ORGANIZATION
Grumman Aerospace Corporation		Air Force Office of Scientific Research

6c. ADDRESS (City, State, and ZIP Code)	7b. ADDRESS (City, State, and ZIP Code)
Mail Stop A08-35 Corporate Research Center Bethpage, New York 11714-3580	Bolling AFB, Building 410 Bolling AFB, Washington, DC 20332

8a. NAME OF FUNDING/SPONSORING ORGANIZATION	8b OFFICE SYMBOL (If applicable)	9 PROCUREMENT INSTRUMENT IDENTIFICATION NUMBER
AFOSR/ Bolling AFB, DC 20332	NA	F49620-85C-0115

8c. ADDRESS (City, State, and ZIP Code)	10 SOURCE OF FUNDING NUMBERS			
	PROGRAM ELEMENT NO	PROJECT NO	TASK NO	WORK UNIT ACCESSION NO
AFOSR/ NA Bolling AFB, DC 20332	61102F	2307	A4	

11 TITLE (Include Security Classification)
On the Prediction of Highly Vortical Flows Using an Euler Equation Model; Part II.

12 PERSONAL AUTHOR(S)
Frank Marconi

13a TYPE OF REPORT	13b TIME COVERED	14 DATE OF REPORT (Year, Month, Day)	15 PAGE COUNT
FINAL	FROM 7/31/85 TO 7/31/87	87/10/30	13

16 SUPPLEMENTARY NOTATION

17 COSATI CODES			18 SUBJECT TERMS (Continue on reverse if necessary and identify by block number)
FIELD	GROUP	SUB-GROUP	Fluid Mechanics, Vortex Flows Supersonic Flows

DTIC ELECTE JAN 07 1988 S C E D

19 ABSTRACT (Continue on reverse if necessary and identify by block number)

An investigation of the power of the Euler equations in the prediction of conical separated flows is presented. These equations are solved numerically for the highly vortical supersonic flow about simple bodies. Two sources of vorticity are studied; the first is the flow field shock system and the second is the vorticity shed into the flow field from a separating boundary layer. Both sources of vorticity are found to produce separation and vortices. In the case of shed vorticity, the surface point from which the vorticity is shed (i.e., separation point) is determined empirically. At very high angles of attack the only stable separated solution is found to be asymmetric. Solutions obtained with both sources of vorticity are studied in detail, compared with each other and with potential calculations and experimental data.

20 DISTRIBUTION/AVAILABILITY OF ABSTRACT	21 ABSTRACT SECURITY CLASSIFICATION
☒ UNCLASSIFIED/UNLIMITED ☐ SAME AS RPT ☐ DTIC USERS	UNCLASSIFIED

22a NAME OF RESPONSIBLE INDIVIDUAL	22b TELEPHONE (Include Area Code)	22c OFFICE SYMBOL
HE HELIN	202 767 6911	AFOSR/NA

DD FORM 1473, 84 MAR — 83 APR edition may be used until exhausted. All other editions are obsolete.

SECURITY CLASSIFICATION OF THIS PAGE
UNCLASSIFIED

REPORT RE-739

ON THE PREDICTION OF HIGHLY VORTICAL FLOWS USING AN EULER EQUATION MODEL PART II

OCTOBER 1987

prepared by

Frank Marconi
Fluid Mechanics Directorate
Grumman Corporate Research Center
Bethpage, New York 11714-3580

Final Report on
Contract F49620-85-C-0115

prepared for

USAF Office of Scientific Research
Building 410
Bolling AFB, Washington, DC 20332

REPORT RE-739

ON THE PREDICTION OF HIGHLY VORTICAL *FLOWS USING AN EULER EQUATION MODEL* PART II

OCTOBER 1987

prepared by

Frank Marconi
Fluid Mechanics Directorate
Grumman Corporate Research Center
Bethpage, New York 11714-3580

Final Report on
Contract F49620-85-C-0115

prepared for

USAF Office of Scientific Research
Building 410
Bolling AFB, Washington, DC 20332

Approved by: Richard A. Schneuing

Richard A. Schneuing, V.P.
Corporate Research Center

SUMMARY

A three-year investigation of the power of the Euler equations in the prediction of separated flows has been conducted. The preliminary work for this study was conducted from 6/84 to 6/85 under AFOSR Contract F49620-84-C-0056 and is reported upon in Part I of this report. Here, only the work conducted in the last two years of this research project will be discussed, except when background material from Part I is essential to the completeness of this report.

The Euler equations are solved numerically for the highly vortical supersonic flow about simple geometries. Two sources of vorticity are investigated; the first is the flow field shock system and the second is the vorticity shed from a separating boundary layer. In the case of shed vorticity, the surface point from which the vorticity is shed (i.e., separation point) is determined empirically. Solutions obtained with both sources of vorticity are studied in detail and the relationship between the two is discussed. The complex interaction between shock-vorticity-produced vortices and the shock system itself is shown to result in interesting shock/vortex patterns. The vorticity shedding model developed in this effort was successfully applied to flat-plate-delta-wing and simple three-dimensional flows. Less success was achieved in applying the model to subsonic flows. A very exciting result was found in an investigation of very high angle-of-attack flows. It was found that the symmetric solution for the separated flow about cones became unstable for angles of attack higher than two and a half times the cone half angle. At these angles of attack, only asymmetric solutions exist, as noted experimentally.

CONTENTS

ILLUSTRATIONS

ILLUSTRATIONS (cont'd.)

ILLUSTRATIONS (cont'd.)

1. INTRODUCTION

Separation and the formation of vortices in the three-dimensional flow about wings and forebodies at high angles of attack constitute an important aspect of advanced vehicle design. The phenomenon will be especially important at maneuver conditions for the next generation fighter aircraft, since the flight envelopes of these vehicles may extend to high angles of attack at supersonic speeds. An understanding of three-dimensional separation and accompanying vortex formation may help in adding to the aerodynamic efficiency of these aircraft. Design efforts which try to take advantage of vortex lift or utilize vortex flaps will surely benefit from basic studies of separated flows. Controllability problems associated with vortex interactions and asymmetric forebody separation will benefit from an understanding of flow separation. If separated flows can be studied accurately and efficiently using computational techniques, the development costs of these aircraft will be significantly reduced.

This report presents a numerical study of separation and accompanying vortices in the flow about delta wings and simple forebodies at supersonic speeds. The governing equations considered in this investigation are inviscid (i.e., Euler's equation). It is well known that separation zones (i.e., spirals or closed separation bubbles in 2-D flow) are associated with the existence of vorticity in the flow.[1,2,3,4] There are two sources of vorticity in the high Reynolds-number flows about supersonic aircraft: first, the vorticity in the boundary layer, and second, the vorticity produced by shock waves. When boundary layer separation occurs, the vorticity of the boundary layer is shed into the flow field and may, to a good approximation, be considered confined to an infinitesimal sheet which rolls into a vortex. This approximation has been used in conjunction with linearized flow field models for many years (see, for example, Ref 5 and 6) with good results. The present author[7] showed preliminary Euler calculations which indicated that the more exact flow field model made the computation of vortex flows simpler and at the same time more accurate. At flight Reynolds numbers ($> 10^6$), viscous effects are confined to thin flow regimes (boundary layers and vortex sheets) with the majority of the flow inviscid in nature. This fact makes the solution of the Navier-Stokes equations with a unified procedure (no special treatment of

sheets or boundary layers) very difficult. The Euler equations combined with special treatments for sheets and boundary layer may turn out to be a more reliable and accurate approach to the prediction of these flows. The power of the Euler equation model lies in its ability to transport vorticity while avoiding the evaluation of the boundary layer details. The extent to which the Euler equations can be used to predict separated flows is a major goal of this work.

In the past several years, a number of investigators have studied numerical solutions to the Euler equations exhibiting separation. In Ref 8, Salas showed how shock vorticity can cause separation at the base of a cylinder. Rizzi et al[9] and Murman[10] have shown solutions to Euler's equations with leading edge separation. In Ref 9 and 10, the source of vorticity is unclear; there is no evidence of strong shock waves. Both authors indicate the possibility that separation is caused by numerical viscosity. In Ref 10, the wing is a flat plate delta; therefore, there must be a singularity at the leading edge. The numerical scheme used could implicitly introduce a Kutta condition at the leading edge and shed vorticity into the flow field. R. Newsome[11] showed Euler solutions over an elliptic delta wing with finite thickness. His crude grid results exhibited leading edge separation (before any crossflow shock); his very fine grid results exhibited separation after a crossflow shock. The numerical schemes of Ref 9, 10, and 11 require the addition of artificial viscosity for stability. Their research has indicated a small sensitivity of separation zones to reductions in artificial viscosity. It seems that these separation zones are Reynolds number independent (even numerical Reynolds number independent) and one must be very careful in controlling artificial viscosity. It is generally agreed today that the Euler separation of the type shown in Ref 9, 10, and 11 is due to explicitly added dissipation. It is interesting to note that the separated flows of Ref 9, 10, and 11 compare well (at least qualitatively) with experimental data even though the source of vorticity is numerical in nature, particularly when the separation point is obvious, as in the case of the flat-plate delta wings of Ref 10.

In the Euler calculations presented here, separation occurs only when a well-defined source of vorticity is present. In addition to vorticity shed from the boundary layer, shock waves in supersonic conical flow can produce

enough vorticity to induce separation. This type of separation is qualitatively similar to that produced by vorticity shed from a boundary layer. With boundary layer vorticity excluded, any comparison with experimental data will be poor. It is difficult to assess the relative magnitude of the vorticity introduced into the flow from shocks and the boundary layer. It should be pointed out that experimental data show large regions of separated flow with no significant shock vorticity. This seems to indicate that vorticity shed from the boundary layer is much larger than that produced by shocks. In addition, boundary layer separation has a tendency to reduce shock strengths and, therefore, shock vorticity. Nevertheless, the calculations presented here show that shock vorticity may play an important role in the separation process. The author investigated the effects of shock vorticity on circular cones[7,12] (Ref 12 is included in Appendix A for completeness) and on elliptic delta wings,[13] and found that at high angle of attack a crossflow shock (Fig. 1) can produce enough vorticity to cause separation. The interaction of the shock and vortex system will be discussed in detail later in this report. In addition, the relationship between shed and shock vorticity will be outlined.

Most geometries considered in this work are either delta wings with similar cross sections or circular cones, so that each section normal to the z axis (Fig. 1) is self similar and the geometry is conical. The flow is assumed supersonic everywhere and separation lines are assumed to be on conical rays. With these assumptions, it follows that the flow is conical (i.e., all flow variables are independent of the spherical radius r (Fig. 1)). However, the basic features of the flow, including separation and vortices, are three-dimensional in nature. In addition, the models used here have been extended to fully three-dimensional flow and these results will be presented later in this report.

Our previous work in highly vortical flows[7,12,13] will not be presented in this report, as this was covered before in Part I. The overall computational procedure will be outlined and the model for shedding vorticity from specified separation points will be discussed. Flow fields with shock-vorticity-induced separation will be studied, in addition to flows with vorticity shed from both primary and secondary boundary layer separation points. A detailed comparison of these two different sources of vorticity

will be presented. The investigation of the computed flow fields will be aided by comparisons with experimental data and computations of other researchers. Finally, the findings of this work will be summarized.

2. COMPUTATIONAL PROCEDURE

2.1 OVERALL COMPUTATIONAL PROCEDURE, SHOCK VORTICITY ALONE

Although employing a number of new features, the overall numerical procedure used in this study is essentially standard.[14] The fully three-dimensional Euler equations are solved with an explicit marching technique. The marching direction, z (Fig. 1), is an iterative coordinate for the conical flow. The scheme is restricted by the fact that the axial component of velocity, W (Fig. 1), must be supersonic everywhere. The marching scheme is continued until the flow field is invariant with respect to the computational marching direction, except for a scale factor for conical flow, and to the end of the body considered for fully three-dimensional flows. The finite difference scheme used is Moretti's characteristic-based λ-scheme.[15] The bow shock and the primary crossflow shock are fit and are forced to satisfy the exact Rankine-Hugoniot jump conditions. The bow shock is fit as the outermost boundary of the flow field. On the low-pressure side of the bow shock, freestream conditions exist. The crossflow shock is fit as an internal boundary of the flow field with its low-pressure side being computed as the computation proceeds.[16]

The crossflow shock computation is a critical part of the overall procedure, particularly since it plays such a critical role in separation. As mentioned in Section 1, it is the vorticity produced by the crossflow shock that is significant. Any scheme that captures the crossflow shock and introduces additional artificial viscosity to stabilize it runs the risk of distorting the separation and vortex. The bow shock also introduces vorticity into the flow field, but not enough to produce separation. The crossflow shock is caused by the fact that at a large incidence the crossflow component of the velocity, $\sqrt{u^2+v^2}$ (Fig. 1), becomes supercritical. The flow expands in going around the body, and the crossflow can become supercritical if the incidence is high enough. This component of velocity must be small in the lee symmetry plane due to the boundary conditions. A supercritical crossflow generally passes through a relatively normal shock before stagnating in the lee plane on the surface. The crossflow shock exists to turn the three-dimensional flow parallel to the lee symmetry plane. The variation in strength of the crossflow shock can be quite large. The shock is strongest at

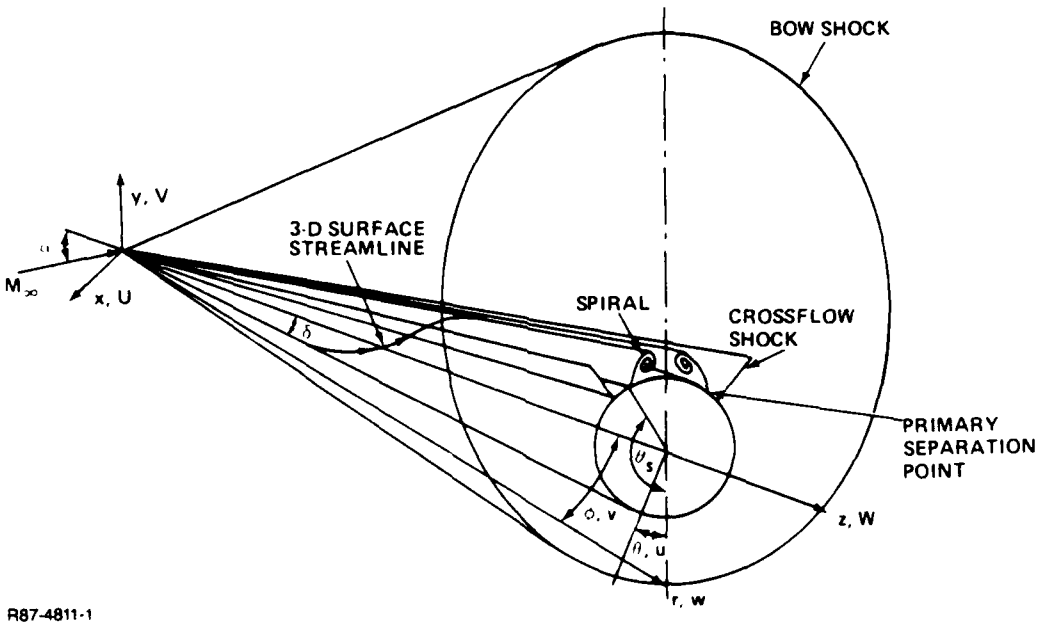

Fig. 1 Three-Dimensional Sketch of Flow Field & Coordinate System

the body where the crossflow is highly supersonic and approaches zero strength in the field where the crossflow becomes sonic. It is this variation in strength that produces a crossflow entropy gradient and thus radial vorticity. This vorticity in turn causes shock-induced separation.

The low-pressure side of the crossflow shock is computed with one-sided differences away from the shock. This is consistent with the fact that the crossflow is supersonic. The Rankine-Hugoniot conditions, together with the compatibility condition along a bicharacteristic reaching the shock on its high-pressure side, supply enough information to compute the deviation of each shock point from a conical ray in addition to all the primitive variables on its high-pressure side. The bicharacteristic used is the one in the plane containing the local normal to the shock and the marching direction. All shock points are computed with the post-correction scheme proposed by Rudman[17] and independently by deNeef.[18] The shocks converge (i.e., each shock point becomes aligned with a conical ray) with the rest of the flow field. In all the computations presented here, the last crossflow shock point fit had a normal Mach number of approximately 1.05 (pressure ratio of 1.12). The finite difference scheme was able to capture weaker shock points. In addition, the finite difference scheme was used to capture all reverse crossflow shocks and oblique crossflow shocks in the flow field (to be discussed later). These shocks are usually weak and the scheme can capture them accurately.

The computational grid used in this work is developed in stages. In the first stage, the flat wing section in a constant z plane is mapped to a circle. This step is omitted in the case of a circular cone. The mapping is a simple Joukowski transformation and will not be detailed here. Next, a polar coordinate system is used in the mapped space. An exponential stretching is used in the radial direction to cluster grid points near the surface in order to resolve the complex flow near separation. The Joukowski mapping clusters grid points in the circumferential direction automatically. When thin ellipses (axis ratios > 10) were first considered,[13] solutions with large truncation error at the wing leading edge were found. One result of this truncation error was the production of vorticity at the leading edge. There was little error in entropy at the leading edge (i.e., entropy was constant on streamlines), but the vorticity was large, leading to a violation of Crocco's theorem. The error was manifested by a layer in crossflow

velocity at the surface. The crossflow on the body was much lower than that one point away from the body. While this vorticity was never large enough to cause leading edge separation, as in the work of Ref 9, 10, and 11, it did distort the separation behind the crossflow shock. This error was eliminated by increasing the resolution at the wing leading edge. An exponential stretching was used in the circumferential direction in the delta wing results shown here.

Shock-induced inviscid separation produces a contact surface emanating from the separation point (Fig. 1). It is this contact that ultimately spirals to form a vortex. The contact surface has a jump in entropy and an accompanying jump in velocity. In conical flow, entropy is constant on crossflow streamlines. Thus, one can see (Fig. 1) that the entropy on the windward side of the contact comes from the windward stagnation point of a cone and the wing leading edge stagnation point in the case of an ellipse. The streamline that wets the body passes through the base of the crossflow shock to form the high-entropy side of the contact. There are a number of possibilities for the entropy on the lee side of the contact. The crossflow streamlines that wet the body are tracked in each step of the iteration, and the proper entropy is imposed on the surface, including the jump in entropy at the separation point. All entropy discontinuities off the body are captured with the finite difference scheme.

The finite difference scheme used in this work is an explicit marching scheme which is notoriously inefficient for converging to a conical or steady solution. One advantage of the explicit marching scheme is that it is totally "vectorizable." The time-consuming parts of the code (i.e., interior point computation) utilized the vector architecture of the Cray 1 computer. This made the computation about 20 times faster than on an IBM 3033. The computations shown here typically took 20 CPU minutes on the Cray XMP, and the conical grid used had 89 x 89 points in the cross sectional plane. In each case shown, the maximum residual (i.e., the derivative of pressure in the marching direction) was reduced at least six orders of magnitude.

2.2 SHED VORTICITY - COMPUTATIONAL MODELS

In this section, the concept of shedding vorticity from a specified separation point (the intersection of a conical separation line and the cross plane) will be discussed. The conceptual process of shedding vorticity from a

conical surface will force separation and an accompanying spiral. The model used here to force separation at a specified location is founded in the work of J.H.B. Smith.[5] Smith assumed irrotational flow outside a vortex sheet in order to analyze the local flow at separation. The present work uses only the basic concept, which does not depend on the irrotational assumption. In addition, any model of inviscid separation should reduce to that of Smith as the rotationality outside the vortex sheet gets small. The basic concept acquired from Ref 5 is that, at a specified separation point, there is a vortex sheet or contact surface which has a jump in velocity direction. The condition at the intersection of the sheet and a smooth surface (i.e., the separation point) is that the crossflow velocity stagnates on the lee side of the sheet (Fig. 2a). The concept of crossflow applies only to conical flow. The extension of this model to fully 3-D flow will be discussed in another part of this section. The crossflow velocity on the wind side of the sheet is determined by the global solution. In general, the crossflow velocity on the wind side of the sheet is finite. The vortex sheet is a stream surface and the pressure is continuous across it. In the case of isentropic irrotational flow considered in Ref 5, these conditions imply that the modulus of velocity is continuous across the sheet. If the crossflow stagnates on both sides of the sheet ($u = v = 0$) at separation, the isentropic condition implies that the radial component of velocity (w, Fig. 1) is continuous and the sheet does not exist, i.e., no vorticity is shed into the flow field. These arguments conclude that, in isentropic flow, the separating sheet must leave the cone surface tangentially if the wing side crossflow is subsonic. If the surface crossflow is subsonic just upstream of separation and the sheet leaves the surface at any angle relative to the surface, then the flow on the windside of the sheet must stagnate and no vorticity will be shed into the flow. On the other hand, if the crossflow is supersonic, the sheet can leave the surface at an angle, an oblique crossflow shock will occur, and the flow on the wind side of sheet will not stagnate so that vorticity is shed. This phenomenon will be discussed further in this section. None of these arguments holds for the highly nonisentropic flow discussed in the previous section, where the flow stagnates on both sides of the separating sheet. In these cases, vorticity is not shed from the surface; only shock vorticity is present.

Separation was forced in the calculations presented here simply by using a double point at separation in order to allow for a jump in crossflow

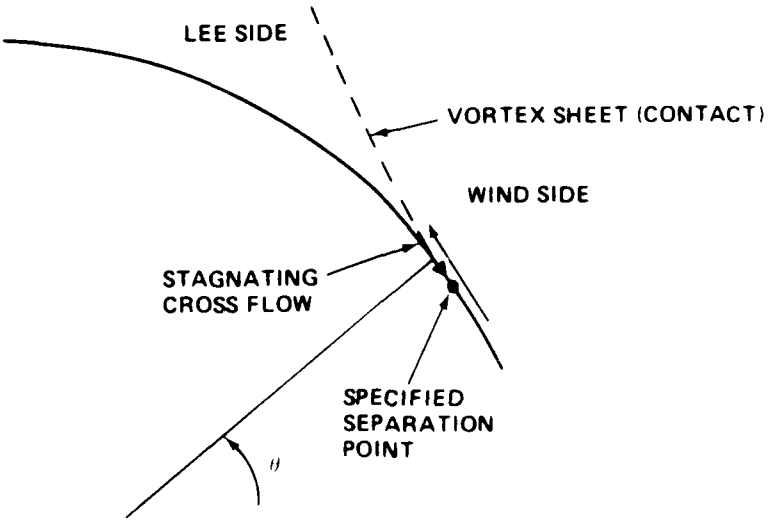

a) Subcritical

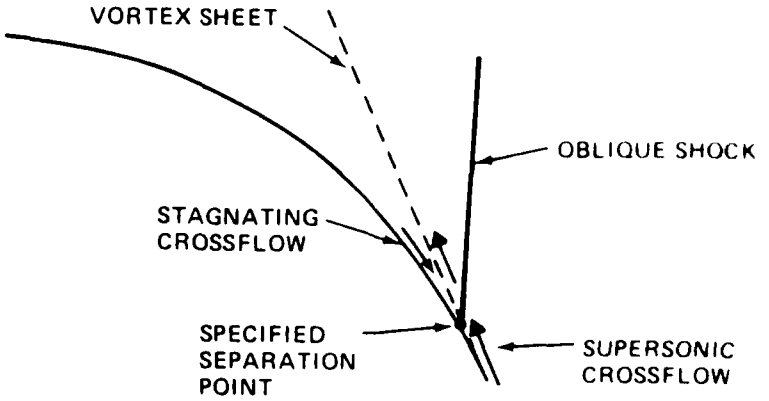

b) Supercritical

R87-4811-2

Fig. 2 Sketch of Forced Separation Model

velocity. The crossflow velocity (u) on the wind side of the sheet is determined by the governing crossflow momentum equation, as at any other surface point. The crossflow component (v) must vanish at every surface point from the boundary condition. The crossflow velocity on the lee side of the sheet is set to zero ($u = 0$) in order to force separation at a specified point.

The separation point in this forced separation model exhibits a jump in crossflow velocity. The crossflow on the wind side (Fig. 23a) of the separation is evaluated in each step of the iteration from the momentum equation tangent to the body in the cross plane. The remaining primitive variables are computed at this point with the same governing equations as at any other body point, with the boundary condition ($v = 0$) satisfied. All circumferential velocity derivatives are taken one-sided in the negative θ direction in order to avoid differencing across the sheet. The point just below the sheet (lee side) is forced to be a crossflow stagnation point ($u = v = 0$). The pressure is continuous across the sheet, so that its value on the wind side could theoretically be used on the lee side at separation. Difficulties were encountered in computing the pressure in a small region just after separation. The computation of the pressure in this region will be discussed in the next paragraph. The entropy at the lee side point is computed in the standard way, i.e., conserved along the streamline that wets the lee side of the body. If the pressure is known in addition to the entropy and total temperature (the flow is assumed adiabatic), the last component of velocity (w) (Fig. 1) can be evaluated from the energy equation. Again, circumferential derivatives of the velocities across the sheet at the body grid points near separation are avoided. Differences in entropy across the sheet are avoided naturally by the λ-scheme, as in the shock-induced separation discussed in the previous section.

The difficulty encountered in the evaluation of the pressure on the lee side of the separation point can be traced to the numerical computation of the derivatives of velocities in a direction normal to the surface. The derivatives appear in the continuity equation from which the pressure is evaluated. These velocities are discontinuous across the sheet and, since the sheet lies so close to the surface at separation, there is no way to resolve the flow in the region between the surface and the sheet near separation. The

behavior of the pressure in this region was evaluated analytically by Smith[5] and numerically by Fiddes[6] under the assumption of slender-body theory. The results of Fiddes show a pressure plateau on the surface just after separation. The full Euler equations predict that the pressure derivative along the surface (p_θ) becomes zero at the lee side of the separation point, where the crossflow stagnates. In the present calculation it has been difficult to obtain this type of pressure behavior. A number of procedures have been attempted with varying degrees of success, but none has been totally satisfactory. In Ref 7 the author showed preliminary results which exhibited a pressure plateau after separation, but the scheme used there proved unstable when the vortex sheet was moved during the iteration process. A reformulation of dependent variables has alleviated the problem. Currently, as long as the crossflow is subsonic (Fig. 2a) just before separation, no special treatment is used in evaluating the pressure except for circumferential and radial grid clusterings. Because of the difficulties associated with the pressure evaluation in the region on the surface just after separation, the results of the next section should be considered somewhat preliminary.

In the case of supersonic crossflow (Fig. 2b), differencing of pressure across the separation point proved to be unstable. The results of a number of numerical experiments indicate that the model for the inviscid flow in this case should be such that the sheet leaves the surface at an angle relative to it and an associated shock occurs at separation. The flow structure is sketched in Fig. 2b. This model does not violate the concepts of vorticity shedding proposed by Smith,[5] since the flow on the wind side of the separation point need not stagnate, and thus a jump in velocity exists across the sheet. In order to capture the shock at separation in one mesh interval, no pressure derivatives were taken across the separation point on the cone surface. In addition a small pressure plateau is imposed just after separation, the level being taken from just downstream of separation.

Secondary separation is forced by shedding vorticity from the body in the reverse crossflow region produced by primary separation. The model is the same as was just outlined for primary separation. Both separation point locations are obtained from experimental data. The only free parameters in the problem as posed here are the locations of the separation points. In the work of Ref 6, primary separation points were found iteratively by matching an

inviscid solution (slender-body theory) to a boundary layer solution. The procedure just outlined is directly applicable to fully three-dimensional flows if the crossflow is replaced by the flow in a plane locally normal to the separation line. Consider Fig. 3, where the separation point location in each plane Z = constant is specified (i.e., experimentally). Given all these separation locations, a separation line can be constructed (see sketch in Fig. 3). In each marching step of the calculation, the plane normal to separation line can be determined and the model just outlined can be applied locally in each of these planes. The zero-crossflow condition becomes equivalent to forcing the surface velocity vector parallel to the separation line, as it should.

2.3 SEPARATION CONDITION AT SHARP WING LEADING EDGE

The flow at the leading edge of the zero-thickness delta wing is singular. Powell and Murman have been successful in computing these flows with no consideration of this singularity.[24]

Salas[19] investigated the conical flow with a singular expansion corner. The flow at the wing leading edge is similar. Figure 4 depicts the flow situation in the crossflow plane. The singularity is two-dimensional in a plane normal to the wing leading edge (the crossflow plane) since all derivatives normal to this plane are zero for a conical flow. The velocity component normal to this plane is unchanged through the singularity.

The crossflow stagnates just inboard of the leading edge on the wind side of the sheet. It rapidly accelerates to sonic at the leading edge. The sonic line is followed by a centered Prandtl-Meyer expansion. The flow cannot expand through a deflection $\delta > \nu_{max} = 130.5$. At a deflection of 130.5°, the Mach number would be infinite and the pressure zero. Hence, the flow separates to form a vortex sheet that spirals downstream. The deflection angle δ is such that the pressure on the wind side of the sheet matches that at the crossflow stagnation point on the lee side of the sheet.

During the computation, δ is evaluated from the local flow directions, expanding the sonic crossflow through the Prandtl-Meyer to get the pressure on either side of the sheet at the leading edge. The singular behavior is imposed at each step of the iteration, and the deflection δ is converged with the rest of the flow field.

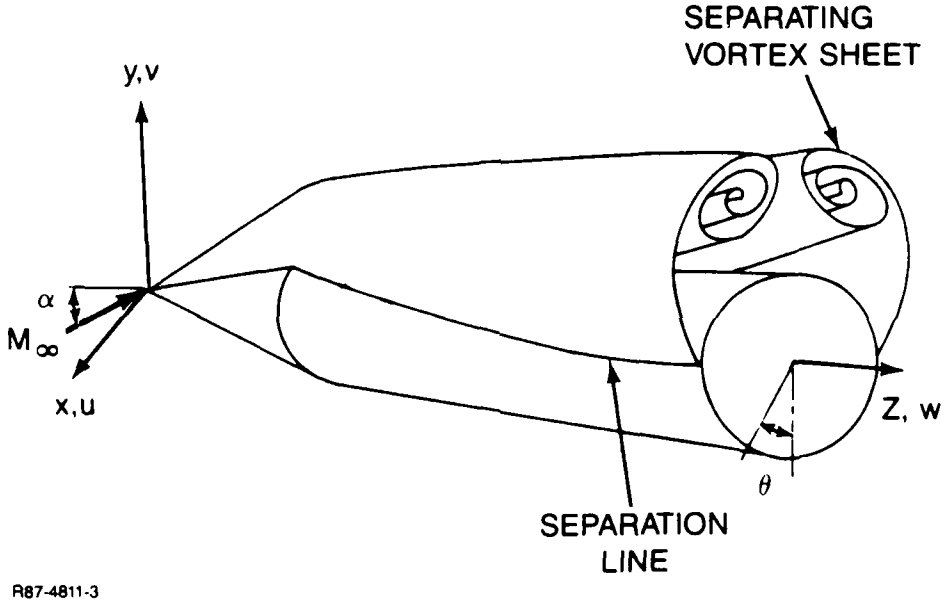

Fig. 3 Sketch of Three-dimensional Separated Flow

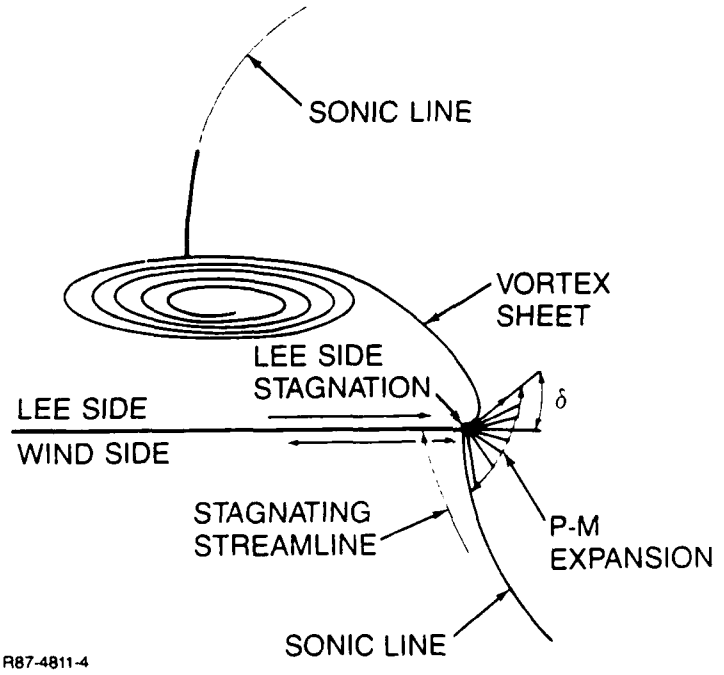

Fig. 4 Sketch of Singularity at Wing Leading Edge

3. COMPARISON OF SHOCK VORTICITY AND SHED VORTICITY

In an effort to gain a better understanding of the relationship between shock vorticity and vorticity shed from the surface of a smooth body, the flow about the 5° cone tested by Rainbird[20] was computed with a number of different separation point locations specified. The case considered was $M_\infty = 4.25$ and $\alpha = 12.35°$. This flow is supercritical and, with no vorticity shed from the cone surface, the crossflow shock produces enough vorticity to cause separation. Figures 5 and 6 show the crossflow streamlines and isobars, respectively, for this flow with no vorticity shed from the body. Separation for this case is computed to be at $\theta = 151.3°$. Figure 5 indicates that the separating streamlines leave the surface at a large angle (57°) relative to it. As shown by the author in Ref 12, when only shock vorticity is present, there is no jump in crossflow velocity at the separation point, which is consistent with the fact that no vorticity is being shed from the surface. It should be pointed out that in the computational results in this section all crossflow shocks are captured. Figure 6 indicates that the shock is captured very sharply (see the closely spaced isobars). Additionally, these captured shock results compare very well with the shock fit results for this case (Ref 12).

Figures 7 and 8 show results for the other extremes of separation point location studied ($\theta = 115°$). Figure 7 shows the crossflow streamlines. The secondary separation shown is due to a strong reverse crossflow shock (see Fig. 8), and the third vortex off the surface is similar to the one discussed previously. In Fig. 8, the isobars are shown, and they indicate an oblique shock at the specified primary separation point. The jump in velocity at the separation point is significant with separation specified at $\theta = 115°$, indicating significant vorticity being shed from the surface. A comparison of Fig. 5 and 7 shows that the extent of the vortical regions is comparable, while the two sources of vorticity are very different.

The relationship between shock vorticity and shed vorticity is made clearer by considering Fig. 9. The figure shows the jump in crossflow velocity vs separation point location. The jump in crossflow velocity is directly related to the vorticity shed into the flow field from the separation point. The shock configuration transition from an oblique crossflow shock to

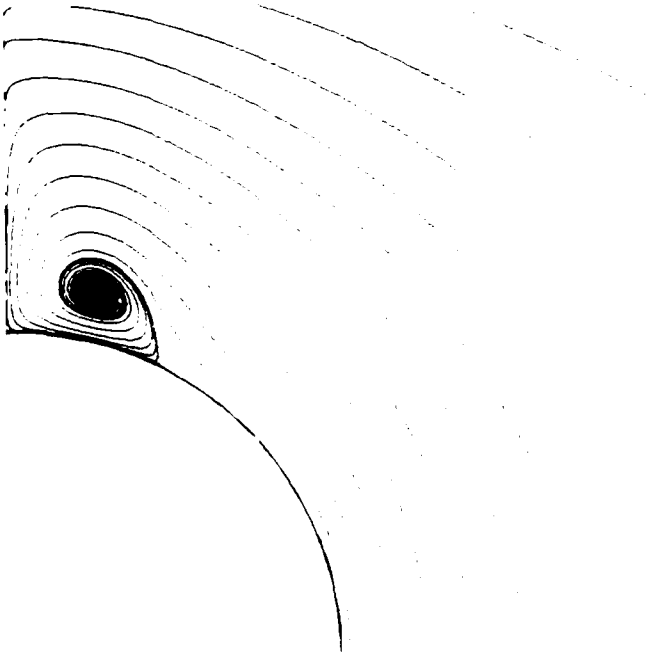

R87-4811-5

Fig. 5 Crossflow Streamlines on the 5° Circular Cone (M_∞ = 4.25, α = 12.35°) Separation Due to Shock Vorticity Alone at θ = 151.3°

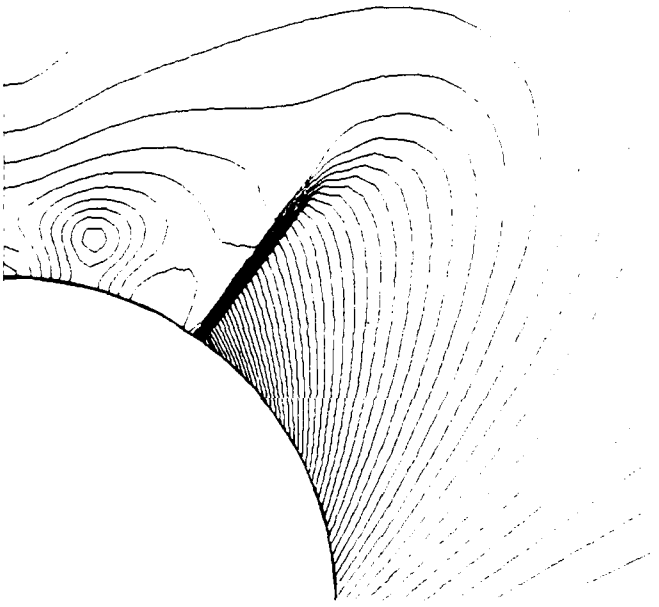

R87-4811-6

Fig. 6 Isobars on the 5° Circular Cone (M_∞ = 4.25, α = 12.35°) Separation Due to Shock Vorticity Alone at θ = 151.3°

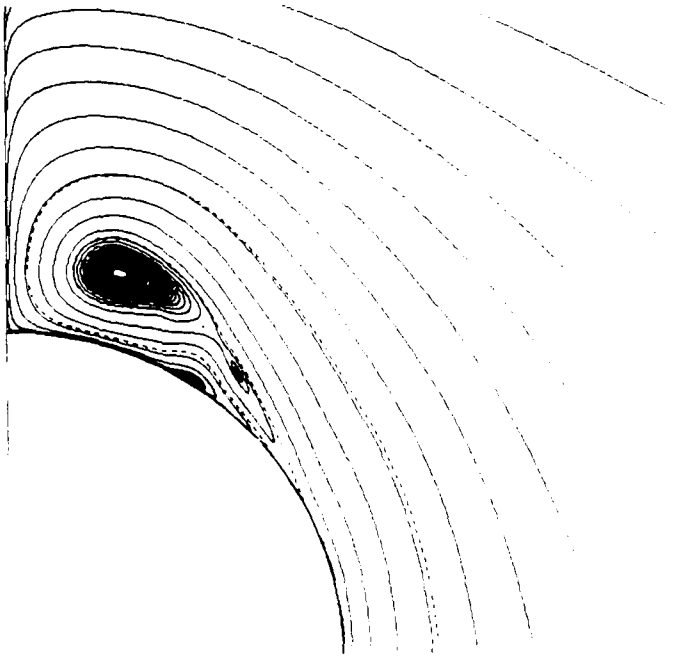

R87-4811-7

Fig. 7 Crossflow Streamlines on the 5° Circular Cone (M_∞ = 4.25, α = 12.35°) Separation Forced at θ = 115°

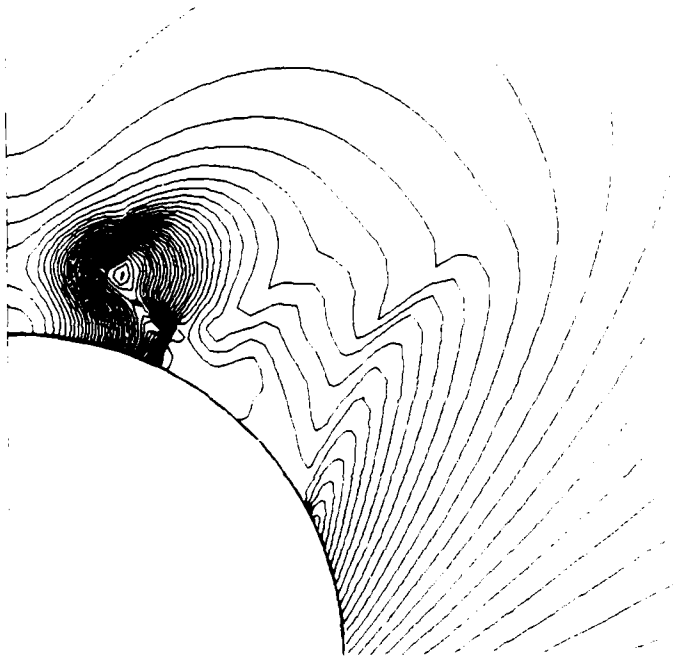

R87-4811-8

Fig. 8 Isobars on the 5° Circular Cone ($M_\infty = 4.25$, $\alpha = 12.35°$) Separation Forced at $\theta \approx 115°$

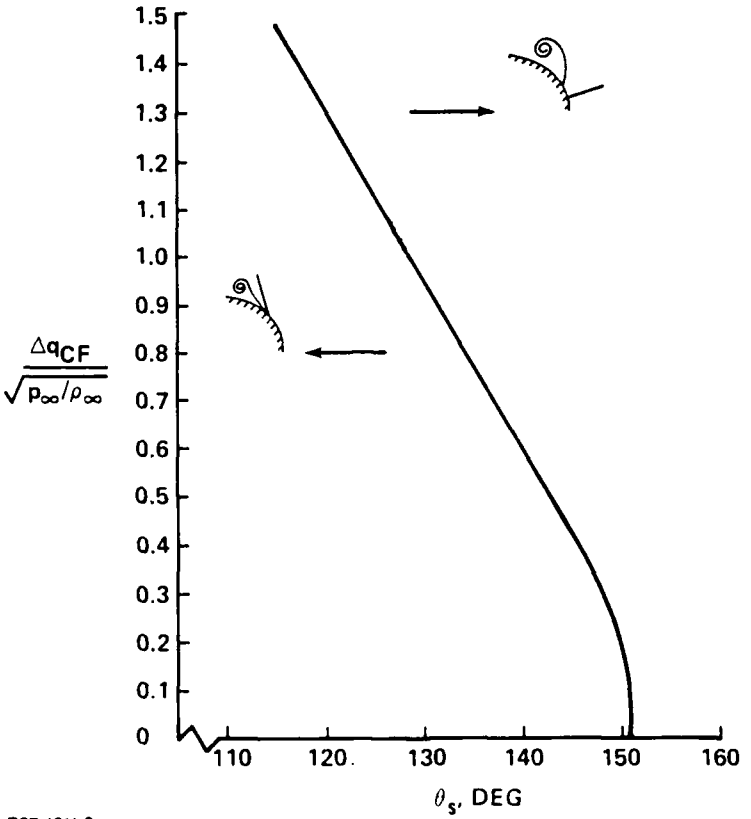

R87-4811-9

Fig. 9 Vorticity Shed into the Flow Field as a Function of Separation Point Location

a detached normal crossflow shock occurs at about $\theta_s \approx 128°$ (indicated by the shaded area in Fig. 9). It should be pointed out that the jump in velocity at the separation point in the oblique shock cases was computed by subtracting the oblique shock velocity jump from the numerical results. Thus, the jumps in velocity in Fig. 9 represent the jumps across the vortex sheet at separation. The figure shows that this velocity jump goes to zero smoothly as the separation point location due to shock vorticity alone is approached (θ_s = 151.3°). This indicates that separation due to shock vorticity alone and that due to shed vorticity are related. In fact, it would seem that separation due to shock vorticity alone is a particular solution of the set of solutions in which vorticity is shed from the surface. In this particular solution, the value of the vorticity shed is zero. Additional details of this investigation can be found in Ref 21, which is included here as Appendix B.

4. COMPLEX SHOCK PATTERNS AND VORTICES

In an investigation of high Mach-number, high angle-of-attack flows, a number of interesting flow phenomena were discovered. These were due to the very high vorticity imparted into the flow from the shock system and the interaction of the resulting vortices with that same shock system.

In this computational investigation, a single cone is considered. The half angle is 10°, and two Mach numbers (5 and 10) were studied. At a freestream Mach number of 5, the shock system becomes complex at an angle of attack of 25°. Figure 10 shows the crossflow streamlines and Fig. 11 the isobars. The crossflow shock exhibits a slope discontinuity as it passes over the top of the vortex, which it created. This discontinuity in shock slope is accompanied by an additional shock, which extends toward the lee plane. This shock is captured but is clearly seen in the isobar plot of Fig. 11. The crossflow shock is no longer simple, but has a triple point separating two portions of shock.

Around the primary vortex a "pinwheel"[22] shock pattern is formed. The crossflow shock becomes oblique to the flow just off the surface so that the crossflow behind the shock is supersonic just off the surface (see the sonic line plot of Fig. 12). The bundle of supersonic crossflow extends to the triple point. This flow must be shocked in order to meet the symmetry condition in the lee plane, and so a crossflow shock sits on top of the vortex (Fig. 11). As lee plane flow is accelerated by the vortex, it becomes supersonic, so that another sonic bubble is formed attached to the lee plane (Fig. 12). This supersonic flow must be shocked to meet the surface boundary condition. Note in Fig. 11 that the shock is normal to the lee plane just above the body. Finally, the surface flow is accelerated under the primary vortex and becomes supersonic (see the third sonic bubble in Fig. 12). This flow is shocked in order to become tangent to the inside of the separation line. This process of expanding and shocking as the flow moves around the vortex sets up a system of three shocks which the author first referred to as the pinwheel type in Ref 22. This shock system is clearly shown in the isobars of Fig. 11.

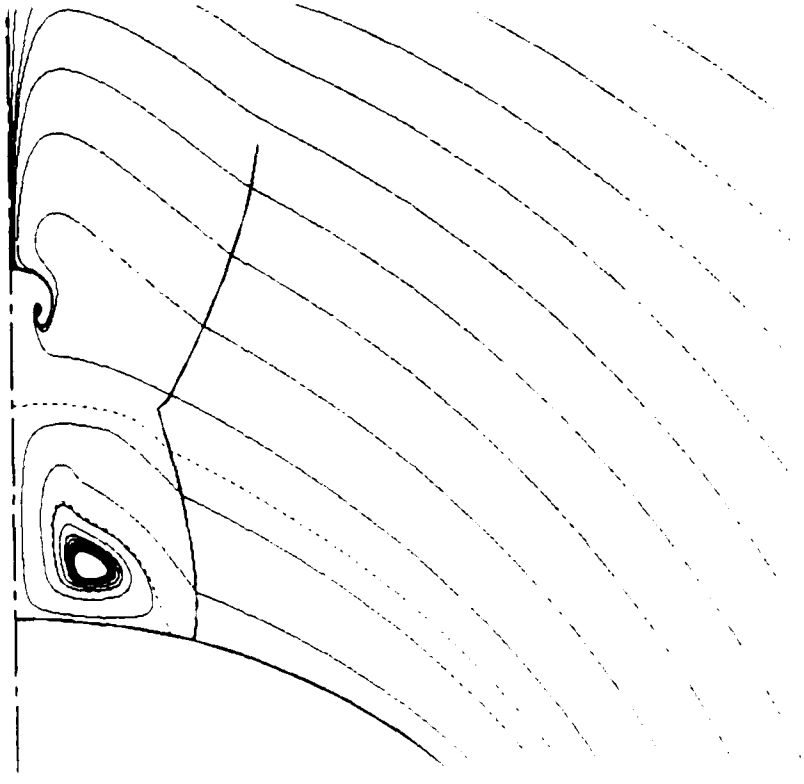

R87-4811-10

Fig. 10 Crossflow Streamlines and Shock 10° Cone, $M_\infty = 5$, $\alpha = 25°$

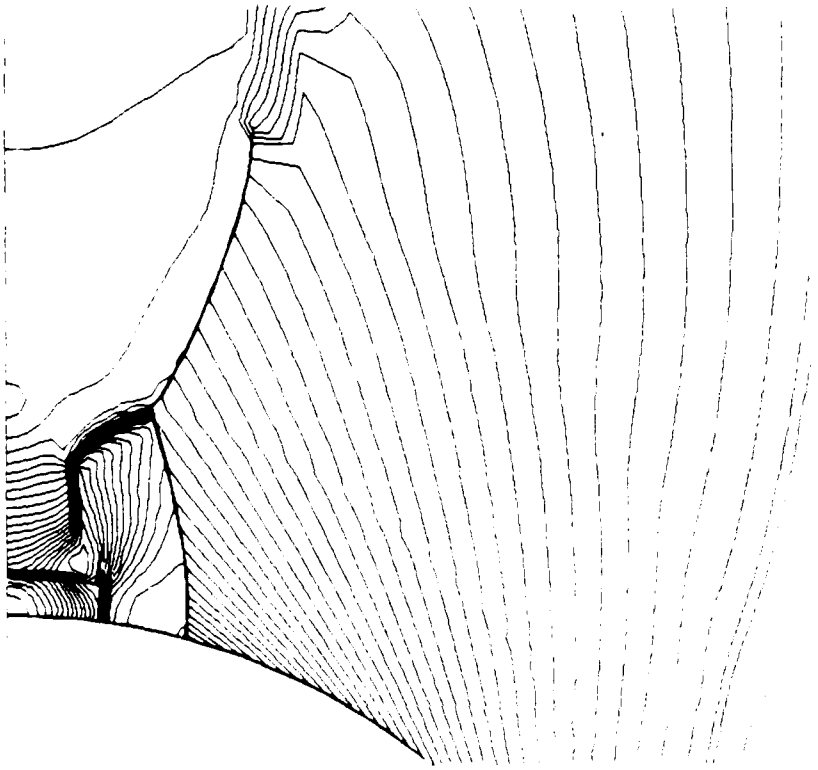

R87-4811-11

Fig. 11 Isobars and Shocks 10° Cone, $M_\infty = 5$, $\alpha = 25°$

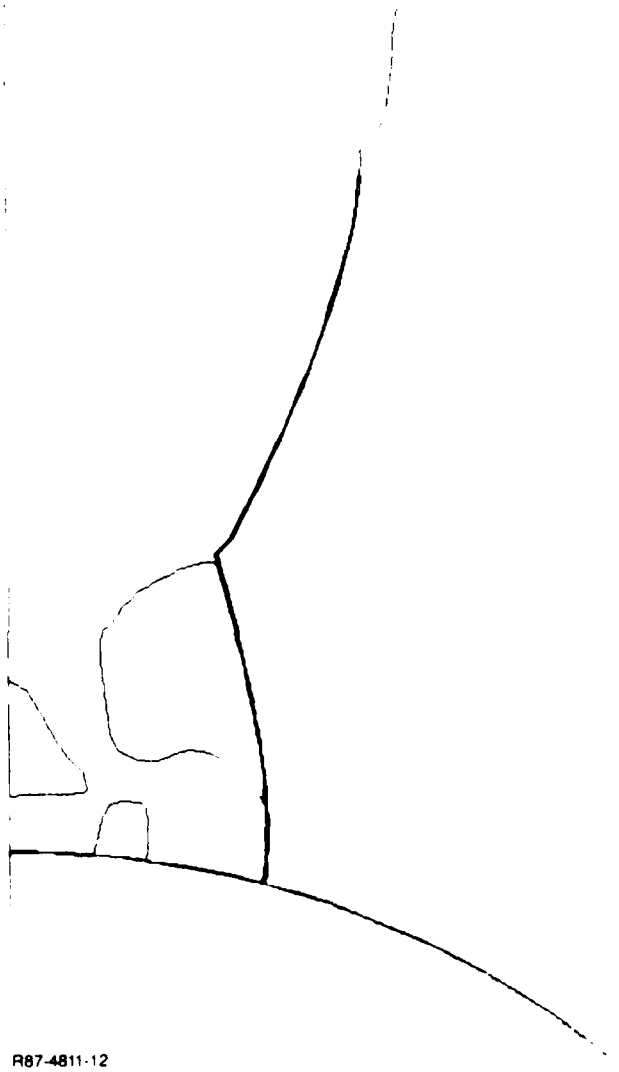

R87-4811-12

Fig. 12 Crossflow Sonic Lines and Shock 10° Cone, $M_\infty = 5$, $\alpha = 25$

Complex shock patterns occur at $\alpha = 20°$ for $M_\infty = 10$ instead of $\alpha = 25°$ at $M_\infty = 5$. Figures 13 and 14 show the crossflow streamlines and isobars, respectively, for the $M_\infty = 10$ and $\alpha = 20°$ case. Figure 14 shows the pinwheel-type shock pattern discussed previously, in addition to the triple point in the crossflow shock. It should be noted that there is no secondary vortex in this case; instead, there is a simple node in the lee plane above the primary vortex.

The last case considered is $M_\infty = 10$ and $\alpha = 25°$. Figure 15 shows the streamlines and Fig. 16 the isobars. Again, the pinwheel shock pattern is quite evident in addition to the triple point. The primary crossflow shock has a maximum normal Mach number of 3.8 at the surface and is quite strong. The captured reverse crossflow shock has a normal Mach number of 1.8. This has a secondary vortex above the main vortex, in addition to a simple node in the lee plane halfway between the body and the bow shock (not shown in the figure). The secondary spiral node above the main vortex is seen more clearly in the expanded view of its region shown in Fig. 17. Figure 17 is an expanded view of the dashed box in Fig. 15. It can be seen that the node does not form a large vortex as does the primary vortex, but seems to spiral at the node. Additional details of this work can be found in Ref 23, which is included here as Appendix C.

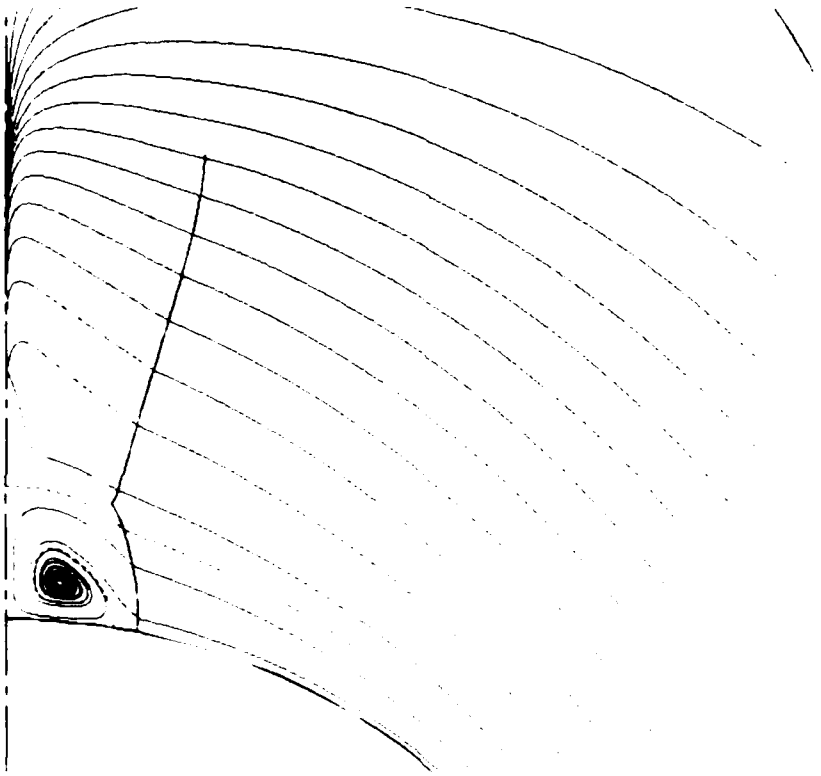

R87-4811-13

Fig. 13 Crossflow Streamlines and Shock 10° Cone, $M_\infty = 10$, $\alpha = 20°$

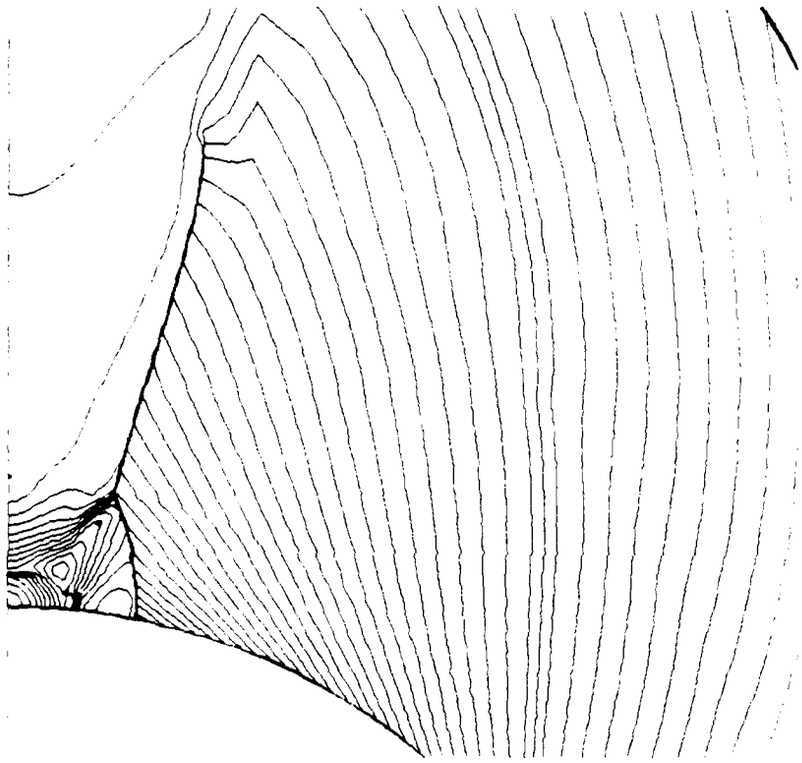

R87-4811-14

Fig. 14 Isobars and Shocks 10° Cone, $M_\infty = 10$, $\alpha = 25°$

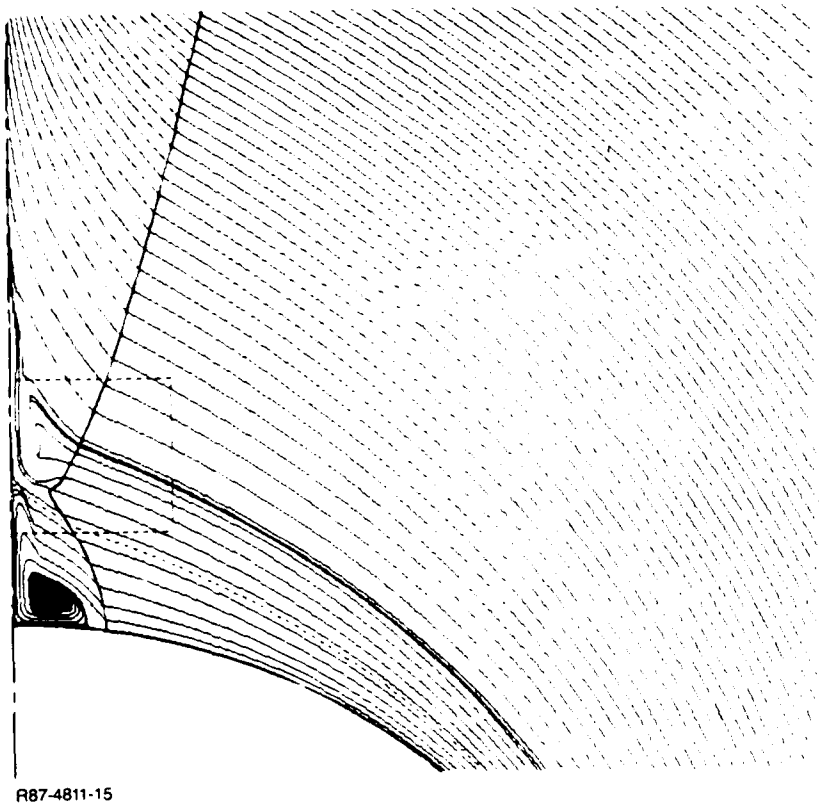

R87-4811-15

Fig. 15 Crossflow Streamlines and Shocks 10° Cone, $M_{\infty} = 10$, $\alpha = 25^{\circ}$

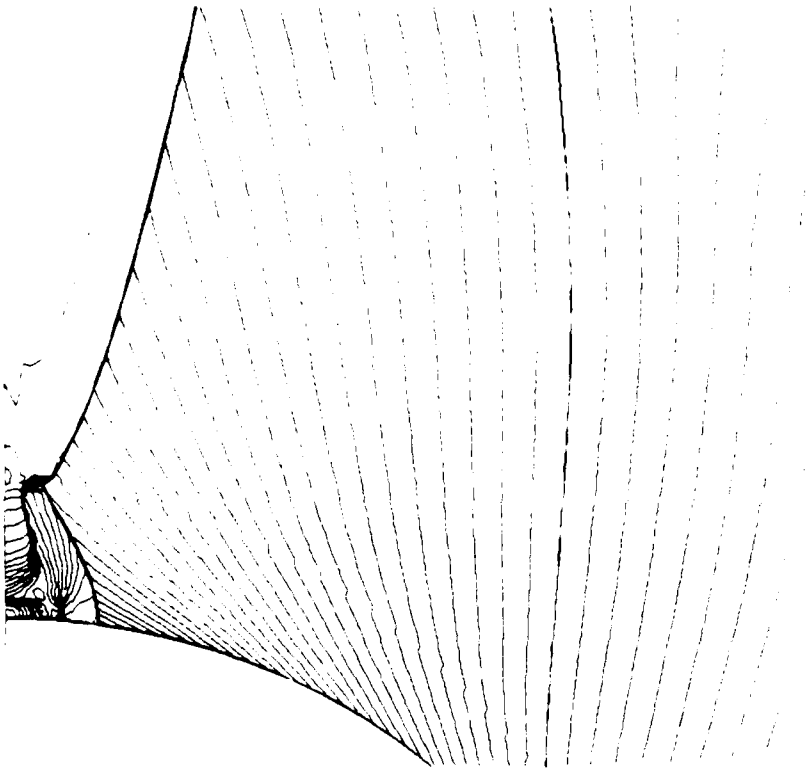

R87-4811-16

Fig. 16 Isobars and Shocks 10° Cone, $M_\infty = 10$, $\alpha = 25°$

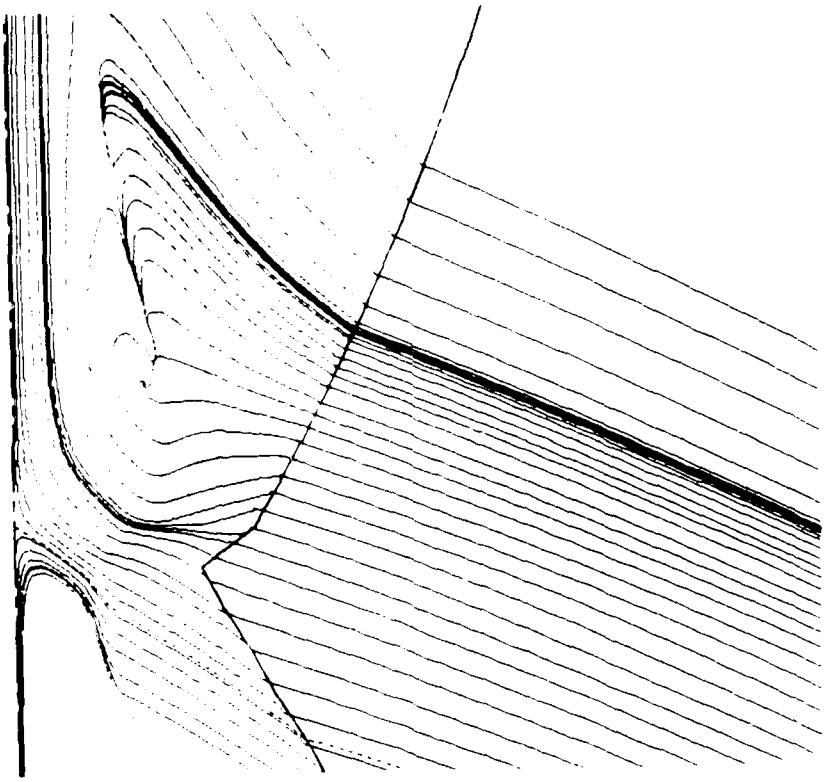

R87-4811-17

Fig. 17 Expanded View of Crossflow Streamlines 10° Cone, $M_\infty = 10$, $\alpha = 25°$

5. DELTA WING FLOWS

Over the past several years a number of researchers investigating separated flow about sharp leading edge wings have concluded that there exists a close relationship between flow separation and computed total pressure loss (see, for example, Ref 24). This is not surprising in light of Crocco's equation which relates vorticity to the gradient of entropy (i.e., total pressure). But this conclusion seems inconsistent with the classical model for inviscid separated flow. The classical model[4,5,6] is one of isentropic irrotational flow with a infinitesimally thin region of vorticity, a vortex sheet. This apparent inconsistency was investigated, and it was found that a zero total pressure loss Euler solution with leading edge separation does exist.

In all the cases considered in this investigation, the shock system produces very little entropy. The question then arises as to how Crocco's relation $\nabla H_o - T\nabla S - \vec{V} \times \vec{\omega} = 0$ is satisfied by a separated flow with vorticity and no entropy or total enthalpy gradients. The exact inviscid solution is irrotational ($\vec{\omega} = 0$) everywhere outside the vortex sheet and away from the vortex core. These flows have been computed for many years using irrotational models (see Ref 25, for example) with the sheet and the vortex core being modeled by singularities. Modern Euler solvers capcure the sheet and the vortex core as part of the solution. Powell and Murman[26] showed two different ways that Crocco's relation could be satisfied by an Euler solver: a strictly conservative formulation in which entropy gradients generated at the wing leading edge are balanced by $\vec{V} \times \vec{\omega}$ (H_o is constant) and a modified conservative scheme which substituted S = constant for the axial momentum equation. In the latter formulation, $\nabla S = \vec{V} \times \vec{\omega} = 0$ and again $\nabla H_o = 0$. The present formulation is closer to the second of these. Since entropy is tracked very accurately along streamlines, the present formulation differs from the second of Powell and Murman's in that all momentum equations are satisfied.

If we consider a 75° sweep delta at a low supersonic Mach number (M_∞ = 1.5) and small angle of attack (α = 4°), then the shock system (only a bow shock) produces less than 1% total pressure loss. The present calculation predicts that result very accurately. Figure 2a shows contour lines of the

modulus of vorticity, and Fig. 2b shows the crossflow streamlines. The vortex is formed because of the presence of the vorticity which comes from the leading edge. The flow separates because an attached leading edge requires expansion beyond the vacuum limit, as discussed in Section 2 of this report. The sheet is spread over a few grid cells near the leading edge and gets thicker as it wraps around the vortex core. Unlike the calculations of Ref 24, no total pressure loss is associated with this separation. In the core of the vortex, Crocco's relation is satisfied to within the accuracy of the calculation. The gradient of total enthalpy is at a machine zero, and the gradient of entropy ∇S is less than 10^{-10}, so that only the $\vec{\nabla} \times \vec{\omega}$ remains. This term has a local maximum near the core of 10^{-2} ($|\vec{\omega}| = O(1)$ at the core), which is within the accuracy of the calculation. There are larger values of $\vec{\nabla}x\vec{\omega}(10^{-1})$ at the wing leading edge due to the singularity there. These findings are similar to those of Ref 26.

The case discussed in the preceding paragraph is one in which the flow is irrotational outside the vortex sheet and away from the vortex core (see Fig. 18a). The exact solution to the differential Euler equations is approached as the sheet approaches an infinitesimal region and the core approaches a point. In the exact solution, Crocco's relation is not expected to be satisfied across the vortex sheet; velocities are discontinuous and their derivatives do not exist. It can be shown that the flow velocity must be parallel to the vorticity vector at the spiral node at the end of the vortex sheet (the vortex core). The exact solution satisfies Crocco's relation by forcing $\vec{\nabla} \times \vec{\omega} \to 0$ as the core is approached. The vortex core has the same behavior in the present calculation.

Figure 18 shows a comparison of the surface pressure computed using the present technique and that computed using the fully conservative procedure of Powell and Murman.[27] The wing is swept 75° and the free stream conditions are $M_\infty = 1.95$ and $\alpha = 10°$. The flow is separated at the leading edge, as can be seen from the crossflow streamlines of Fig. 20a (the dashed lines are crossflow stagnating streamlines). The reverse flow becomes supersonic under the vortex and is shocked at $x/x_{LE} \approx 0.75$; note the clustering of isobars in Fig. 20b. The comparison of Fig. 19 indicates that the two procedures are predicting the same static pressure. The results of Powell and Murman exhibit a 65% loss in total pressure at the vortex core, while the shock system

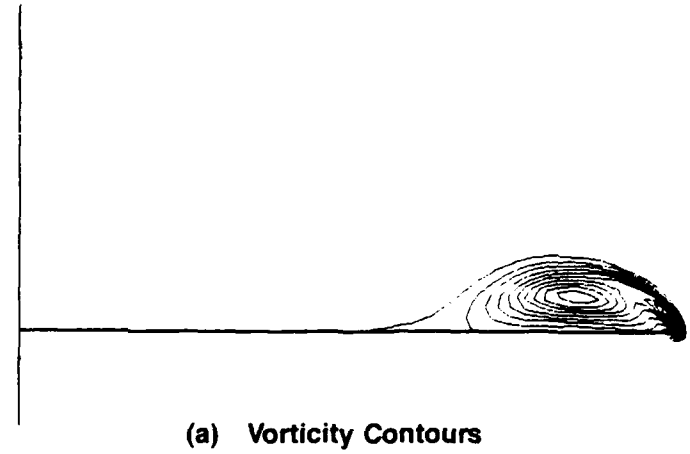

(a) Vorticity Contours

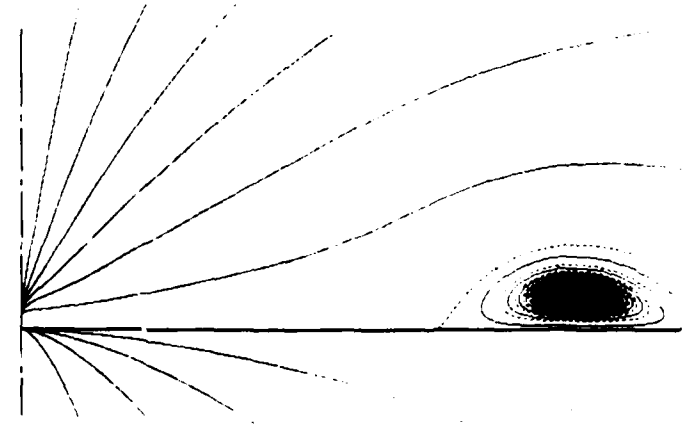

(b) Crossflow Streamlines

R87-4811-18

Fig. 18 Vorticity Contours and Streamlines for Flat Plate Delta with $\lambda = 75^{\circ}$, $M_{\infty} = 1.7$ and $\alpha = 4^{\circ}$

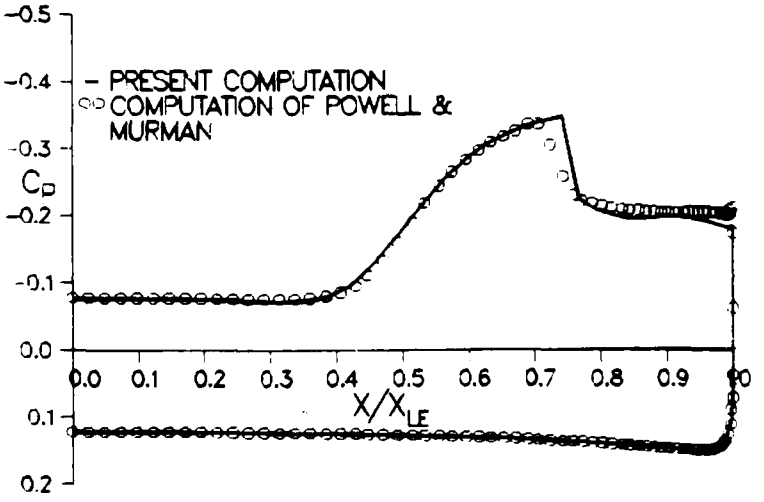

R87-4811-19

Fig. 19 Surface Pressure Comparison, $\lambda = 75^\circ$, $M_\infty = 1.95$, $\alpha = 10^\circ$

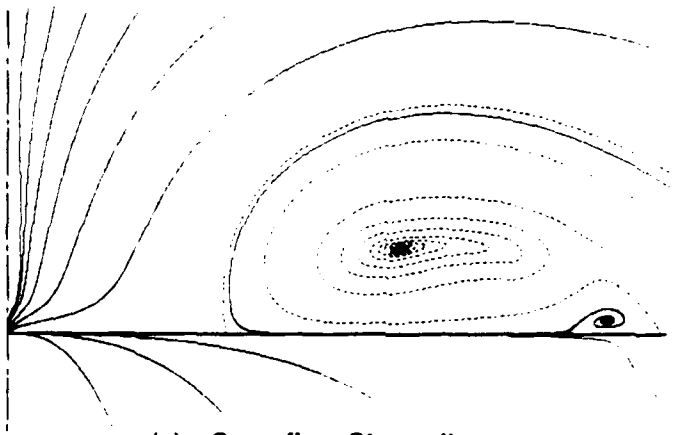

(a) Crossflow Streamlines

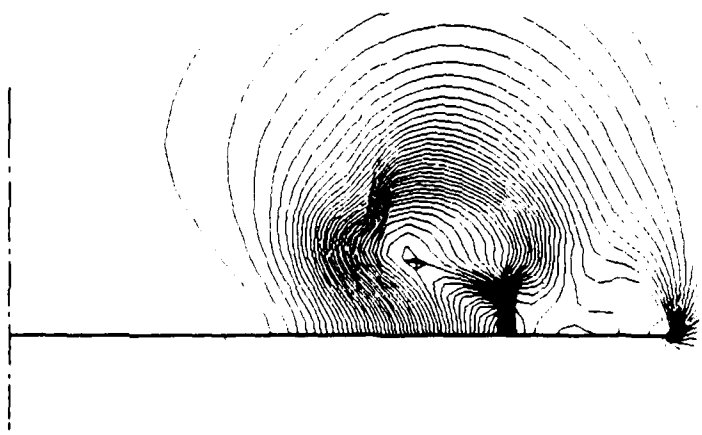

(b) Isobars

R87-4811-20

Fig. 20 Crossflow Streamlines and Isobars, $\lambda = 75^{\circ}$, $M_{\infty} = 1.95$, $\alpha = 10^{\circ}$

produces a maximum total pressure loss of only 30%. Figure 21 compares the surface crossflow Mach number computed by the two calculations. For the sake of clarity, this Mach number is plotted vs normalized arc length (i.e., 0 to 1 is the wind side and 1 to 2 is the lee). Here again the comparison is generally good. There are small discrepancies just beyond the leading edge in addition to those near the lee plane of symmetry. In Ref 26, Powell and Murman found that the major discrepancy between results that conserve entropy and those that do not is in the radial component of Mach number. The computations presented here seem to indicate the same result.

The flow at the leading edge of the zero-thickness delta wing is singular. Powell and Murman have been successful in computing these flows with no consideration of this singularity. The results presented here in Fig. 18-21 were also computed with no consideration for this singularity. The wing leading edge was avoided, i.e., no grid point was placed there. A Kutta-type condition was developed for sharp leading edge wings, and was outlined in Section 2 of this report. Figure 22a shows a comparison of the surface pressure distribution computed with and without the singularity included. The wing sweep is 75° and $M_\infty = 1.7$ and $\alpha = 12°$. The differences in the pressures are very small and confined to the area of the tip. Figure 22b shows a comparison of the computed surface crossflow Mach number distribution. Here again the differences are small and confined to the leading edge region. It should be noted that the sonic velocity at the tip ($s/x_{LE} = 1$) is indicated by the symbol ($M_{CF} = 1.$), as is the flow after the centered expansion ($M_{CF} = 1.3$). In all the results that follow, the singular tip solution is computed explicitly.

In comparing the results of inviscid separated flow calculations with experimental data, one will find significant discrepancies under the main vortex. A large part of these discrepancies is due to secondary separation. In Ref 7, this author presented a model for shedding vorticity from a smooth surface in order to force separation at a specified location in an Euler calculation. In Ref 20, this work was extended to include secondary separation, i.e., separation of the reverse flow under the main vortex.

Figure 23 shows a comparison of computed surface pressure and experimental data.[29] The wing is swept 75°, $M_\infty = 1.7$ and $\alpha = 12°$. Also shown in the figure are the computed results of Powell and Murman which were first

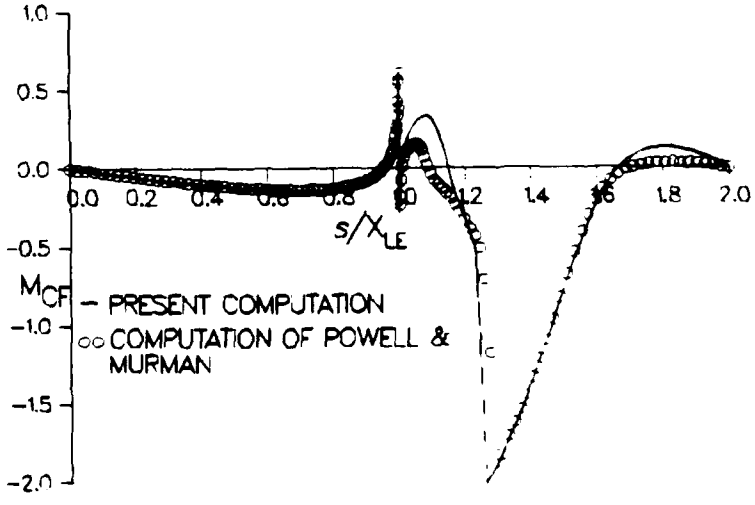

R87-4811-21

Fig. 21 Comparison of Surface Crossflow Mach Number, $\lambda = 75^\circ$, $M_\infty = 1.95$, $\alpha = 10^\circ$

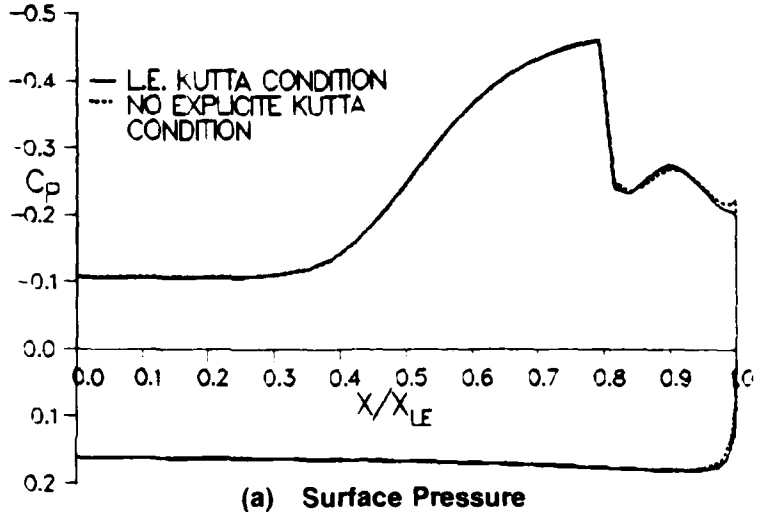

(a) Surface Pressure

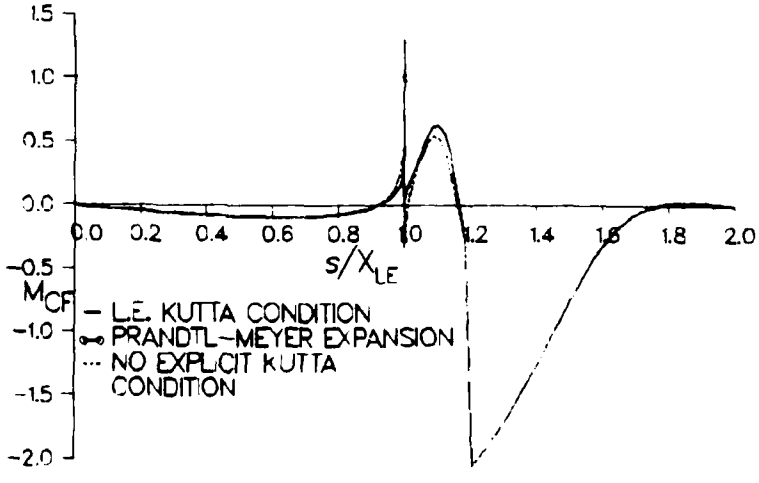

(b) Surface Crossflow Mach Number

R87-4811-22

Fig. 22 Comparison of Results with and without Kutta Condition Imposed
$\lambda = 75°$, $M_\infty = 1.7$, $\alpha = 12°$

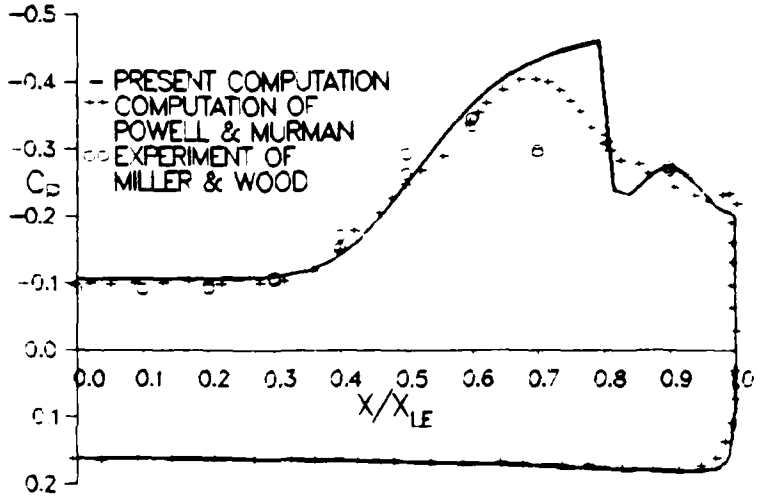

R87-4811-23

Fig. 23 Surface Pressure Comparison, $\lambda = 75^\circ$, $M_\infty = 1.7$, $\alpha = 12^\circ$

presented in Ref 30. Both the Euler computations predict the lee side pressures quite well, except in the region under the main vortex ($x/x_{LE} > 0.6$). Figure 24a shows the crossflow streamlines, which indicate that the vortex is centered above $x/x_{LE} = 0.6$. Figure 24a shows a separation of the reverse flow which is due totally to shock vorticity and is downstream of the secondary separation location noted experimentally. The shock that causes this separation is the reverse crossflow shock located at $x/x_{LE} \approx 0.8$. Figure 11b shows the isobars from which the shock can be seen clearly.

The experimental data of Miller and Wood[29] included cross-sectional vapor-screen photographs from which secondary vortices can be seen. The location of secondary separation was difficult to determine from these pictures, but an attempt was made. Figure 25 shows a comparison among computed surface pressures, secondary separation forced at $x/x_{LE} = 0.7$, and the experimental data. The figure shows a significant improvement in the comparison in the pressures for $x/x_{LE} > 0.6$. From the comparison of Fig. 25, one might get the impression that the Euler results with secondary separation predict the flow fields very accurately. Experience with more detailed experimental data indicates that the test data are flat for $x/x_{LE} > 0.6$. The overexpansions of the Euler result under the main vortex ($0.6 < x/x_{LE} < 0.7$) and the secondary vortex ($0.8 < x/x_{LE} < 0.9$) are areas where discrepancies exist. These discrepancies are due either to boundary layer thickening or to viscous effects not accounted for by the boundary layer equations.

Figure 26a shows the crossflow streamlines with secondary separation at $x/x_{LE} = 0.7$. A comparison of Fig. 26a and 26a indicates that the forced secondary vortex is larger than that caused by the reverse crossflow shock. The secondary separation is forced to occur in a supersonic reverse crossflow region. Therefore, a shock is produced before the vortex. Figure 26b shows isobars that indicate the shock clearly at $x/x_{LE} = 0.7$. It must be remembered that while this shock's vorticity may contribute to this secondary vortex, it is the additional vorticity shedding that causes this secondary separation. These comparisons are typical; additional examples can be found in Ref 31.

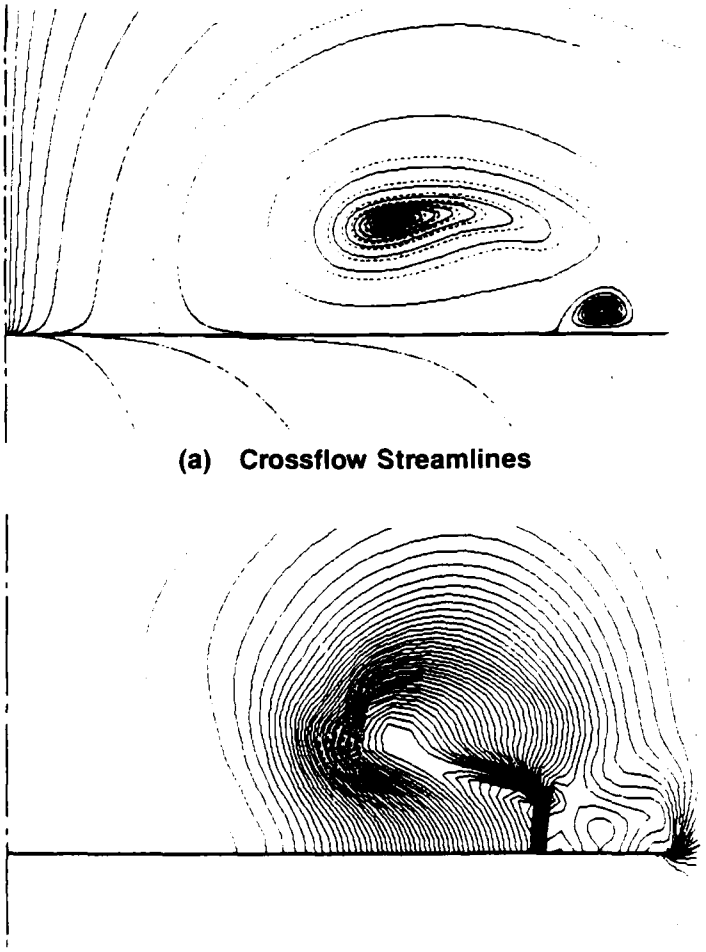

(a) Crossflow Streamlines

(b) Isobars

R87-4811-24

Fig. 24 Crossflow Streamlines and Isobars, $\lambda = 75^\circ$, $M_\infty = 1.7$, $\alpha = 12^\circ$

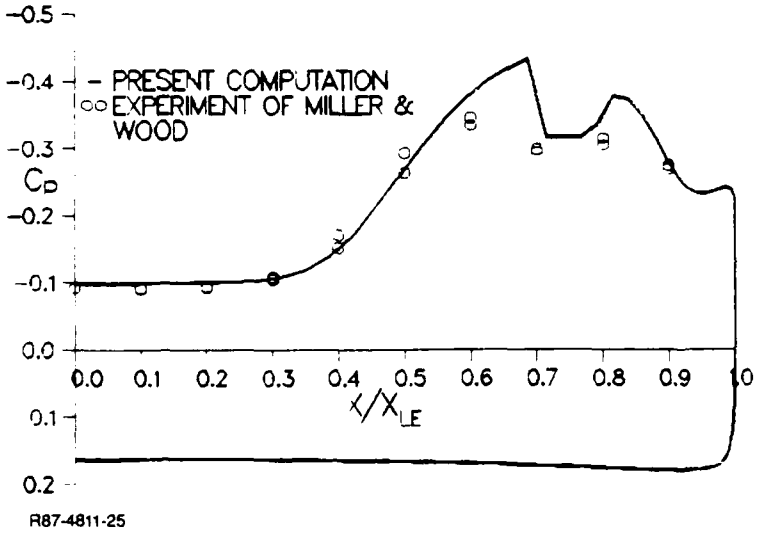

Fig. 25 Surface Pressure Comparison, $\lambda = 75^\circ$, $M_\infty = 1.7$, $\alpha = 12^\circ$, Secondary Separation Forced at $x/x_{LE} = 0.7$

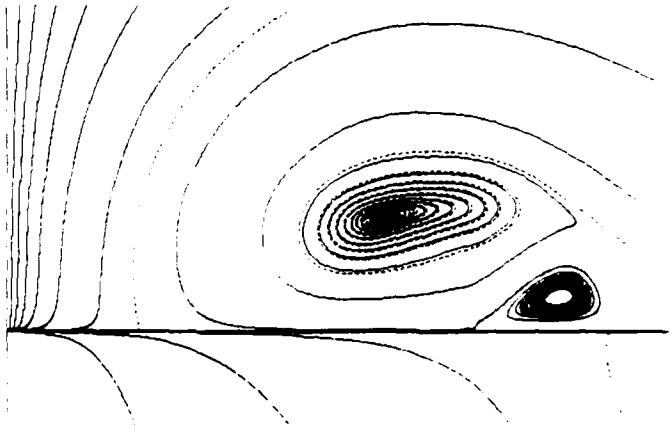

(a) Crossflow Streamlines

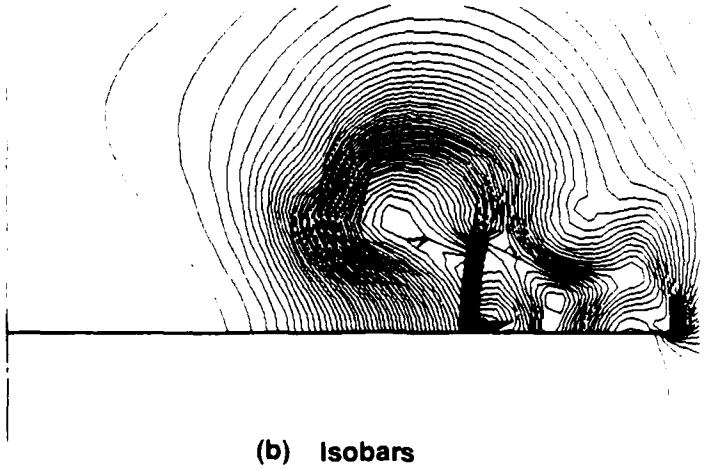

(b) Isobars

R87-4811-26

Fig. 26 Streamlines and Isobars, $\lambda = 75^\circ$, $M_\infty = 1.7$, $\alpha = 12^\circ$, Secondary Separation Forced at $x/x_{LE} = 0.7$

6. FULLY THREE-DIMENSIONAL FLOWS

In this section the application of the vorticity-shedding model used for conical flows to fully three-dimensional flows is demonstrated. The computational procedure has already been discussed in Section 2 of this report. The present study is restricted to simple three-dimensional configurations. The first is a cone/cylinder configuration tested by E.J. Landrum[12] at NASA's Langley Research Center. The free-stream Mach was 2.3 and the cone half-angle was 9.46°. The conical portion of the body ended at Z/L = .45. The configuration is shown in Fig. 27. Also shown in the figure are the surface stream lines for the 20° angle-of-attack case. The primary separation line is clearly indicated by the discontinuity in the slope of the streamlines coming from the wind side of the body. The location of this line was obtained from the experimental data. The streamline picture of Fig. 27 is easier to understand if, in addition, the conical crossflow streamlines are considered. Figure 28a shows the crossflow streamlines on the conical portion of the body (Z < .45). First, one sees that the streamlines coming from the wind plane leave the body at the separation point (dashed line, intersecting the body at 113° from the wind plane, is the separating streamline); this should be kept in mind when studying Fig. 27. Under the main vortex, there is a small secondary vortex which is caused by the vorticity produced by a reverse crossflow shock. The crossflow isobars are shown in Fig. 28b. This shock is indicated by the clustered isobars under the main vortex. There is a crossflow reattachment line (dashed line, Fig. 28a) on the body at 124° from the lee plane. These features can be seen in the surface streamlines of Fig. 27. This case and all those to follow have a supersonic crossflow approaching primary separation. As mentioned in Section 2, an oblique crossflow shock occurs at the separation point, which can be seen in the isobars of Fig. 28b. This oblique shock is not captured as sharply as the normal reverse crossflow shock.

Figure 29 shows a comparison of the computed surface pressure and the experimental data. Figure 29a is for the conical flow Z/L < .45; Fig. 29b and 29c are at Z/L = .675 and .925, respectively, of Landrum.[33] The polar angle θ is measured from the wind plane as shown in Fig. 1. In the figure, the primary separation is denoted by a jump in pressure due to the oblique

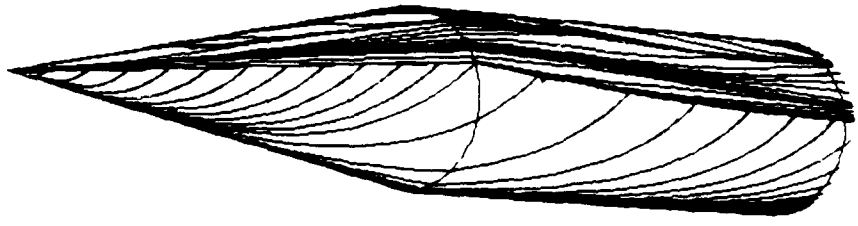

R87-4811-27

Fig. 27 Surface Streamlines, Cone/Cylinder, $M_\infty = 2.3$, $\alpha = 20^\circ$

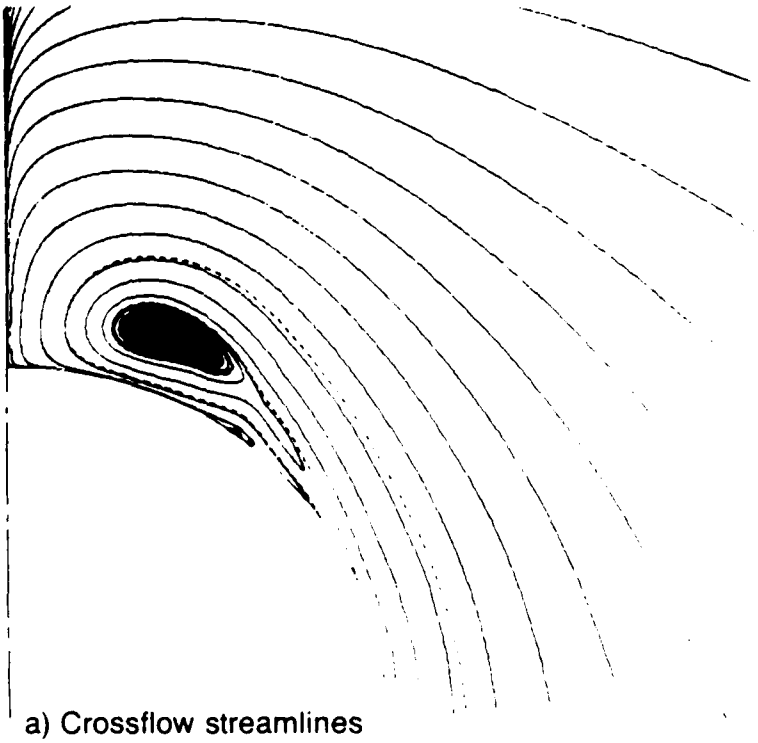

a) Crossflow streamlines

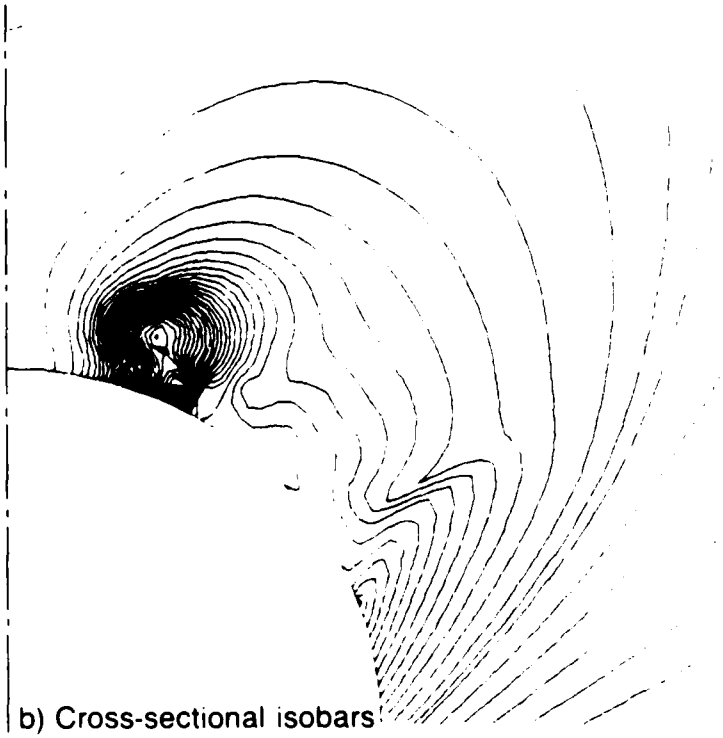

b) Cross-sectional isobars

R87-4811-28

Fig. 28 Crossflow Streamlines and Isobars on Cone/Cylinder ($Z/L < 45$), $M_\infty = 2.3$, $\alpha = 20^\circ$

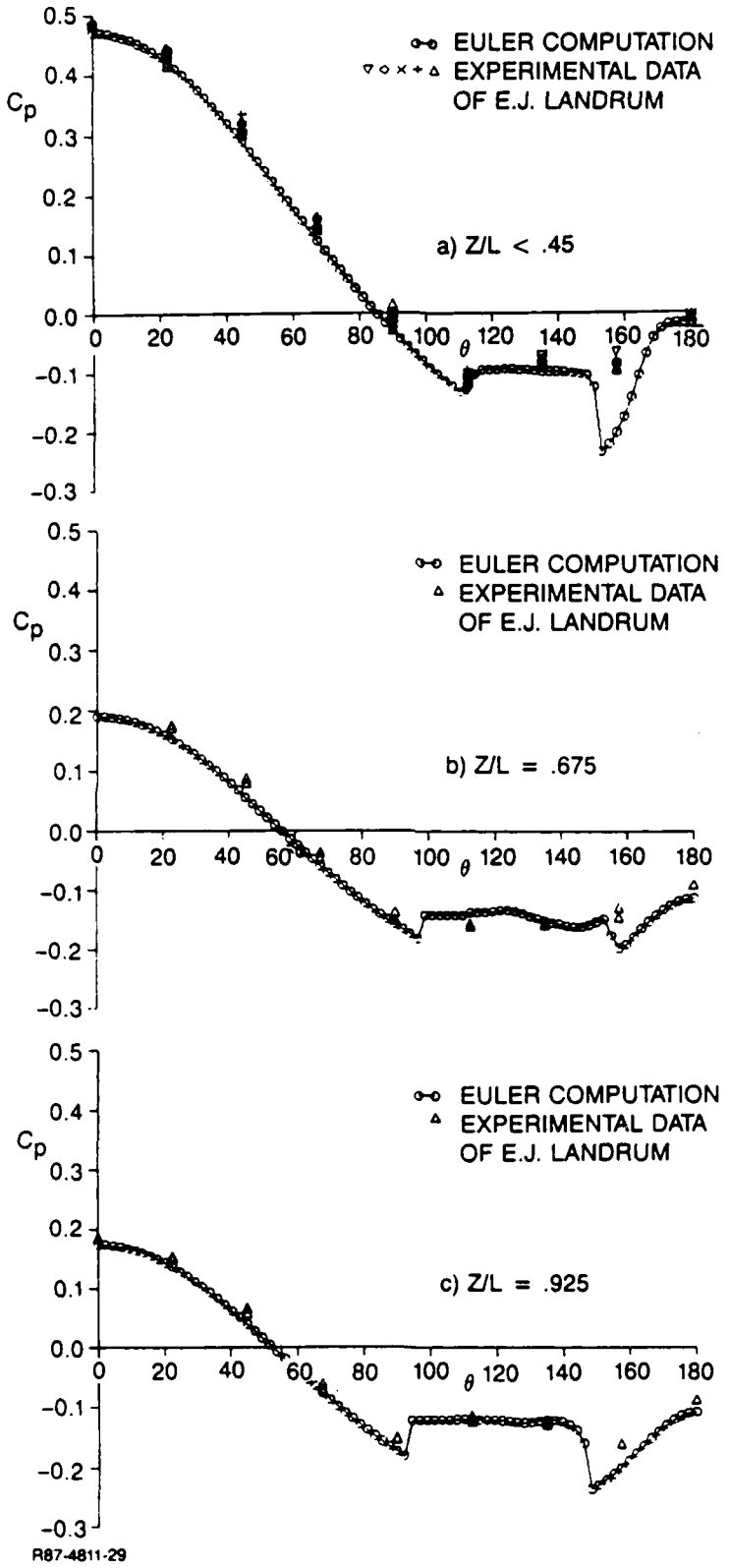

Fig. 29 Surface Pressure Comparison, Cone/Cylinder, $M_\infty = 2.3$, $\alpha = 20^\circ$

crossflow shock mentioned previously. The pressure comparison is good upstream of the primary separation; in addition, the plateau pressure just past separation is predicted quite well. The lee plane region is not predicted so well. The pressure in the lee plane itself is predicted accurately, but the inviscid reverse flow expands rapidly to a supersonic reverse Mach number region which is terminated by a reverse crossflow shock. While reverse crossflow shocks have been noted experimentally,[32] they seem too strong in inviscid calculations. This is similar to the result found for the delta wing calculations discussed in the previous section.

The last case considered here (more detail can be found in Ref 22) is a missile configuration with elliptical cross sections. The configuration was tested at NASA's Langley Research Center[34] and computed with a Navier-Stokes solver by Newsome.[35] The missile is made up of a series of 3:1 elliptical sections. The computation was performed at $M_\infty = 2.5$, $\alpha = 20°$ and $\beta = 0$ (tests were conducted at yaw). Primary separation occurred near the leading edge of the configuration; the location of the separation line was obtained from the computational results of Newsome.[35]

Figure 30 shows a comparison of surface pressures computed with the Euler solver, the Navier-Stokes solver[35] and that found experimentally.[34] Figure 11a shows a station near the apex of the body (Z/L = 0.3). The separation point is indicated by the compression (shock) at $\theta \approx 100°$ in the Euler solution. The comparison before separation is good except for some upstream influence seen in both the experiment and the Navier-Stokes calculation and absent in the Euler solution. In this flow field as in the others presented here, the local crossflow is supersonic at separation. The pressure plateau after separation is predicted well by both computations. The Euler computation predicts supersonic reverse crossflow and a shock at $\theta \approx 120°$. Surprisingly, it seems that the Navier-Stokes solution has the same pressure distribution in this region. In this calculation, the experimental data do not seem to show this behavior, but its scatter at $\theta \approx 135°$ is large and makes it difficult to tell whether a compression does or does not occur in this region. Figure 30 shows stations farther downstream. The features are similar to those in Fig. 29. The final two sections shown in Fig. 30 show a sharp shock at the primary separation point, in addition to a sharp reverse crossflow shock. At this station the Navier-Stokes computation shows no sign

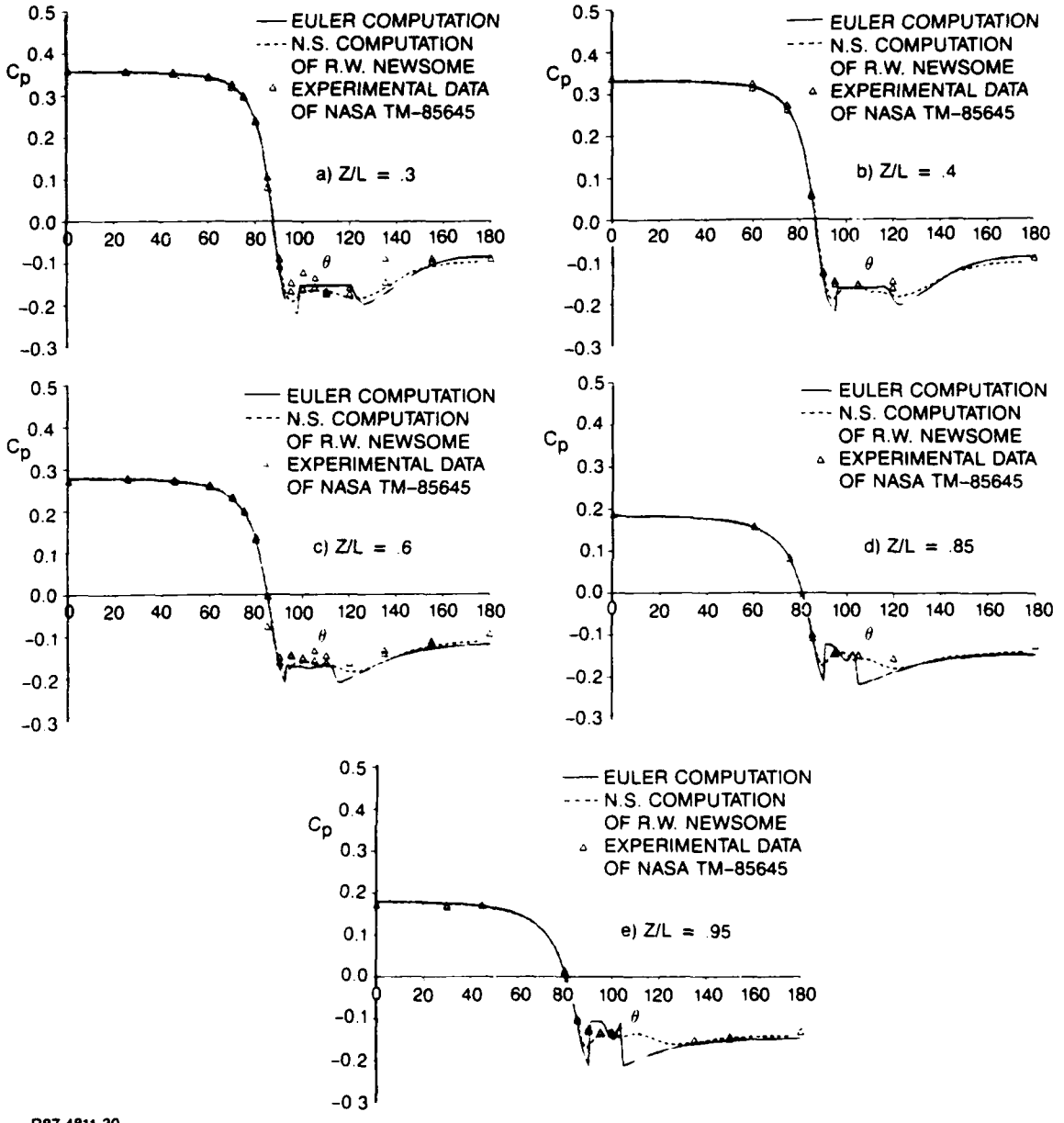

R87-4811-30

Fig. 30 Surface Pressure Comparison, Elliptic Missile, $M_\infty = 2.5$ and $\alpha = 20°$

of supersonic reverse crossflow. It should be pointed out that secondary separation was noted in the experiment and Navier-Stokes calculation was not included in the Euler computation for the reasons discussed previously. Here again, the Euler computation predicts the separated flow surface pressures well, except in the region under the vortex.

7. SUBSONIC FLOWS

The separation model developed here was incorporated into a fully conservative, time-dependent, two-dimensional code in order to test its capability in predicting subsonic flows. The code utilized Van Leer's[36] flux vector splitting technique to develop a finite difference scheme. The effort was unsuccessful in that the model did not cause separation. It seemed that the smearing inherent in the scheme was the cause of the difficulty. Unlike the λ Scheme,[15] the conservative scheme spread the vortex sheet evenly on the surface at the separation point. As discussed in Section 2 of this report, the λ Scheme naturally avoids differentiating the entropy and in some sense the velocity at a point where the velocity changes sign, i.e., the separation point. This property seems to be needed in order to force separation within the model used here. An attempt was made to incorporate the model into a conservative central difference code, again with no success. Both these schemes are notorious for spreading convective currents. In Ref 37 it was found that both these schemes were inaccurate for boundary layer flows because of this smearing.

An unsteady λ Scheme code was written to substantiate the suspicion stated above. The separation model used in supersonic flow was successful in forcing separation on a cylinder at $M_\infty = 0.3$ (nearly incompressible). The results are shown in Fig. 31. Separation was forced at 150° from the forward stagnation point, as can be seen in the streamlines of Fig. 31a. It should be noted that symmetry was assumed in the computation. The surface pressure is shown in Fig. 31b. These results indicate that the model can be used in the subsonic region, but not in conjunction with a conservative formulation.

The original intent of this aspect of the work was to incorporate the flow-separation model into an existing subsonic, conservative, three-dimensional code. Since the available codes were able to predict flow separation with the model, in its present form this aspect of the work was delayed to a future effort.

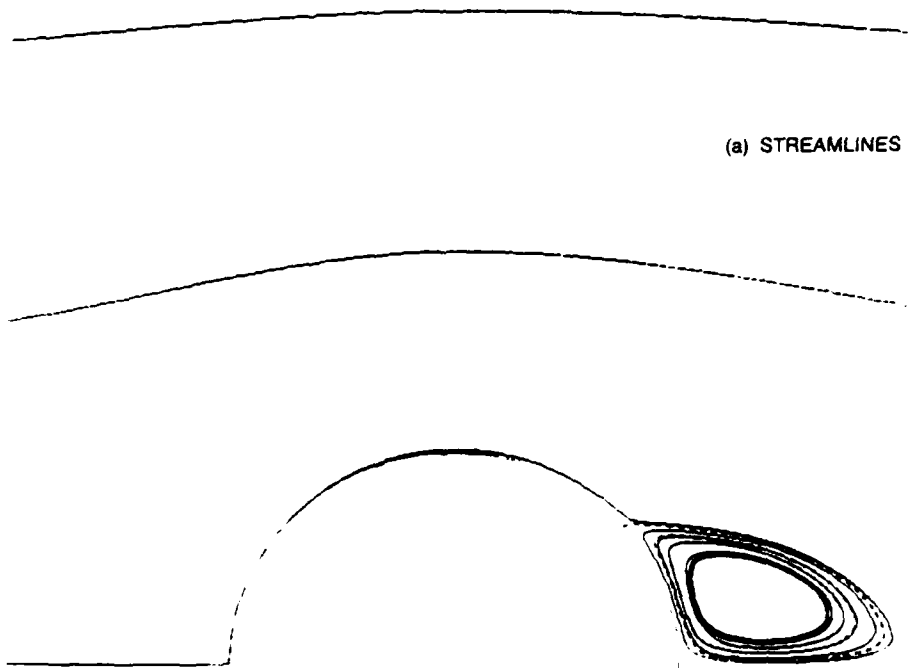

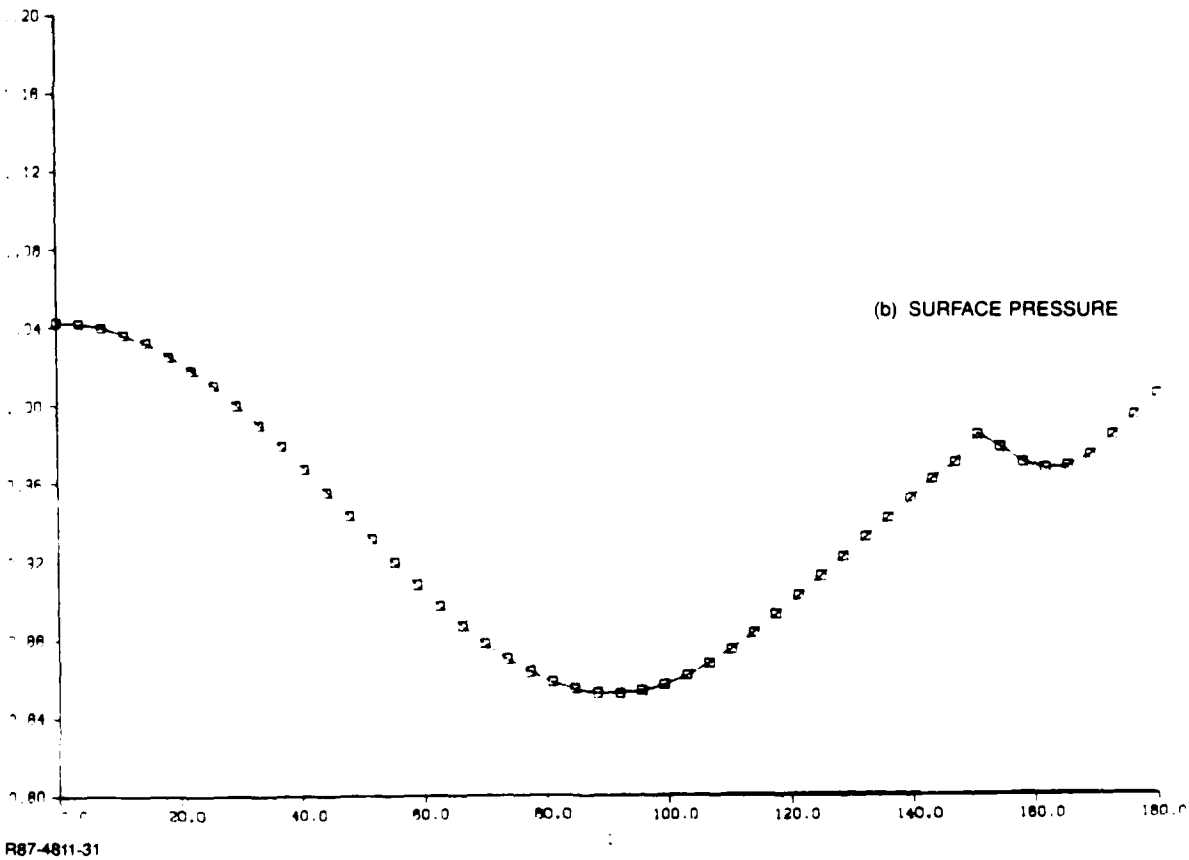

R87-4811-31

Fig. 31 Two-Dimension Cylinder at M_∞ = .3, Separation Forced at 150° from the Forward Stagnation Point

8. ASYMMETRIC FLOWS

In the late 1940's, the phenomenon of lateral instability due to asymmetric vortex formation was discovered. On slender-nosed aircraft flying at a high angle of attack ($\alpha \approx 3$ x nose half angle), the flow which should be symmetric about the plane containing the free stream velocity vector can be very asymmetric due to the vortices. While the separation points are slightly asymmetric, the resulting vortices are very asymmetric, resulting in large side forces and lateral instability. The cause of this asymmetry has been debated since it was first discovered. The basic issue of whether it is a viscous or inviscid phenomenon is still uncertain. The inviscid flow separation model used here is an ideal tool for investigating this issue.

One of the first indications that this phenomenon was inviscid in nature came from the work of Fiddes.[38] He showed small disturbance calculations with vortex sheets modeled by vortex filaments that exhibit asymmetric vortices. The geometry was a slender cone and the flow was incompressible. Fiddes showed that two solutions existed for a symmetrically separated flow. One solution being symmetric, the resulting vortices were symmetric, and the other solution asymmetric. The second, asymmetric, solution exists only in the very high angle-of-attack regime, $\alpha >$ 2 x cone half angle. At these conditions, the asymmetric solution compares much better with experimental data than does the symmetric one. Of course, in the wind tunnel experiment Fiddes[38] found that in asymmetric flow the separation points cannot be symmetric. Very small asymmetries in the separation locations resulted in very large side forces, indicating very large asymmetries in the vortex locations. Computationally, Fiddes found that for slightly asymmetric separation point locations there existed two solutions, one which was slightly asymmetric and the other very asymmetric. Another indication that the phenomenon is inviscid is that experimental data indicate an insensitivity of the onset of the raise in side force to Reynolds number.

The question of whether the small disturbance approximation could be the cause of the asymmetry in Fiddes computation can be answered quite simply by the Euler computation presented here. The work presented here is confined to the supersonic regime, where experimentalists find reduced side forces.[39] The Euler code used here in conjunction with the flow-separation model was able to

predict asymmetric flows. Figure 32 shows a bifurcation map for a 7° cone at $M_\infty = 1.6$ with separation forces symmetrically at $\theta = 25°$ and 55°. The plot shows the vertical location of the vortices as a function of relative incidence. Below an $\alpha/\delta = 2.3$, only one solution exists, i.e., the symmetric one. When the angle of attack is increased further, two solutions exist: the symmetric and the asymmetric. Note the three vortex locations in Fig. 32. The two asymmetric vortex locations bracket the symmetric one. Unlike Fiddes, finding the symmetric solution was found to be unstable in the present computation. The only way to achieve a symmetric solution was to enforce a symmetry condition. If the symmetry conditions were relaxed after a symmetric solution was converged, the solution could revert to an asymmetric one.

Figures 33 to 36 show results for this 7° cone at $M_\infty = 1.6$ and $\alpha = 20°$. Figure 33 shows the crossflow streamlines in the vicinity of the lee plane; the asymmetry of the vortices is obvious. The separation points are placed symmetrically ($\theta = 25°$ and 155°) as is the case in all the calculations to follow. Figure 34 shows the surface pressure distribution; it should be pointed out that θ is measured counterclockwise. The crossflow is locally supersonic so that shocks precede the separation points (see the isobars of Fig. 35). The vortex to the left is much closer to the surface (Fig. 33) than that on the right; this can be seen in its influence on the surface pressure. The minimum surface pressure at $\theta = 210°$ is a result of this vortex interaction. The isobars of Fig. 35 show the shocks before the separation points and the closed isobars representing the local minimum in pressure at the vortex centers. While the asymmetry is significant, it is localized in supersonic flow because of the limited domain of influence. Figure 34 shows that the surface pressure is symmetric, i.e., unaffected, before the separation points. This is the reason side forces due to asymmetries decrease with increasing Mach number. The asymmetry may be significant, but because its domain of influence is limited, the side forces may be small. Figure 36 shows the whole crossflow plane with the streamlines; note that the flow looks symmetric except in the vicinity of the vortices.

Figures 37 and 38 show the same 20° angle-of-attack case with symmetry enforced. Figure 37 shows the crossflow streamlines and Fig. 38 the surface pressure distribution. Note that the asymmetric vortices of Fig. 33 bracket those of Fig. 37. Figures 39 and 40 show results of a computation at small

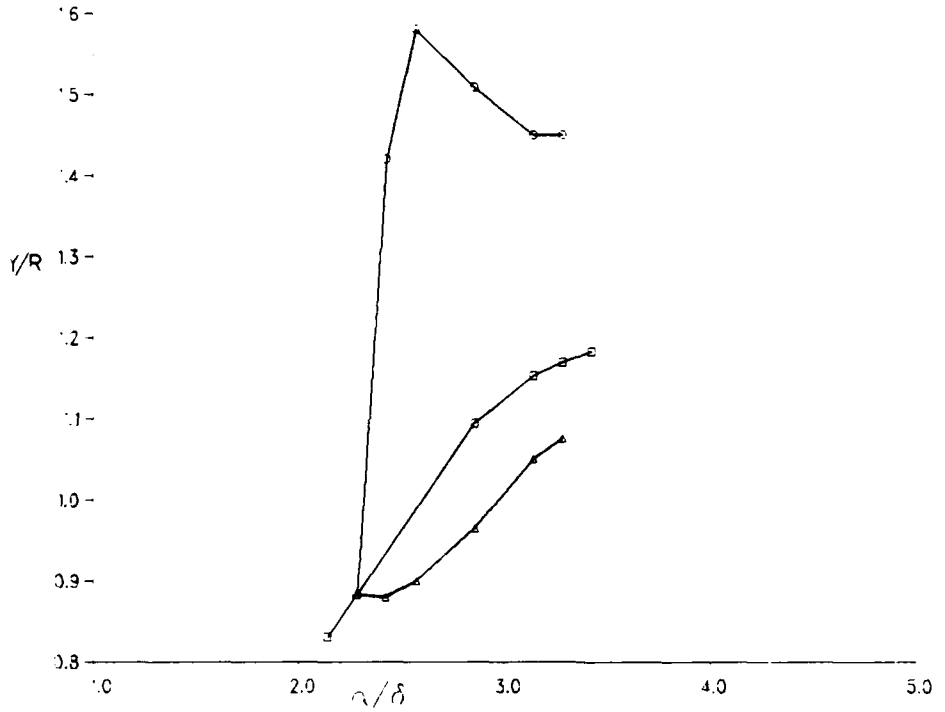

R87-4811-32

Fig. 32 Bifurcation Map, 7° Cone at $M_\infty = 1.6$, Symmetric Separation ($\theta_1 = 25°$, $\theta_2 = 155°$)

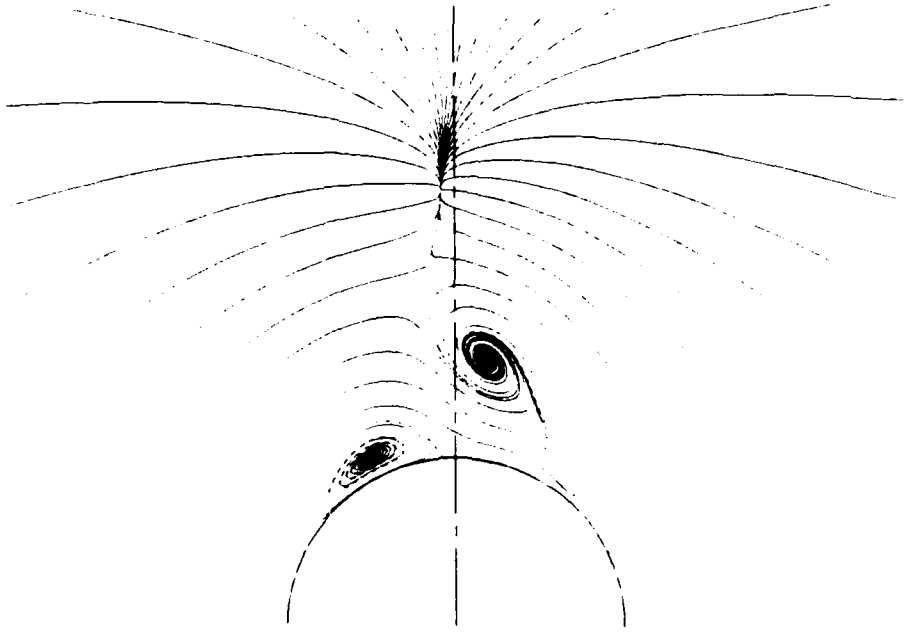

R87-4811-33

Fig. 33 Crossflow Streamlines, 7° Cone at $M_\infty = 1.6$, $\alpha = 20°$

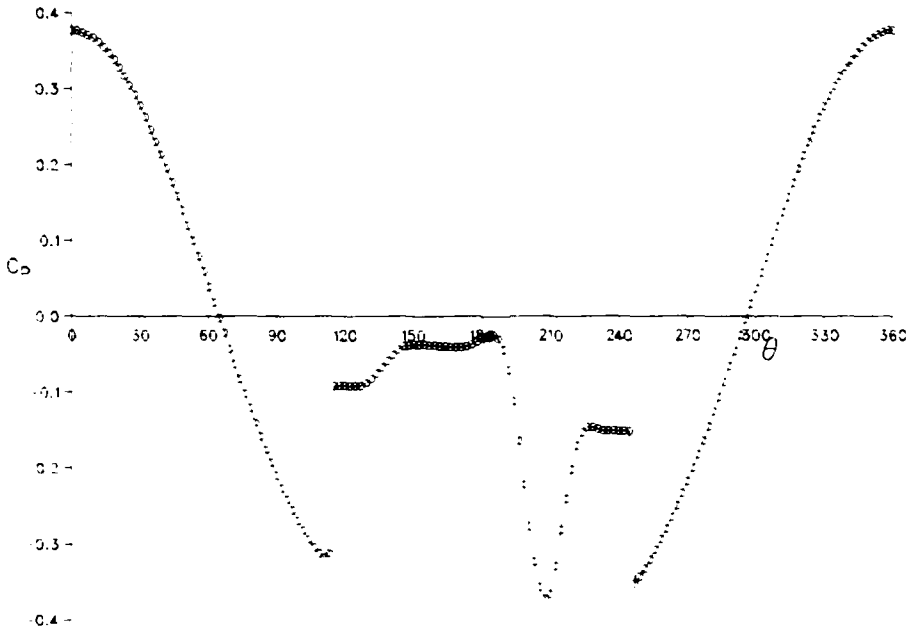

R87-4811-34

Fig. 34 Surface Pressure Distribution 7° Cone at $M_\infty = 1.6$, $\alpha = 20°$

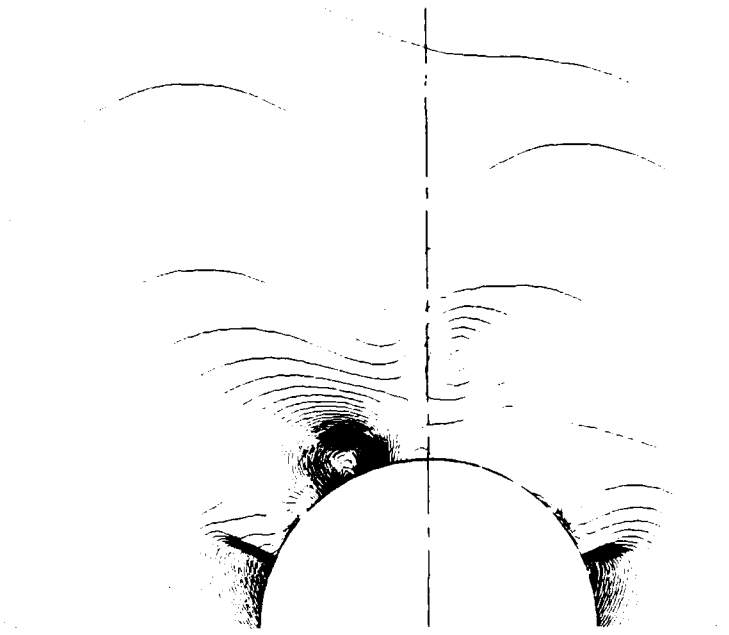

R87-4811-35

Fig. 35 Cross Sectional Isobars 7° Cone at $M_\infty = 1.6$, $\alpha = 20^\circ$

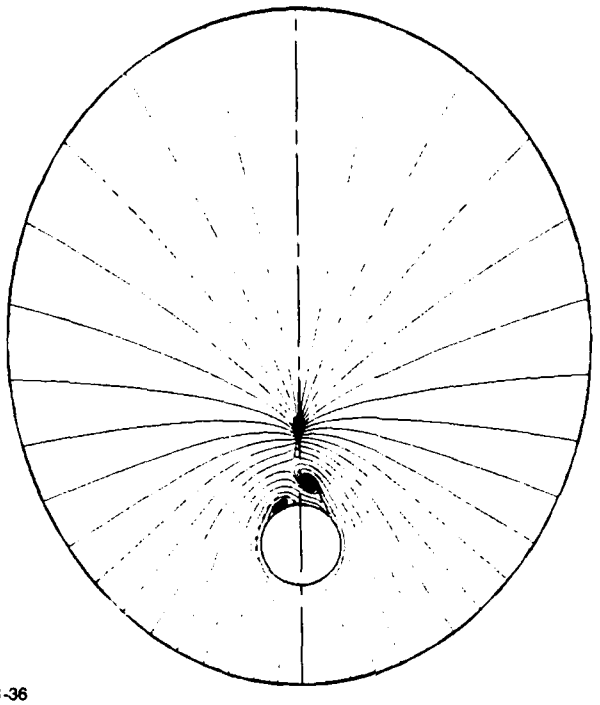

R87-4811-36

Fig. 36 Crossflow Streamlines (Whole Plane) 7° Cone, $M_\infty = 1.6$, $\alpha = 20°$

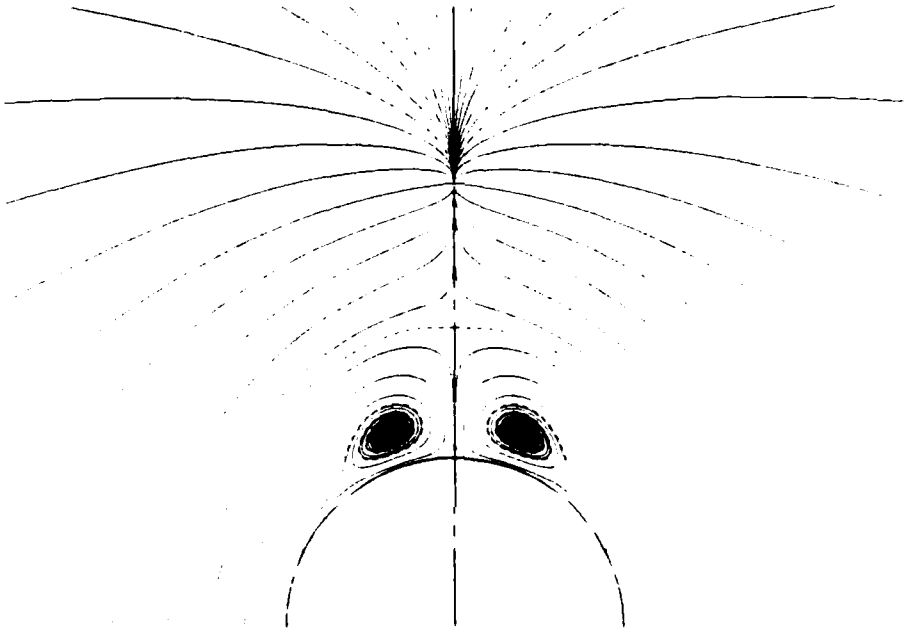

R87-4811-37

Fig. 37 Crossflow Streamlines 7° Cone, $M_\infty = 1.6$, $\alpha = 20°$

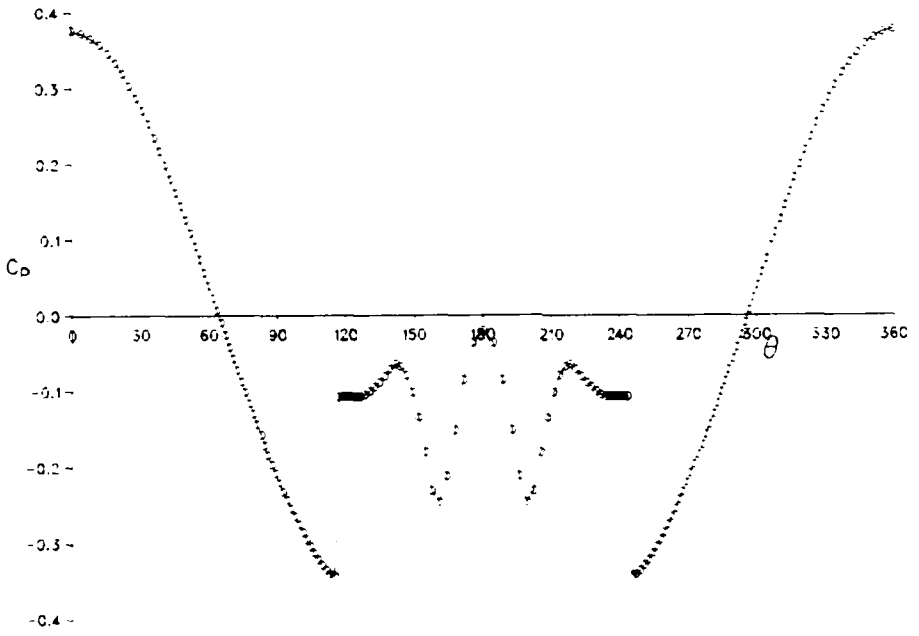

R87-4811-38

Fig. 38 Surface Pressure Distribution 7° Cone, $M_\infty = 1.6$, $\alpha = 20°$

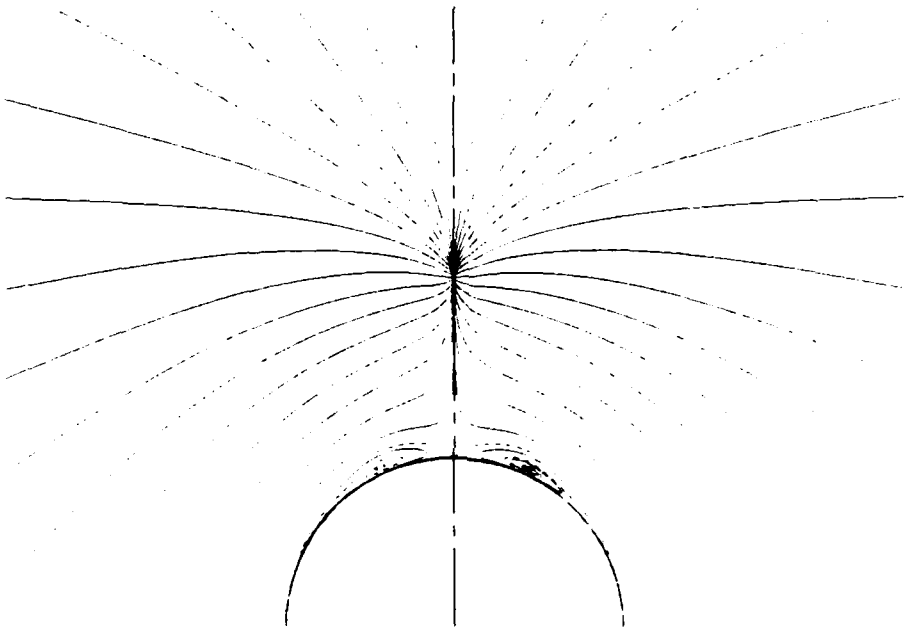

R87-4811-39

Fig. 39 Crossflow Streamlines 7° Cone at $M_\infty = 1.6$, $\alpha = 15°$

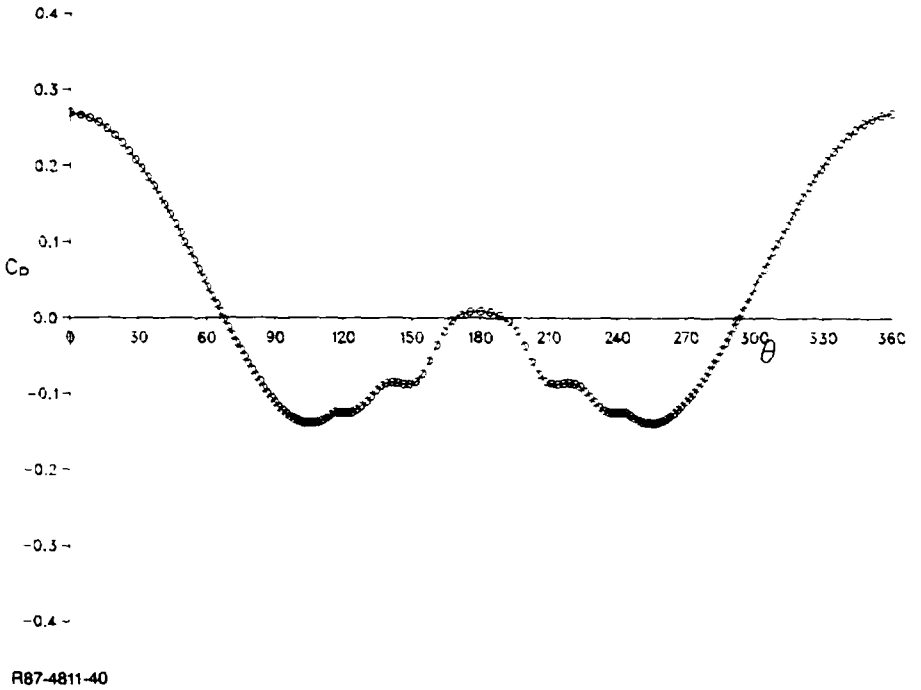

Fig. 40 Surface Pressure Distribution 7° Cone, $M_\infty = 1.6$, $\alpha = 15°$

enough angles of attack (α = 15°) so that only a symmetrical solution exists. Figure 39 shows the crossflow streamlines and Fig. 40 the surface pressure. It should be pointed out that this calculation was performed with no symmetry condition imposed, indicating that the code is capable of producing symmetrical results.

Figure 32 indicates that the flow becomes asymmetric quickly above α/δ = 2.3; this is reinforced in Fig. 41. The figure shows the crossflow streamlines at α = 19° (α/δ = 2.7) to be very asymmetric. Figure 42 shows the surface pressure which seems to indicate no shock at separation on the right side and a small shock on the left side. Because the vortex sheet leaves the body at such a large angle on the right side it seems the flow is inhibited from expanding supersonically, while the left-side, shallow vortex allows the flow to expand. Figure 32 indicates a maximum in asymmetry at α = 19°. Figures 43, 44, and 45 show results for a higher angle of attack α = 23°, α/δ = 3.3. While the vortices seem to approach the same height above the cone (see Fig. 43), the flow is by no means approaching symmetry. This is reinforced by the surface pressure plot of Fig. 44. It seems that the vortex height may not be the best indication of asymmetry. The asymmetries in this flow is further evidenced in Fig. 45, the isobars.

The investigation of asymmetric flows is incomplete and will continue. The ability of this method to predict the onset of asymmetries and the details of these flows will be studied. Computed results will be compared with experimental data. The method presented here has a good chance of contributing to an understanding of this phenomenon. It seems that the interaction of the two vortices is the cause of the asymmetries; this will be investigated.

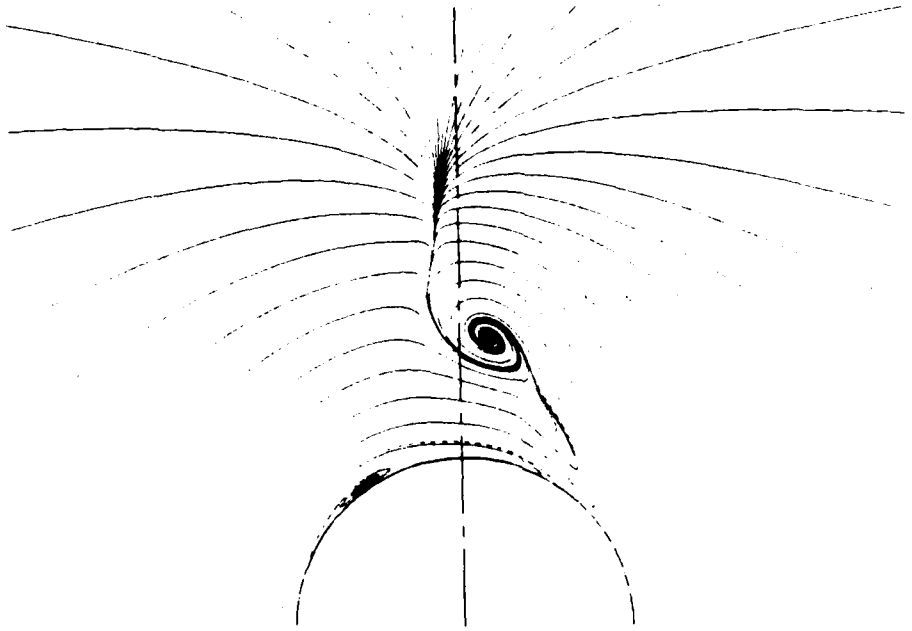

R87-4811-41

Fig. 41 Crossflow Streamlines 7° Cone, $M_\infty = 1.6$, $\alpha = 19°$

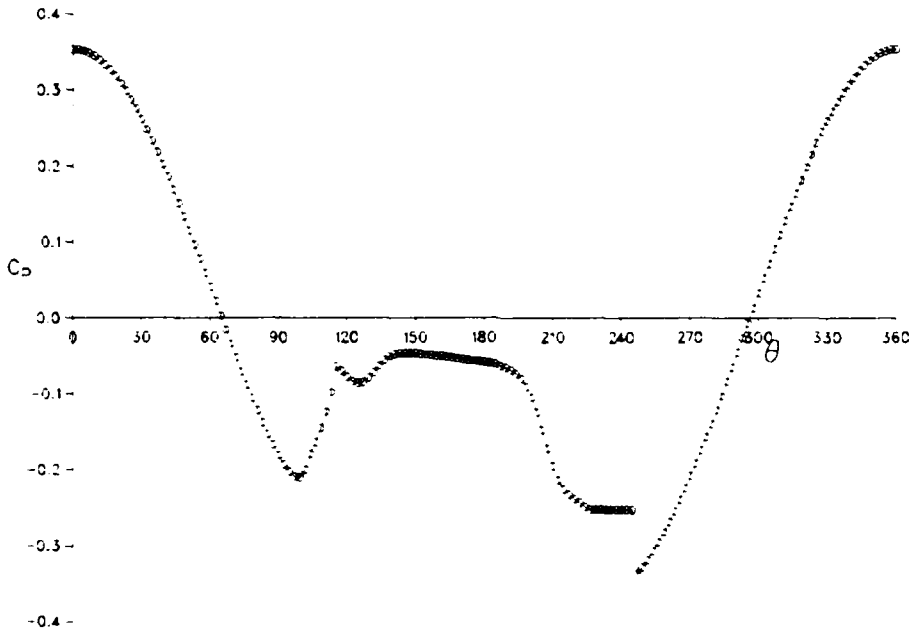

R87-4811-42

Fig. 42 Surface Pressure Distribution 7° Cone, $M_\infty = 1.6$, $\alpha = 19°$

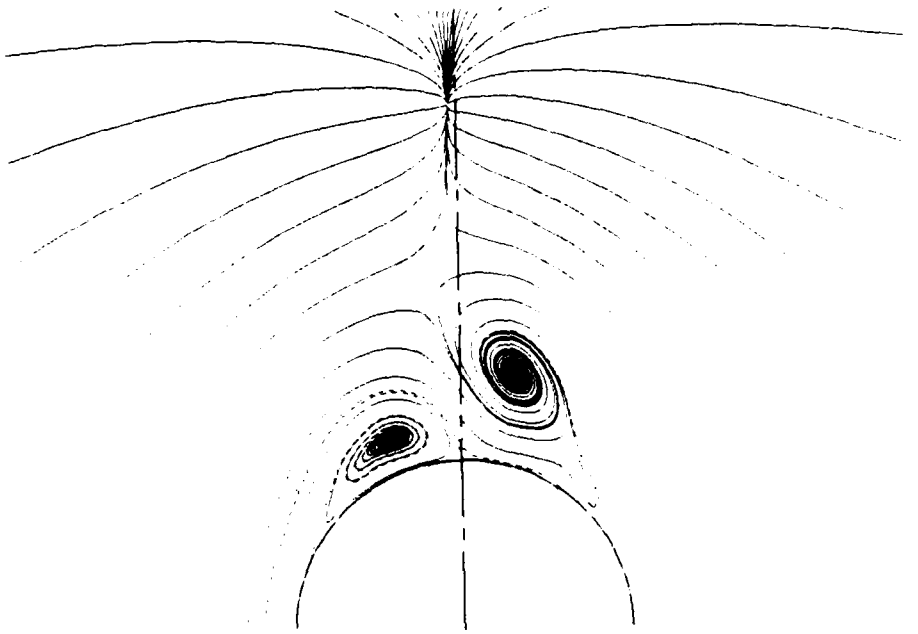

R87-4811-43

Fig. 43 Crossflow Streamlines 7° Cone, $M_\infty = 1.6$, $\alpha = 23^\circ$

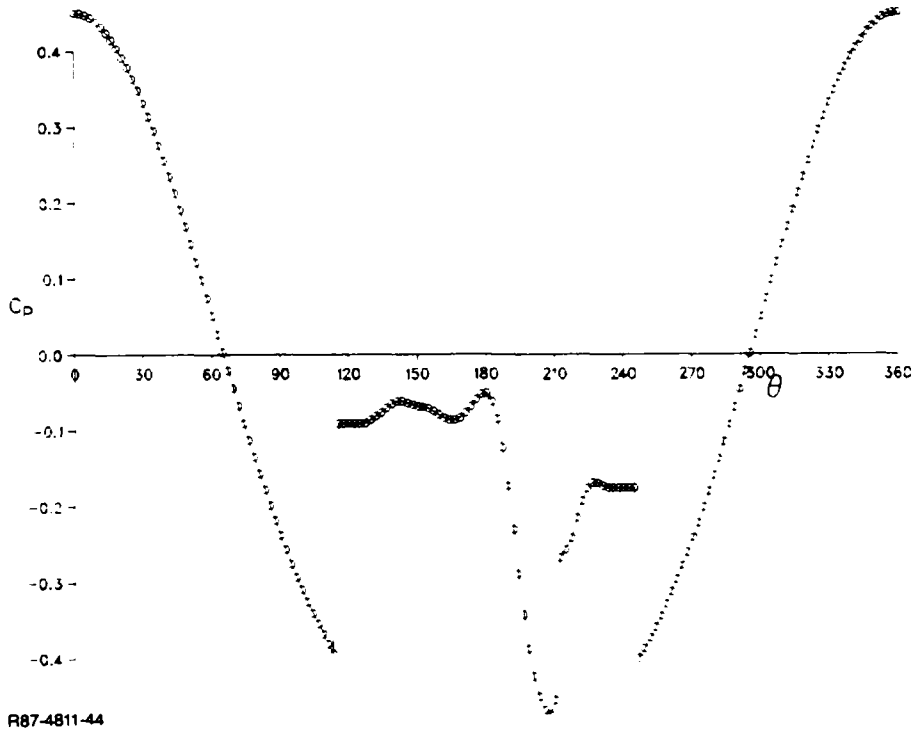

Fig. 44 Surface Pressure Distribution 7° Cone, $M_\infty = 1.6$, $\alpha = 23°$

R87-4811-45

Fig. 45 Cross Sectional Isobars 7° Cone, $M_\infty = 1.6$, $\alpha = 23°$

9. CONCLUSIONS

The main conclusions reached as a result of this work are listed below:

- Shock-vorticity-induced separation and shed-vorticity-induced separation are similar in that the vorticity shed into the flow field is reduced smoothly as the separation point is moved to its shock-induced location (Fig. 9)
- Shock/vortex interaction can cause complex shock patterns (Fig. 10 and 11) which exhibit interesting fluid physics
- The relationship between sharp leading-edge separation and total pressure losses is weaker than has been published in recent years
- The inclusion of a proper Kutta-type condition at the leading edge of a sharp leading-edge wing does not affect results very much (Fig. 22)
- Secondary separation is influenced by viscous effects more than primary separation (Fig. 26)
- The separation model was simply extendable to fully three-dimensional flow
- Difficulty was encountered in trying to apply the separation model to conservative schemes
- Asymmetric flow can be predicted with the separation model used here, indicating that the asymmetric vortex flow phenomenon is inviscid in nature.

10. REFERENCES

1. Küchemann , D., "Inviscid Shear Flow Near the Trailing Edge of an Aerofoil," R.A.E. TR 67068 (1967).

2. Fraenkel, L.E., "On Corner Eddies in Plane Inviscid Shear Flow," J Fluid Mechanics, Vol 11, pp 400-406 (1961).

3. Smith, P.D., "A Note on the Computation of the Inviscid Rotational Flow Past the Trailing Edge of an Airfoil," R.A.E. TM 1217 (1970).

4. Smith, J.H.B., "Remarks on the Structure of Conical Flow," Progress in Aeronautical Sciences, Vol 12, pp 241-271 (1972).

5. Smith, J.H.B., "Behavior of a Vortex Sheet Separating from a Smooth Surface," R.A.E. TR 77058 (1977).

6. Fiddes, S.F., "A Theory of the Separated Flow Past a Slender Cone at Incidence," AGARD CP 291, pp 30-1 to 30-14 (1981).

7. Marconi, F., "The Spiral Singularity in the Supersonic Inviscid Flow Over a Cone," AIAA Paper 83-1665 (1983).

8. Salas, M.D., "Recent Developments in Transonic Euler Flow Over a Circular Cylinder," NASA TM 83282 (1982).

9. Rizzi, A., Erickson, L., Schmidt, W., and Hitzel, S., "Numerical Solutions of the Euler Equations Simulating Vortex Flows Around Wings," AGARD CP-342, pp 21-1 to 21-14 (1983).

10. Murman, E., "Solutions of the Conical Euler Equations for Flat Plate Geometries - Preliminary Results," MIT CFDL-TR-84-4 (1984).

11. Newsome, R., "A Comparison of Euler and Navier-Stokes Solutions for Supersonic Flow Over a Conical Delta Wing," AIAA Paper 85-0111 (1985).

12. Marconi, F., "Supersonic Conical Separation Due to Shock Vorticity," AIAA J, Vol 22, No. 8, pp 1048-1055 (1984).

13. Marconi, F., "Shock Induced Vortices on Elliptic Cones in Supersonic Flow," AIAA Paper No. 85-0433 (1985).

14. Marconi, F., "Supersonic Inviscid, Conical Corner Flow Fields," AIAA J, Vol 18, No. 1, pp 78-84 (1980).

15. Moretti, G., "The λ-Scheme," Computers and Fields, Vol 7, pp 191-205 (1979).

16. Marconi, F., Salas, M.D., and Yaeger, L., "Development of a Computer Code for Calculating the Steady Super/Hypersonic Inviscid Flow Around Real Configurations," NASA CR-2675 (1976).

17. Rudman, S., "Multinozzle Plume Flow Fields - Structure and Numerical Calculations," AIAA Paper 77-710 (1977).

18. deNeef, T., and Moretti, G., "Shock Fitting for Everybody," Computers and Fluids, Vol 8, pp 327-334 (1980).

19. Salas, M.D., "Numerical Study of Flow Fields About Asymmetric External Conical Corners," AIAA J, Vol 20, No. 12, 1982, pp 1661-1667

20. Rainbird, W.J., "The External Flow About Yawed Circular Cones," AGARD CP30, 1968.

21. Marconi, F., "Conical, Separated Flows with Shock and Shed Vorticity," AIAA J, Vol 25, No. 1, 1987, pp 173-175.

22. Marconi, F., "Fully Three-Dimensional Separated Flows Computed with the Euler Equations," AIAA Paper 87-0451, 1987.

23. Marconi, F., "Complex Shock Patterns and Vortices in Inviscid Supersonic Flows," to be published in Journal of Computer and Fluids.

24. Powell, K.G., Murman, E.M., Perez, E., and Baron, J.R., "Total Pressure Loss in Vortical Solutions of the Conical Euler Equations," AIAA Paper No. 85-1701, 1985.

25. Hoeijmakers, H.W.H., "Computational Vortex Flow Aerodynamics," AGARD CP-342, pp 18-1 to 18-35, 1983.

26. Powell, K.G. and Murman, E.M., "Two Different Ways of Satisfying Crocco's Relation," SIAM Conf, Boston, MA, Aug 1986.

27. Powell, K.G., and Murman, E.M., Private Communication.

28. Marconi, F., "On the Prediction of Highly Vortical Flows Using an Euler Equation Model," Proc of Vortex Dominated Flows Conf, NASA Langley, June 1985.

29. Miller, D.S., and Wood, R.M., "Lee-Side Flow Over Delta Wings a Supersonic Speeds," NASA TP 2430, 1985.

30. Miller, D.S., Wood, R.M., and Covell, P.F., "An Overview of the Fundamental Aerodynamics Branch's Research Activities in Wing Leading Edge Vortex Flows at Supersonic Speeds," NASA CP 2416, Vol 1, 1985.

31. Marconi, F., "Flat Plate Delta Wing Separated Flows with Zero Total Pressure Losses," AIAA Paper No. 87-0038, 1987.

32. Vorropoulos, G., and Wandth, J.F., "Laser Velocimetry Study of Compressibility Effects on the Flow Field of a Delta Wing," AGARD CP-342, 1982.

33. Landrum, E.J., "Wind-Tunnel Pressure Data at Mach Numbers from 1.6 to 4.63 for a Series of Bodies of Revolution at Angles of Attack from -4° to 60°," NASA TMX 3558, 1977.

34. Allen, J.M., Hernandez, G., and Lamb, M., "Body Surface Pressure Data on Two Monoplane-Wing Missile Configurations with Elliptical Cross-Section at Mach 2.5," NASA TM 85645, 1983.

35. Newsome, R.W., and Adams, M.S., "Numerical Simulation of Vortical Flow Over an Elliptical Body Missile at High Angle of Attack," AIAA Paper 86-0559, 1986.

36. Anderson, W.K., Thomas, J.L., and Van Leer, B., "Comparison of Finite Volume Flux Vector Splittings for the Euler Equations," AIAA J, Vol 24, No. 9, 1986, p 1453.

37. Van Leer, B., Thomas, J., Roe, P.L., and Newsome, R.W., "A Comparison of Numerical Formulas for the Euler and Navier-Stokes Equations," Proc of the AIAA 8th Computational Fluid Dynamics Conf, 1987.

38. Fiddes, S.P., "Separated Flow About Cones at Incidence - Theory and Experiment," Proc of Symp on Studies of Vortex Dominated Flow, NASA/LRC, 1985.

39. Peak, D.J., Owen, F.K., and Higuchi, H., "Symmetrical Asymmetrical Separations About a Yawed Cone," AGARD-CP-247, pp 16-1 to 16-27, 1979.

APPENDIX A

SUPERSONIC CONICAL SEPARATION DUE TO SHOCK VORTICITY

Supersonic Conical Separation Due to Shock Vorticity

F. Marconi

Reprinted from
AIAA Journal Volume 22 Number 8 August 1984 Page 1048
AMERICAN INSTITUTE OF AERONAUTICS AND ASTRONAUTICS • 1633 BROADWAY • NEW YORK, N.Y. 10019

Supersonic Conical Separation Due to Shock Vorticity

Frank Marconi*
Grumman Aerospace Corporation, Bethpage, New York

A numerical study of the conical, supersonic, inviscid flow about circular slender cones at large incidence is presented. Although the flow is assumed inviscid, separation and an accompanying spiral are found. This phenomenon is shown to be a valid solution to Euler's equations, i.e., valid in the sense of being independent of any numerical viscosity. The separation and spiral are caused solely by the vorticity produced by a cross-flow shock. The resulting separated flowfields are compared to full potential calculations and to experimental data.

Introduction

THREE-DIMENSIONAL separated flows are, in general, accompanied by the spiraling of streamlines into a vortex. The phenomenon is important in many flow situations: the flow about the leading edge of a wing; the flow behind bluff bodies; and the flow on the lee side of slender bodies at large angles of attack. The control of vortices for increased aerodynamic efficiency has been studied by aircraft designers for many years and was the subject of a recent paper by Rao.[1] The current paper is a numerical study of spiraling vortex flow about slender cones flying at supersonic speeds and large incidence. Although the cones considered here may be slender, the full inviscid Euler equations are solved. An understanding of these flowfields has direct applicability to missile aerodynamics and to the aerodynamics of aircraft forebodies.

All geometries considered in this numerical study are circular cross-section cones, so that while the flow is in a real sense three-dimensional, all flow variables depend on only two coordinates. The flowfield is assumed supersonic everywhere and conical. In addition, the gas is assumed ideal with a ratio of specific heats of 1.4 (i.e., air). It should be realized that while the assumption of conical flow does simplify the numerical problem, the conclusions reached have more general applicability. The basic features of the flowfield are essentially unchanged in the fully three-dimensional flow.

Conical streamline spirals occur in the separation region on the leeward side of slender cones at large angles of attack (see Figs. 1 and 2). The existence of this type of flow pattern in purely inviscid flow has been the subject of study for many years. Küchemann[2] proved analytically that for two-dimensional flow with distributed vorticity, inviscid separation can occur. Two-dimensional flow separation is accompanied by a closed recirculation zone. The streamlines "trapped" inside this recirculation zone cannot be tracked back upstream where all flowfield conditions are known. Flow properties that are transmitted along streamlines (for example, entropy and vorticity) must somehow be determined inside the closed recirculation zone. Fraenkel[3] found closed-form solutions for the incompressible two-dimensional flow over cylinders with closed recirculation zones caused by distributed vorticity in the freestream. Smith[4] used the analytical work of Küchemann to numerically compute recirculation zones at the trailing edge of a two-dimensional airfoil. The vorticity in this case was imposed at a finite distance upstream of the trailing edge. This situation is similar to vorticity being generated by a transonic shock near the trailing edge of an airfoil. More recently, a number of researchers working on solutions to Euler's equations in two-dimensional transonic flow[5,6] have found inviscid separation and recirculation zones behind cylinders and airfoils. Salas[5] showed how Euler solutions with transonic shocks can exhibit recirculation zones behind cylinders. The vorticity and entropy trapped in the recirculation zone are said to be determined by the time-dependent computation used to asymptote to a steady solution.

In fully three-dimensional flow and the conical flows considered here, separation is not accompanied by a closed recirculation zone but by spiraling streamlines.[7] This point is important because in the conical flow all streamlines originate in the freestream where all flowfield quantities are known. Therefore, entropy and vorticity can be uniquely determined everywhere, along with the flowfield and, in particular, the required shock system. Figure 1 shows a three-dimensional surface streamline starting from the windward plane wetting the body surface and getting swept up into the spiral. Figure 2 is a sketch showing how the cross-flow streamlines, which start outside the bow shock, pass through the shock system, and ultimately get swept up into the spiral singularity or a lee plane node (Fig. 2b). The dashed line of Fig. 2b divides the flow that is swept into the spiral node from that which goes into the lee plane node. Cross-flow streamlines are defined as the intersection of fully three-dimensional stream surfaces and the surface of a sphere centered at the apex of the cone. Their direction in the x-y plane (Fig. 2) can be defined as the ratio of the two components of the cross-flow velocity u and v (Fig. 1).

In the current paper, separation will be loosely defined as the process by which a stream surface originally on the cone leaves the cone surface and ultimately forms an infinitely turning spiral (see Figs. 1 and 2). Separation occurs along a line in conical flow; the intersection of this line and the cross-flow plane will be referred to as the separation point. In a review paper on conical streamline singularities, Smith[8] showed analytically that a conical spiral singularity can exist only in flows with vorticity. In particular, he found that a finite radial (spherical r, Fig. 1) component of vorticity was a necessary while not sufficient condition for the existence of a spiral. It seems clear that separation and an accompanying spiral are linked to the generation of vorticity and not to the details of the viscous processes involved.

There are three ways of introducing vorticity in an otherwise irrotational flow: 1) by specifying vorticity in the freestream, as was done in Refs. 3 and 4; 2) through shock waves; and 3) by shedding vorticity from the boundary layer at a separation point. In this paper only the vorticity produced by the shock system will be discussed in detail. It should be noted that currently only through solutions of the Euler

Presented as Paper 83-1665 at the AIAA 16th Fluid and Plasma Dynamics Conference, Danvers, Mass., July 12-14, 1983; submitted July 30, 1983; revision received Nov. 18, 1983.

*Senior Staff Scientist, Research and Development Center. Member AIAA.

equations can this aspect of the flow be modeled (i.e., full potential shocks do not generate vorticity). The third mechanism of vorticity introduction, shedding, has been studied extensively by Smith[9,10] and Fiddes.[11] The current author has shown preliminary Euler solutions that use this model to force separation at a specified location.[12]

In order to shed vorticity, the flow is modeled by assuming that there exists an infinitesimally thin sheet of infinite vorticity across which there is a jump in velocity. The rest of the flow can be assumed irrotational. The vortex sheet will generally roll up into a spiral. The sheet is forced to originate at a separation point by imposing a Kutta condition. At sharp edges (sharp wing tip, for example), the condition is similar to that imposed at wing trailing edges in three-dimensional flow to exclude singularities due to flow turning around sharp edges. For smooth bodies, the proper Kutta condition to be imposed to start a vortex sheet in an otherwise completely irrotational flow has been studied in detail in Refs. 9 and 10. The location of the origin of shedding on the body is the only free parameter and is specified to match the boundary-layer separation point. In contrast to bodies with salient edges, where the edge is taken as the separation point, smooth bodies require that the separation point be computed from a boundary layer coupled to an inviscid flow iteration[11] or from experimental data. Calculations including forced separation from a shedding vortex sheet have been performed for a number of years (for example, the early work of Bryson[13]). More recently, Rizzi[14] has shown solutions to Euler's equations with separation from sharp leading edge wings, and Nielsen[15] has shown solutions to Euler's equations with separation from smooth bodies. It should be pointed out that the work of Refs. 14 and 15 seem inconsistent with the analysis of Refs. 9 and 10 for the flow near the origin of this sheet (i.e., the separation point), while the present author has used the model of Ref. 9 to force separation at a specified location.[12]

It should be made clear at this point that the two mechanisms of vorticity introduction, shock waves and shedding, both produce valid solutions to Euler's equations with separation and spirals. While the two mechanisms produce similar flowfield structures, the details of the separation and spiraling sheet are different. The differences in detail are outlined in Ref. 12. The main difference should be clear. The separation caused by the shock vorticity occurs with no additional conditions and uniquely determines separation point location, while the forced separation point location is arbitrary. It is the arbitrariness of the separation point location that allows the freedom necessary to match the boundary-layer separation point location. The separation point in the shock-induced case may bear little relation to the real viscous flow, but the shock-produced vorticity can play a role in the structure of the real separated flow. The point here is that the vorticity in the flowfield comes from two sources—shock waves and shed from the boundary layer—both of which contribute to the quantitative structure of the flow. Only the shock vorticity will be considered herein, so it is not surprising that the comparisons with experimental data are poor in some sense; in particular, the separation point locations are significantly different.

The intent of this paper is to show that the vorticity produced by shock waves can cause separation and that solutions to the inviscid Euler equations exhibiting this phenomenon are valid, in the sense of being independent of any numerical artifices. The qualitative structure of the separated flow produced by shock vorticity will be shown to be the same as that produced in the presence of a boundary layer, indicating the possibility of this vorticity being significant. In the section that follows, the overall computational procedure will be outlined. The issues of convergence both in terms of iteration scheme and grid refinement will be addressed in this section. Then a detailed study of computational results will be presented including comparisons with experimental data and full potential calculations. The final section of the paper will present a summary of the findings of this work and the future directions of this effort.

Computational Procedure

The overall numerical procedure used in this study, although employing a number of new features, is essentially standard.[16] The fully three-dimensional Euler's equations are solved with an explicit marching technique. The marching direction (z, Fig. 1) is an iterative coordinate for the conical flow considered here. The scheme is restricted by the fact that the axial component of velocity (W, Fig. 1) must be supersonic everywhere. The marching scheme is continued until the flowfield is invariant with respect to the computational marching direction except for a scale factor. The finite-difference scheme used is Moretti's characteristic based λ-scheme.[17] All shock waves in these flowfields are fit and are forced to satisfy the exact Rankine-Hugoniot jump conditions. The bow shock is fit as the outermost boundary of the flowfield. On the low pressure side of the bow shock, freestream conditions exist. The cross-flow shock is fit as an internal boundary of the flowfield with its low pressure side being computed as the computation proceeds.[18]

The cross-flow shock computation is a critical part of the overall procedure, particularly since it plays such a critical role in separation. As mentioned in the previous section, it is the vorticity produced by the cross-flow shock that produces the spiral. Any scheme that captures the cross-flow shock and introduces additional artificial viscosity to stabilize it runs the risk of distorting the separation and spiral. The bow shock

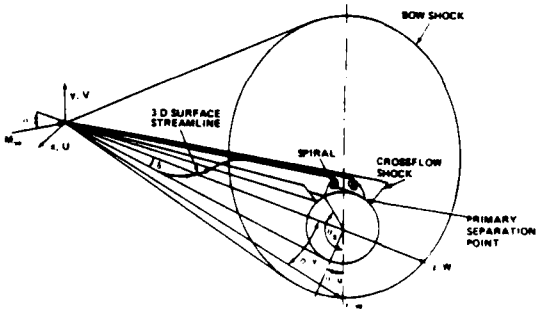

Fig. 1 Three-dimensional sketch of flowfield and coordinate system.

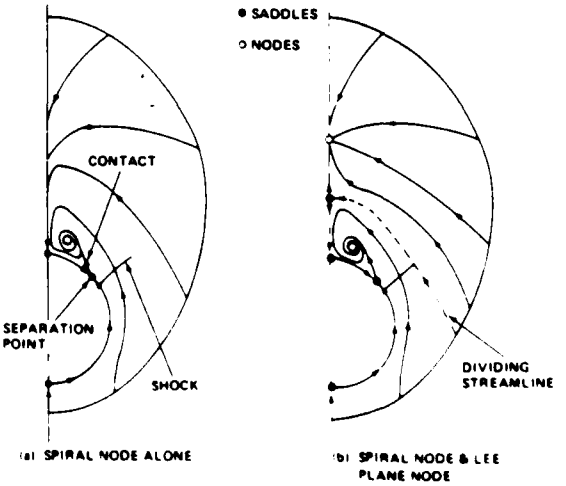

Fig. 2 Sketch of cross-flow streamlines.

also introduces vorticity in the flowfield, but not enough to produce separation. The cross-flow shock is caused by the fact that at a large incidence the θ component of the velocity (u, Fig. 1) becomes supercritical. The flow expands in going from the windward symmetry plane, and u can become supercritical if the incidence is high enough. This component of velocity must vanish in the lee symmetry plane due to the boundary conditions. A supercritical cross flow generally passes through a relatively normal shock before stagnating in the lee plane. The cross-flow shock exists to turn the three-dimensional flow parallel to the lee symmetry plane. The variation in strength of the cross-flow shock can be quite large. The shock is strongest at the body where u is highly supersonic and approaches zero strength in the field where u becomes sonic. It is this variation in strength that produces a cross-flow entropy gradient and thus radial vorticity. This vorticity, in turn, causes shock-induced separation.

The low-pressure side of the cross-flow shock is computed with one-sided differences away from the shock. This is consistent with the fact that the cross flow is supersonic. The Rankine-Hugoniot conditions and the compatibility condition along a bicharacteristic reaching the shock on its high-pressure side supply enough information to compute the deviation of each shock point from a conical ray in addition to all the primitive variables on its high-pressure side. The bicharacteristic used is the one in the plane containing the local normal to the shock and the marching direction. All shock points are computed with the postcorrection scheme proposed by Rudman[19] and independently by deNeef.[20] The shocks converge (i.e., each shock point becomes aligned with a conical ray) with the rest of the flowfield. In all the computations presented here, the last cross-flow shock point fit had a normal Mach number of about 1.05 (pressure ratio of 1.12). The finite difference scheme was able to capture weaker shock points.

An exponential stretching is used to cluster grid points near the surface of the cone. This is important because flow conditions that exhibit the spiral singularity also exhibit large gradients near the body behind the cross-flow shock. Without the stretching, the radial resolution behind the shock can be too coarse to pick up the separation and spiral (see, for example, the Euler calculations made using a procedure very similar to the one used here without a stretching present in Ref. 21). The stretching is of the form:

$$r = -(1/\beta)\ln(1-(1-e^{-\beta})X)(C-B)/\beta + B \qquad (1)$$

where r is the polar radius in the x-y plane (not to be confused with the spherical radius r of Fig. 1), and X is the computational coordinate going from 0 on the body to 1 at the bow shock. The other computational coordinate is Y, which is a linearly normalized polar angle θ. Y is normalized to go from 0 in the windward symmetry plane to 1 on the low-pressure side of the cross-flow shock and from 0 again on the high-pressure side of the shock to 1 in the lee plane. The transformation to the final computational plane is completed by $Z=z$. In the transformation, Eq. (1), B and C are the polar radii of the body and bow shock, and β is a clustering parameter. The grid points are evenly spaced in each X-Y plane. The transformation, Eq. (1), clusters grid points near the body depending on the value of β used. The transformation approaches linear as β goes to zero. All of the calculations shown here were performed with $\beta=2.5$. The gradient in the strength of the cross-flow shock is quite large, which is the reason for the large vorticity produced behind it. The clustering of grid points near the body allows for enough resolution to compute this shock decay properly. The number of points required to resolve this phenomenon without a stretching would be inordinately large.

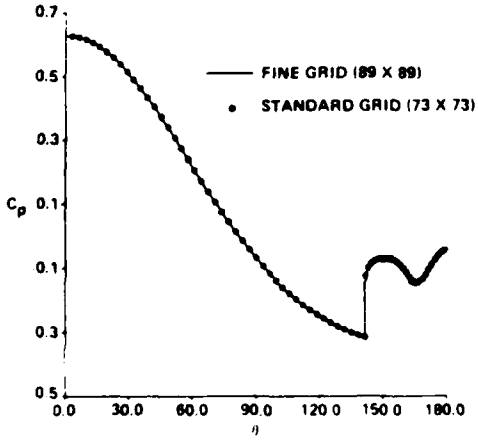

Fig. 3 Comparison of computation with two grids, surface pressure ($M_\infty = 2$, $\delta = 10$ deg, $\alpha = 25$ deg).

Shock-induced inviscid separation produces a contact surface emanating from the separation point (Fig. 2). It is this contact that ultimately spirals. The contact surface has a jump in entropy and an accompanying jump in velocity. In conical flow, entropy is constant on cross-flow streamlines. With this fact, one can see (Fig. 2) that the entropy on the wind side of the contact comes from the wind symmetry plane bow shock. The streamline wets the body and passes through the base of the cross-flow shock. This is the high entropy side of the contact. There are two possibilities for the entropy on the lee side of the contact. The one shown in Fig. 2a corresponds to the lee bow shock entropy wetting the lee side of the cone and ending up on the lee side of the contact. There is a possibility of a saddle point existing in the lee symmetry plane off the body as shown in Fig. 2b. In this case, the entropy on the lee side of the contact would come from this saddle. In either case the cross-flow steamlines that wet the body are tracked in each step of the iteration, and the proper entropy is imposed on the cone including the jump in entropy at the separation point. The entropy discontinuity off the body is captured with the finite difference scheme.

The finite difference scheme[17] used requires that all spatial differences (computational X and Y) be directional, depending on characteristic directions. In the case of entropy, the characteristic direction is the particle path or streamlines, so that both X and Y derivatives of entropy are taken depending on the direction of the local flow. The scheme basically avoids differences across the contact. In order to achieve formal, second-order accuracy, the λ-scheme uses three-point, one-sided differences. In this flowfield, the three-point differences in entropy sometimes required crossing the contact, which caused wiggles. In order to ensure monotonicity at the sheet, these differences in entropy were taken with two-point windward formulas. The sheet was captured between two points until it began to roll up. The region where the sheet rolls up is somewhat smeared, but the scheme seems to describe this region adequately. In any inviscid calculation, approximations must be made for the region near the center of the spiral. In the irrotational calculations of Refs. 11 and 13, the center of the spiral is replaced by a concentrated vortex. One advantage of solving the Euler equations is that this region of concentrated vorticity can be computed automatically.

It was proven by Smith[9] that a forced sheet leaves a smooth body tangent to the surface and that there must be a jump in cross-flow velocity at separation. The cross-flow velocity on the windward side of the sheet is finite, while the cross flow on the lee side stagnates. The arguments of Ref. 9 are based on irrotational and isentropic assumptions and do not hold for flows with cross-flow shocks. It can be shown that when the sheet exhibits a jump in entropy, the cross-flow velocities on either side of the sheet can match and still maintain con-

tinuous pressure across the sheet. Of course the modulus of the velocity must then jump. This jump is absorbed in the radial component of velocity (w, Fig. 1). This seems to be the situation in the inviscid shock-induced separation. Results will be shown later that indicate the continuous variation of cross-flow through the separation point for the shock-induced case.

In order to speed convergence, grid refinement was used in all the calculations shown in this paper. The calculations were started with a 10×10 (polar radial x circumferential) grid. The calculation was continued until a reasonable convergence was reached, and then the grid was halved. The grid was refined three times, the final grid having 73×73 points in each X-Y plane. The iteration was continued on the finest grid until the maximum variation in pressure in the spherical radial (r, Fig. 1) direction was less than 1×10^{-7}. This is the maximum correction in pressure. The solutions are essentially converged at a maximum correction of 10^{-5} so that 10^{-7} is a conservative convergence criterion. This is a reduction of about nine orders of magnitude from the beginning of the iteration. Critical parameters such as shock location and stagnation point location are constant to five places by the time the calculation is stopped.

The sensitivity of this calculation to the initial conditions used was studied early in this work. It was found that the captured shock, coarse grid, initial conditions to the fine grid exhibited a spiral. The spiral was eliminated before starting the shock fit, fine grid calculations with no change in the final result. The spiral simply developed again. In a numerical experiment, a converged high α (with spiral) result was used as initial condition for an $\alpha = 0$ case. The incidence was reduced gradually, and the cross-flow shock was weakened and ultimately was eliminated along with the spiral. The opposite sequence was tried and the spiral reappeared. The numerical experiments indicated an independence of the converged solution to initial conditions.

The finite difference scheme used in this work is an explicit marching scheme that is notoriously inefficient for converging to a conical or steady solution. A number of speed-up procedures were tried, including multigrid and local marching steps.[5] None of these worked. Local marching steps did produce a significant reduction in running times, but proved unstable in the presence of the cross-flow shock. The cross-flow shock was captured with the λ-scheme in the first two coarse grid calculations. The shock was detected and fit from the third grid on. While the captured shock location was significantly off the converged result, this scheme eliminated some shock detection problems. One advantage of the explicit marching scheme used was that it is totally "vectorizable." The time consuming parts of the code (i.e., interior point computation) utilized the vector architecture of the CRAY 1 computer. This made the computation about 20 times faster on the CRAY than on an IBM 3033. All the computations shown in this report took about 30 CPU minutes on the CRAY 1.

Figure 3 shows a comparison of the surface pressure for the flowfield about a 10 deg half-angle cone at $M_\infty = 2$ and $\alpha = 25$ deg. The symbols are the pressure computed with the standard 73×73 grid. The solid line was computed with a finer 89×89 grid. The figure shows that the fine and standard grid surface pressures are virtually identical, indicating that the standard 73×73 grid resolves all flowfield features. In both calculations, about 35% of the circumferential points are behind the cross-flow shock (i.e., 27 points for the 73×73 grid). This flowfield has a shock-induced separation at $\theta = 149.6$ deg, indicated by the minimum in surface pressure behind the shock ($\theta = 165$ deg). This minimum in pressure is just below the core of the spiral. Both computations, 73×73 and 89×89, give the same separation point and spiral location, indicating an independence of the results to numerical viscosity due to truncation error. As a matter of fact, this flowfield was computed with an even coarser grid (37×37) that exhibits the same basic features (i.e., separation and spiral). While it is very difficult to prove the existence of shock-induced inviscid separation, the aforementioned numerical experiments indicate the validity of such solutions. Additionally, the analytical work for two-dimensional flow reported in Refs. 2 and 3 confirm the possibility of such solutions. The uniqueness of the conical flow solution would seem to be on firmer ground because of the absence of closed recirculation zones.

Computational Results

In this section, computational results showing spiraling streamlines due to the vorticity produced by a cross-flow shock will be analyzed. The first configuration considered is a 10-deg cone at $M_\infty = 2$ and $\alpha = 25$ deg. The surface pressure distribution has been shown in Fig. 3. The cross-flow streamlines are shown in Fig. 4, along with the computed bow and cross-flow shocks. The streamlines show saddles in the wind and lee symmetry planes on the cone surface. In addition, there is a saddle at the separation point and a node at the center of the spiral (this configuration is sketched in Fig. 2a). The separation point and spiral can be seen more clearly in the blowup of Fig. 5. If the nodes and saddles are summed using the procedure of Ref. 8, it can be shown that the proper number of nodes and saddles exist in the streamline pattern of Fig. 4. The separation point ($\theta_s = 149.6$ deg) corresponds to

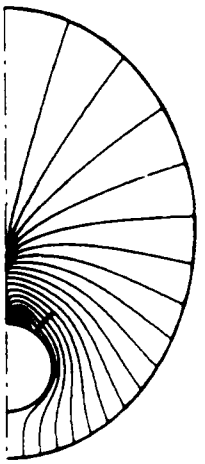

Fig. 4 Cross-flow streamlines in field ($M_\infty = 2$, $\delta = 10$ deg, $\alpha = 25$ deg).

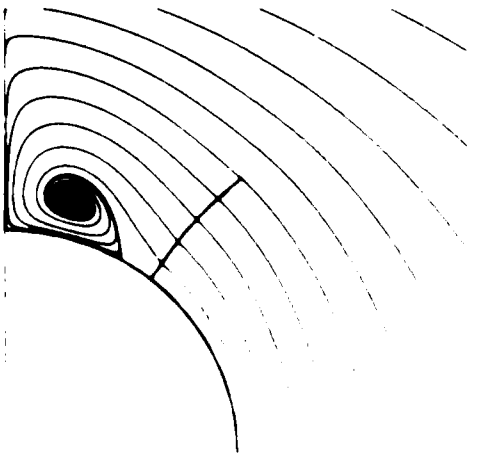

Fig. 5 Cross-flow streamlines near lee plane ($M_\infty = 2$, $\delta = 10$ deg, $\alpha = 25$ deg).

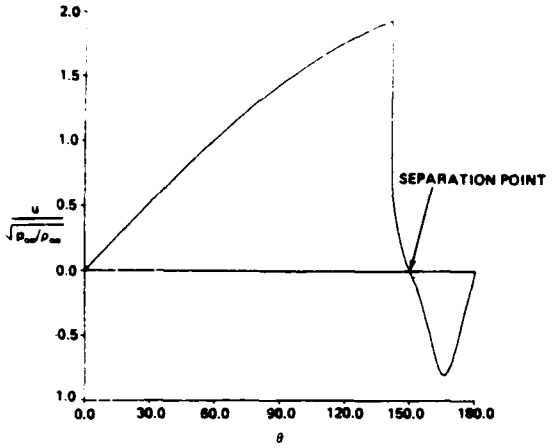

Fig. 6 Surface cross-flow velocity ($M_\infty = 2$, $\delta = 10$ deg, $\alpha = 25$ deg).

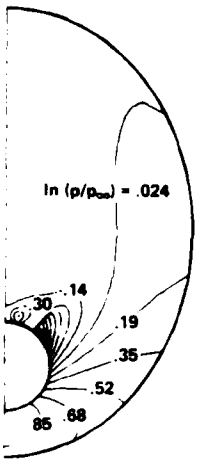

Fig. 7 Isobars in cross plane ($M_\infty = 2$, $\delta = 10$ deg, $\alpha = 25$ deg).

the plateau in pressure (Fig. 3) just after the shock. If one considers the momentum equation in the θ direction, it indicates that $\partial p/\partial\theta = 0$ at a cross-flow stagnation point ($u = v = 0$). The separation point in this flowfield is a real cross-flow stagnation point. The streamlines (Fig. 5) show that the flow moves in the negative θ direction from the lee stagnation point toward the separation point. In doing so, the flow expands (i.e., drop in pressure between $\theta = 180$ deg and $\theta = 165$ deg). The flow then recompresses to the separation point. This recompression phenomenon is the cause of secondary separation. The inviscid separation point location is far from that of the viscous flow. This can be surmised by the fact that the shock is strong enough to separate a boundary layer at its base. The inviscid separation point is too far downstream of the shock. The streamlines of Fig. 5 clearly show how all of the flow is ultimately swept up into the infinitely turning spiral. The apparent power of the Euler equations to describe the region near the center of the spiral should be noted. A detailed study of the streamline pattern near the center of the spiral revealed that the streamlines asymptote to an ellipse. This was first indicated by Smith.[9] It also should be pointed out that Fig. 5 shows that streamlines wrapping around the spiral very rapidly approach the lee side of the separation line (contact). Consider, for example, the third streamline off the cone in Fig. 5. It wraps around the top of the spiral, comes back, and approaches the contact a short distance off the body, creating an entropy layer on the lee side of the contact. This entropy layer tends to weaken the contact.

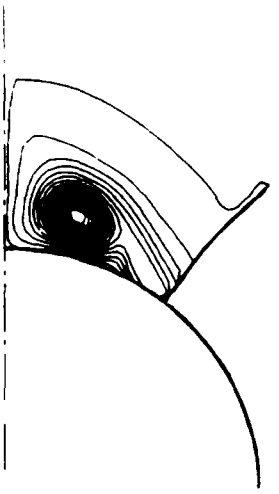

Fig. 8 Lines of constant radial vorticity × spherical radius ($M_\infty = 2$, $\delta = 10$ deg, $\alpha = 25$ deg).

Figure 5 also shows that the separation line leaves the cone at a finite angle. Smith's analysis[9] concluded that at a forced separation the sheet comes off tangent. However, this difference is due to the fact that the separation in the shock-induced case is nonisentropic and is a real cross-flow stagnation point. Figure 6 shows the cross-flow velocity on the surface of the body ($v = 0$ from the body boundary condition). The point to be considered here is that the velocity passes through zero (separation) smoothly. The analysis of Smith indicates that separation occurs at a discontinuity in cross flow, the jump in velocity determining the sheet strength. This is a basic difference between forced and shock-induced separation and is discussed in detail in Ref. 12. The jump in cross-flow velocity in Fig. 6 is due to the shock. It is also interesting to note the maximum negative u that occurs under the spiral. This negative cross flow can become supersonic, causing a second reverse cross-flow shock. A sample of this will be shown later.

Figure 7 shows the isobars for the same case ($M_\infty = 2$, $\delta = 10$ deg, $\alpha = 25$ deg). It should be noted how smoothly the cross-flow shock transitions to zero strength in the field. The most interesting aspect of the figure is the closed isobar at the center of the spiral. It represents an absolute minimum in the flowfield pressure. The component of vorticity in the spherical radial direction is given by:

$$\Omega_r = -\left(u\cos\phi + \frac{\partial u}{\partial \phi}\sin\phi - \frac{\partial v}{\partial \theta}\right)\Big/(r\sin\phi)$$

where u and v are the cross-flow velocities defined in Fig. 1 and r, θ, ϕ are spherical coordinates (Fig. 1). Figure 8 shows lines of constant $r\Omega_r$. The figure shows how the vorticity is distributed and is produced by the cross-flow shock. Note that Ω_r is small until the cross-flow shock, indicating that the bow shock doesn't produce enough vorticity to cause separation on its own. The vorticity produced by the bow shock is an order of magnitude smaller than that produced by the cross-flow shock and two orders of magnitude smaller than that at the center of the spiral. For this reason, there are no contours of vorticity outside the region behind the cross-flow shock in Fig. 8. The vorticity is negative causing the counterclockwise spiraling of this flow, and its absolute magnitude is maximum at the center of the vortex.

The results shown in Figs. 9-11 are all for the same flow conditions ($M_\infty = 2$, $\delta = 10$, $\alpha = 20$ deg). This is a lower angle of attack than the previous case, so that the spiral is smaller

and has moved toward the lee plane. This can be seen by comparing Figs. 5 and 10. It also can be seen from the streamlines (Figs. 9 and 10) that this configuration has an additional saddle/node combination in the lee plane as sketched in Fig. 2b. The dashed line ending at the saddle in the lee plane divides the flow, which is ultimately swept into the spiral node from that which ends up in the node in the lee symmetry plane. The entropy on the dashed streamline ultimately wets the lee side of the contact (separation line). This type of structure has been noticed experimentally.[22] The phenomenon is similar to the standard "liftoff" conical flow structure noticed at lower incidence with no spiral. In the present study, subcritical incidences were computed for the same 10-deg cone at $M_\infty = 2$, and liftoff was observed with no vortex. As the incidence is raised, the flow becomes supercritical and the spiral begins to form near the lee plane. The liftoff remains, as shown in Figs. 9 and 10. As the incidence is raised still further, the spiral gets larger and the liftoff is eliminated (see Figs. 4 and 5). It should be noted that the limiting streamline (dashed line in Fig. 10) seems not to approach the saddle normally. This is possible if distributed vorticity is present in the flow,[23] which is the case here. The isobars in Fig. 11 show that the vortex is so weak that the minimum in pressure at its center does not appear due to the resolution of the contours.

Figure 12 is a plot of the inviscid separation point location vs a measure of shock strength. The cone has a 10-deg half-angle and the freestream Mach number is 2. The cross-flow shock strength was increased by increasing incidence. The pressure ratio used is the one at the base of the shock; of course, all cross-flow shocks go to zero strength at their tips. The pressure ratio used is a good measure of the shock strength variation and thus the vorticity produced by the shock. At each data point, the corresponding α is noted. The plot shows how as the shock strength decreases, the separation point moves to the lee symmetry plane. At the same time, the spiral region is getting smaller. The highest incidence computed was 25 deg, since above that value the axial Mach number on the cone surface approaches sonic, making it impossible to march. At the low end, $\alpha = 19$ deg, the spiral was so small that it was difficult to resolve numerically, and no lower incidences are shown. The interesting feature of this figure is that an extrapolation of the curve would seem to indicate that inviscid separation moves to the lee plane before the shock is eliminated ($p_2/p_1 = 1.$). An extrapolation would indicate that the spiral is eliminated at $p_2/p_1 \approx 1.85$. This corresponds to a normal Mach number slightly above 1.3, which is approximately the region where the full potential

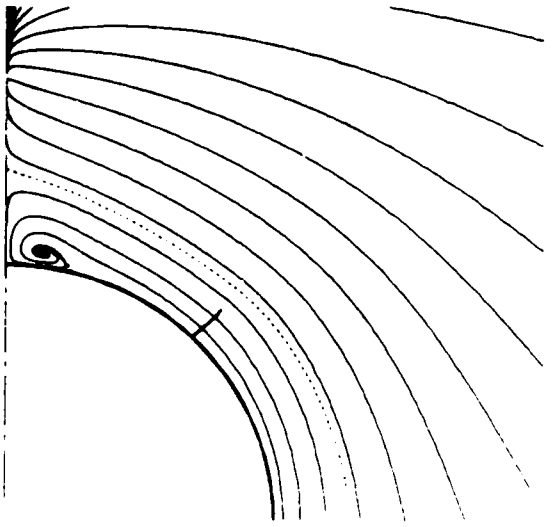

Fig. 10 Cross-flow streamlines near lee plane ($M_\infty = 2$, $\delta = 10$ deg, $\alpha = 20$ deg).

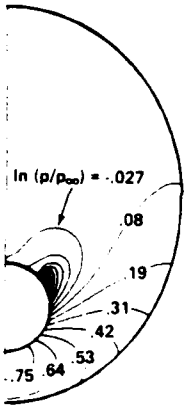

Fig. 11 Isobars in cross plane ($M_\infty = 2$, $\delta = 10$ deg, $\alpha = 20$ deg).

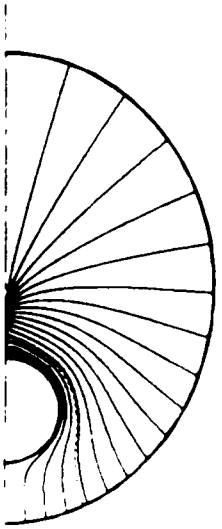

Fig. 9 Cross-flow streamlines ($M_\infty = 2$, $\delta = 10$ deg, $\alpha = 20$ deg).

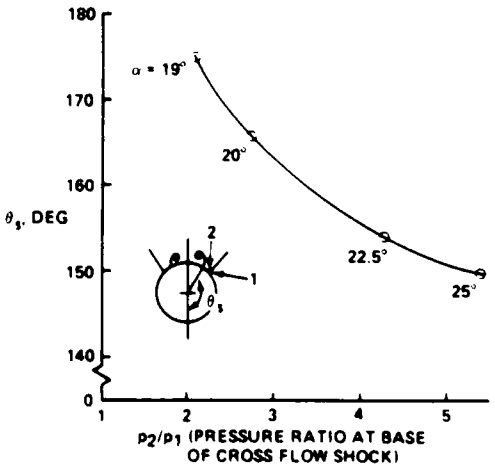

Fig. 12 Inviscid shock-induced separation point location vs shock strength ($M_\infty = 2$, $\alpha = 20$ deg).

approximation is valid for these flowfields. It would seem that below a maximum normal Mach number of 1.3, the cross-flow shock may not produce enough vorticity to cause separation.

Figures 13-15 deal with an interesting case ($M_\infty = 3$, $\delta = 9.46$ deg, and $\alpha = 25$ deg). Figure 13 show the streamlines and the cross-flow shock near the lee plane. The shock exhibits a kink as it passes from the influence of the spiral. Near the cone, the shock must deflect the streamlines upward in order that they may pass over the spiral; beyond the top of the spiral, this is no longer true and the shock acts like a normal shock. The two regions are separated by the kink in the shock, and the shock slope in the cross-flow plane had to be differenced away from this point. Another interesting feature of this flow is the fact that the expansion of the reverse flow from the lee stagnation point is so large that the negative cross flow becomes supersonic near the body. The smooth recompression shown in Fig. 3 is replaced by a reverse cross-flow shock. This phenomenon has been noted experimentally in Ref. 24. The reverse cross-flow shock, which was captured, can be seen in the isobars of Fig. 14. The second (reverse) shock is on the lee side of the primary cross-flow shock. It is indicated by the clustering of the isobars between $\ln(p/p_\infty) = -1.2$ and $\ln(p/p_\infty) = -0.73$ on the cone surface. The shock is not strong enough to produce a secondary inviscid separation, whereas in the experiment of Ref. 24 it was strong enough to separate the boundary layer. The possibility of having secondary separation produced solely by shock vorticity is an interesting topic for future study. The strength of the vortex is also indicated in Fig. 14 by the closed isobars representing a steep pressure minimum at the vortex center.

Figure 15 shows the surface pressure for the $M_\infty = 3$, $\delta = 9.46$ deg, and $\alpha = 25$ deg case. The solid line is the present calculation with shock vorticity-induced separation at $\theta = 155.3$ deg, again at the plateau in pressure just after the primary cross-flow shock. The reverse cross-flow shock can be seen in the pressure distribution at about $\theta = 167$ deg. The shock is captured, and so it is smeared over a mesh interval. The figure also shows the numerical results of Ref. 15. They are also a solution to Euler's equations but with the primary cross-flow shock was captured. In the results of Ref. 15, the separation point was forced to occur at $\theta = 120$ deg in order to match the boundary-layer separation point found experimentally. The forced separation model of Ref. 15 is in contradiction to the analytical work of Smith.[10] In addition, there are anomalies in the results of Ref. 15. Basically the comparison of Fig. 15 shows that the two results are very close, while the separation points are very different. It seems that forcing separation at $\theta = 120$ deg simply inserted a wiggle

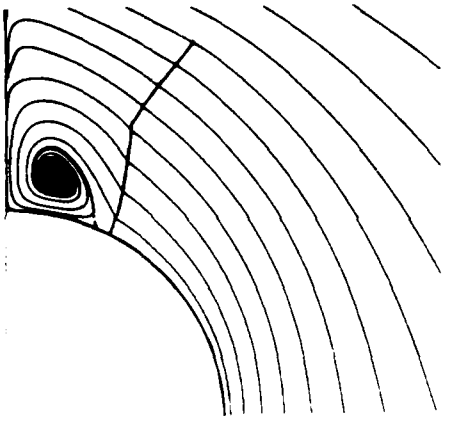

Fig. 13 Cross-flow streamlines near lee plane ($M_\infty = 3$, $\delta = 9.46$ deg, $\alpha = 25$ deg).

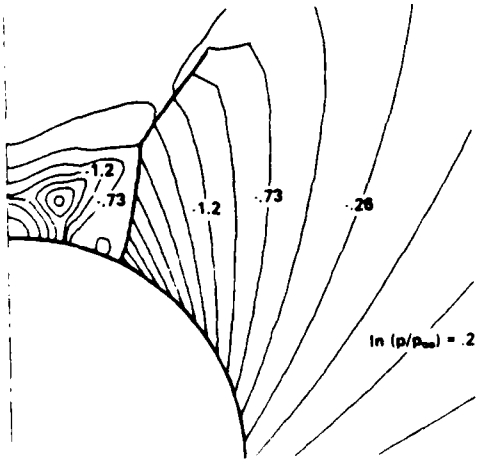

Fig. 14 Isobars near lee plane ($M_\infty = 3$, $\delta = 9.46$ deg, $\alpha = 25$ deg).

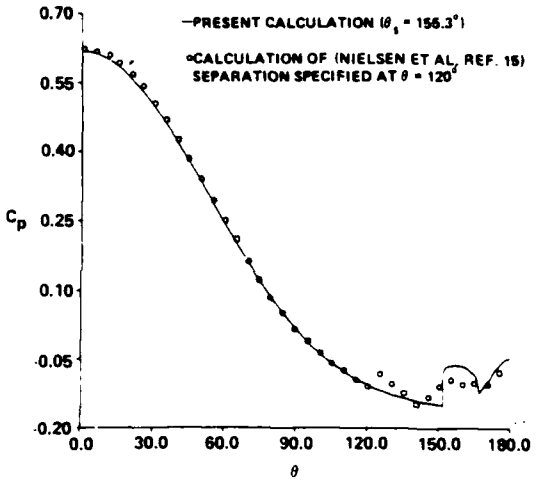

Fig. 15 Surface pressure comparison ($M_\infty = 3$, $\delta = 9.46$ deg, $\alpha = 25$ deg).

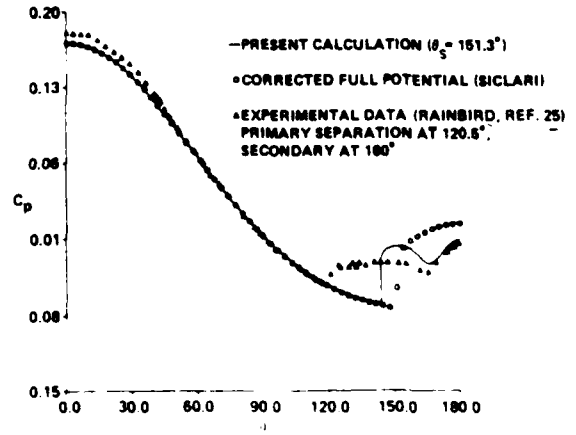

Fig. 16 Surface pressure comparison ($M_\infty = 4.25$, $\delta = 5$ deg, $\alpha = 25$ deg).

in the surface pressure distribution of Ref. 15. The flow then came back to the shock-induced flowfield. The cross-flow shock locations are very close. The shock of Ref. 15 is smeared over a few points but is close to the fit shock of the present calculations. If separation did occur at 120 deg, there must be a cross-flow shock before $\theta = 120$ deg. However, there is no evidence of a shock before separation in the results of Ref. 15.

Figure 16 shows the pressure distribution on a 5-deg cone at $M_\infty = 4.25$ and $\alpha = 12.35$ deg. Compared are the results of the present calculation, those computed using the full potential equation supplied by Siclari, and the experimental results of Rainbird.[25] The potential results of Siclari have been corrected for nonisentropic bow shock effects while maintaining the irrotational assumption. Figure 16 indicates that the Euler and potential results are virtually identical until the shock. The potential result does not exhibit the minimum in pressure behind the shock typical of separation. Potential calculations cannot predict separation or spiraling without a shedding sheet. The comparison between Euler and potential calculations affirms the fact that rotationality is important only after the cross-flow shock. A comparison between the present calculation and the experimental results of Rainbird clearly shows that the vorticity produced by the shock does not separate the flow near the viscous separation point. The experimental data show two separations—primary at $\theta = 120.3$ deg and secondary at 160 deg, while the inviscid separation is at $\theta = 151.3$ deg. The longer plateau in pressure in the experiment behind the primary separation point is due to the secondary separation; otherwise, the Euler and experimental pressure distributions would be similar. It is the expansion and recompression of the reverse flow that causes secondary separation. It should be clear that while the vorticity produced by the cross-flow shock is not the whole separation story, it may play an important role in the process. There are two sources of vorticity in this flowfield—the shock and the boundary layer. Both of these sources of vorticity play a role in separation and the resulting spiral or vortex.

Summary of Findings and Future Work

This study has found that the vorticity produced by a cross-flow shock present in the supersonic flow about cones at high incidence can cause separation and spiraling. A number of important features of these solutions were shown.

1) An independence of these solutions to any numerical artifices; that is, artificial viscosity (truncation error), captured shocks, or initial conditions.

2) Why the conceptual problem associated with the two-dimensional closed-separation bubbles does not exist in conical flow. Since no closed-recirculation zones exist in the conical flow, all quantities transmitted along streamlines can be uniquely defined.

3) The variation of shock-induced separation location with shock strength (Fig. 12), indicating the possibility that the spiral is eliminated before the cross-flow shock.

4) The development of a second reverse cross-flow shock (Figs. 14 and 15) with the possibility of shock-induced secondary separation.

It should be obvious that any computation that relies on the potential flow approximation alone cannot predict these flowfields. While the shock-induced vorticity may play an important role in viscous separation, it is by no means the whole picture (see Fig. 16).

This work has uncovered as many problems as it has solved. The somewhat surprising behavior of the lee plane saddle node combination once the spiral appears must be studied in detail. The saddle node combination (Figs. 9 and 10) that is present at subcritical α's and remains with weak spirals is eliminated as the spiral gets larger (Figs. 4 and 5). The possibility of a second reverse shock (Fig. 15) causing secondary separation is an interesting possibility that must be investigated.

Acknowledgments

The author gratefully express his appreciation to Dr. A. Rubel for his many helpful discussions during the course of this work and Dr. M. Siclari for supplying the full potential calculations. Both are from Grumman's Research and Development Center.

References

[1] Rao, D.M., "Vortical Flow Management for Improved Configuration Aerodynamics—Recent Experiences," AGARD CP-342, 1983, pp. 30-1-30-14.

[2] Küchemann, D. "Inviscid Shear Flow Near the Trailing Edge of an Aerofoil," RAE TR 67068, 1967.

[3] Frankel, L.E., "On Corner Eddies in Plane Inviscid Shear Flow," *Journal of Fluid Mechanics*, Vol. 11, 1961, pp. 400-406.

[4] Smith, P.D., "A Note on the Computation of the Inviscid Rotational Flow Past the Trailing Edge of an Airfoil," RAE TM 1217, 1970.

[5] Salas, M.D., "Recent Developments in Transonic Euler Flow Over a Circular Cylinder," NASA TM 83282, 1982.

[6] Schmidt, W. and Jameson, A., "Recent Developments in Finite Volume Time-Dependent Techniques for Two and Three Dimensional Transonic Flows," in *Computational Fluid Dynamics*, Lecture Series Notes 1982-04, VKE, Brussels, 1982.

[7] Hornung, H.G., "The Vortex Skeleton Model for Three-Dimensional Steady Flows," AGARD CP-342, 1983, pp. 2-1-2-12.

[8] Smith, J.H.B., "Remarks on the Structure of Conical Flow," *Progress in Aeronautical Sciences*, Vol. 12, 1972, pp. 241-271.

[9] Smith, J.H.B., "Behavior of a Vortex Sheet Separating from a Smooth Surface," RAE TR 77058, 1977.

[10] Smith, F.T., "Three-Dimensional Viscous and Inviscid Separation of a Vortex Sheet from a Smooth Non-Slender Body," RAE TR 78097, 1978.

[11] Fiddes, S.F., "A Theory of the Separated Flow Past a Slender Cone at Incidence," AGARD CP 291, 1981, pp. 30-1-30-14.

[12] Marconi, F., "The Spiral Singularity in the Supersonic Inviscid Flow Over a Cone," AIAA Paper 83-1665, July 1983.

[13] Bryson, A.E., "Symmetric Vortex Separation on Circular Cylinders and Cones," *Journal of Applied Mechanics*, Vol. 81, Dec. 1959, pp. 643-648.

[14] Rizzi, A., Ericksson, L., Schmidt, W., and Hitzel, S., "Numerical Solutions of the Euler Equations Simulating Vortex Flows Around Wings," AGARD CP-342, 1983, pp. 21-1-21-14.

[15] Nielsen, J.N., Kuhn, G.D., and Klopfer, G.H., "Euler Solutions of Supersonic Wing-Body Interference at High Incidence Including Vortex Effects," NEAR TR 263, 1982.

[16] Marconi, F., "Supersonic Inviscid, Conical Corner Flow Fields," *AIAA Journal*, Vol. 18, Jan. 1980, pp. 78-84.

[17] Moretti, G., "The λ-Scheme," *Computers and Fields*, Vol. 7, 1979, pp. 191-205.

[18] Marconi, F., Salas, M.D., and Yaeger, L., "Development of a Computer Code for Calculating the Steady Super Hypersonic Inviscid Flow Around Real Configurations," NASA CR-2675, 1976.

[19] Rudman, S., "Multinozzle Plume Flow Fields—Structure and Numerical Calculations," AIAA Paper 77-710, June 1977.

[20] deNeef, T. and Moretti, G., "Shock Fitting for Everybody," *Computers and Fluids*, Vol. 8, 1980, pp. 327-334.

[21] Siclari, J.M., "Investigation of Cross Flow Shocks on Delta Wings in Supersonic Flow," AIAA Paper 79-0345, Jan. 1979.

[22] Peake, D.J., Fisher, D.F., and McRae, D.S., "Flight, Wind Tunnel and Numerical Eperiments with a Slender Cone at Incidence," *AIAA Journal*, Vol. 20, Oct. 1982, pp. 1338-1345.

[23] Rubel, A., "Inviscid Axisymmetric Jet Impingement with Recirculating Stagnation Regions," *AIAA Journal*, Vol. 21, March 1983, pp. 351-357.

[24] Vorropoulos, G. and Wendt, J.F., "Laser Velocimetry Study of Compressibility Effects on the Flow Field of a Delta Wing," AGARD CP-342, 1983, pp. 9-1-9-13.

[25] Rainbird, W.J., "The External Flow Field About Yawed Circular Cones," AGARD CP-30, 1968, pp. 19-1-19-18.

APPENDIX B

CONICAL, SEPARATED FLOWS WITH SHOCK AND SHED VORTICITY

Conical, Separated Flows with Shock and Shed Vorticity

F. Marconi

Reprinted from AIAA Journal Volume 25 Number 1 January 1987 Page 173

AMERICAN INSTITUTE OF AERONAUTICS AND ASTRONAUTICS • 1633 BROADWAY • NEW YORK, N Y 10019

Conical, Separated Flows with Shock and Shed Vorticity

F. Marconi*
Grumman Corporate Research Center
Bethpage, New York

Introduction

THIS investigation deals with the highly vortical flow about circular cones at supersonic speeds and high angle of attack. The author has shown that the shock system of these flows can cause separation and a spiral vortex near the lee plane of the cone.[1] Earlier, Salas[2] showed two-dimensional Euler solutions where shock vorticity had also induced separation. The numerical investigation of Ref. 1 showed that the crossflow shock can produce large entropy gradients and vorticity sufficient to cause separation and a spiral vortex. In addition to shock vorticity, a separating boundary layer can shed vorticity into an otherwise irrotational flow. This phenomenon has been studied with inviscid models for many years. Smith[3] developed a model for shedding vorticity from the surface of a smooth body into the flowfield. The present author[4] was the first to use this model in conjunction with the Euler equations to shed vorticity from both primary and secondary crossflow separation points. An extension of the vorticity shedding model of Ref. 3 to the situation of supersonic crossflow is used in the present investigation. In the case of shock-induced separation, the solution to the Euler equation is unique in that the separation point location is computed along with the shock system and flowfield. On the other hand, the separation point must be prescribed in the case of shed vorticity. There exists a range of separation point locations corresponding to varying amounts of vorticity being shed. This Note presents the results of an investigation of the relationship between shock-vorticity-produced separation and shed-vorticity-produced separation.

Discussion

This study was conducted by numerically evaluating Euler solutions for the flow about a 5 deg cone varying the specified separation point location. The freestream conditions were fixed at $M_\infty = 4.25$ and $\alpha = 12.35$ deg. The flow is conical so that only the crossflow plane (i.e., any plane normal to the cone axis) need be considered. This plane intersects the separation line at a point which will be referred to as the separation point. At the large angle of attack considered here the flow in the crossflow plane is supercritical and so a crossflow shock is present. With no vorticity shed from the cone surface, this crossflow shock is strong enough to produce enough vorticity to cause separation. In addition, shedding vorticity from the cone surface does not eliminate the crossflow shock so that both sources of vorticity are present. Figures 1 and 2 show the crossflow streamlines and isobars, respectively, for the flow with no vorticity shed from the body. Separation for this case is computed to be at $\theta_s = 151.3$ deg from the wind plane. Figure 1 indicates that the separating streamlines leave the surface at a large angle (57 deg in this particular case) relative to the surface. When only shock vorticity is present there is no jump in crossflow velocity at the separation point, consistent with the fact that no vorticity is being shed from the surface. In the case of the shock vorticity alone, the crossflow stagnates on both sides of the separating streamline, and this streamline leaves the surface at a large angle relative to [illegible]. Smith[3] proved that in order to shed vorticity into an otherwise irrotational flow there must be a jump in crossflow velocity at the separation point; the crossflow stagnates only on the lee side of the separating streamline. It should be pointed out that in the computational results presented here all crossflow shocks are captured. Figure 2 indicates that the shock is captured very sharply (see the closely spaced isobars). Additionally, these captured shock results compare well with the [illegible] fit results of Ref. 1.

The model used to shed vorticity from the [illegible] follows the work of Smith.[3] The model is implemented in the computational scheme by using a double grid point at the separation point. One grid point is assumed to lie on the vortex sheet and the other is assumed to lie on the body. In the case of subsonic crossflow, the [illegible] of the sheet are computed as a function of the [illegible] only the flow tangency condition on the [illegible] stagnate on the body side of the sheet. The [illegible] from the flow side of the sheet [illegible] be computed. These [illegible]

Received May 27, 1986; revision received July 10, 1986.

*Senior Staff Scientist. Associate Fellow AIAA.

AD-A190 245 ON THE PREDICTION OF HIGHLY VORTICAL FLOWS USING AN EULER EQUATION MODEL.. (U) GRUMMAN CORP BETHPAGE NY CORPORATE RESEARCH CENTER F MARCONI 30 OCT 87 2/2

UNCLASSIFIED AFOSR-TR-87-1910 F49620-85-C-0115 F/G 20/4 NL

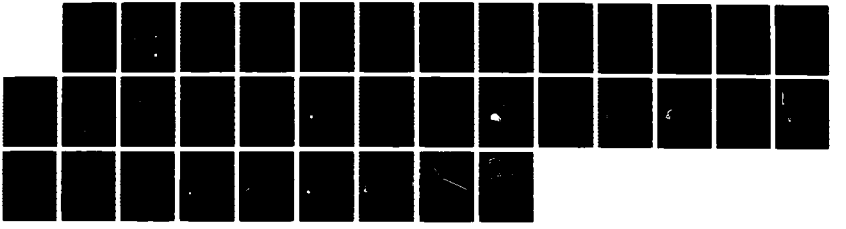

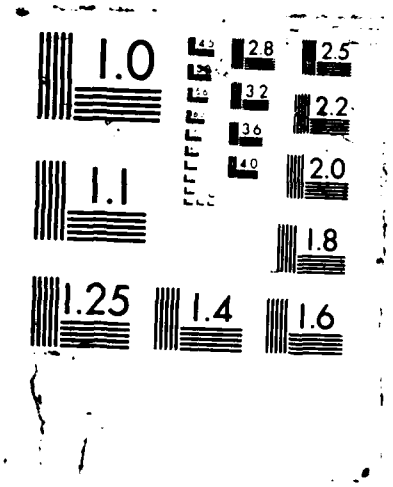
1.0
1.1
1.25
1.4
1.6
1.8
2.0
2.2
2.5
2.8
3.2
3.6
4.0

body tangentially. If the crossflow approaching the separation point is supersonic the model used must be changed. Smith[3] argued that if the separating streamline leaves a smooth surface at a finite angle, then the flow must stagnate on both sides of the separation point and no vorticity will be shed into the flowfield. This argument is true if the flow approaching the separation point is subsonic. However, when the separating flow is supersonic and the separating sheet leaves the body at an angle relative to it, then there can be a jump in crossflow velocity (i.e., vorticity shed). In a locally supersonic flow a slope discontinuity results in a shock, not a stagnation point as in the subsonic case. The new model involves an oblique shock at the separation point unless the deflection is too large, in which case a normal shock is formed and the flow is separated in a locally subsonic flow. The modifications to the computation are as follows: the flow side of the sheet is also on the low-pressure side of the oblique shock at separation so that the pressure there cannot be used on the body side of the sheet. The crossflow on the body side of the sheet is still stagnated with the pressure there being extrapolated from the lee side of separation. With the conditions at the double point defined, no differences are taken across the separation point on the body. Once the sheet leaves the body no provisions are made for it and it is captured over a few mesh points. Reference 4 gives more detail on this procedure.

Figures 3 and 4 show the results for the most windward separation point location computed ($\theta_s = 115$ deg). Figure 3 shows the crossflow streamlines. The secondary separation shown is due to a strong reverse crossflow shock (see Fig. 4); note the third vortex off the surface due to the interaction of the two separations. In Fig. 4, the isobars are shown and they indicate an oblique shock at the specified primary separation pont. The shock is due to the separating sheet leaving the cone surface at an angle relative to it. A similar shock/sheet configuration has been noted experimentally.[4] In the situation of Figs. 3 and 4, the supersonic crossflow passes through the oblique shock and moves outward along the separating streamline. The flow on the lee side of the sheet stagnates at the separation point. With separation specified at $\theta = 115$ deg, the jump in crossflow velocity at the separation point indicates that significant vorticity is being shed from the surface. A comparison of Figs. 1 and 3 shows that the extent of the vortical regions are comparable, whereas the two sources of vorticity are very different.

The relationship between shock vorticity and shed vorticity for conical separated flow is made clear by considering Fig. 5. The figure shows the jump in crossflow velocity (Δq_{CF}) vs separation point location. The jump in crossflow velocity is directly related to the vorticity shed into the flowfield from the separation point. Figure 5 represents all possible Euler solutions for the flow about this cone at these freestream conditions and one specified separation point. No solutions could be found for $\theta_s > 151.3$ deg or $\theta_s < 115$ deg. The experimental

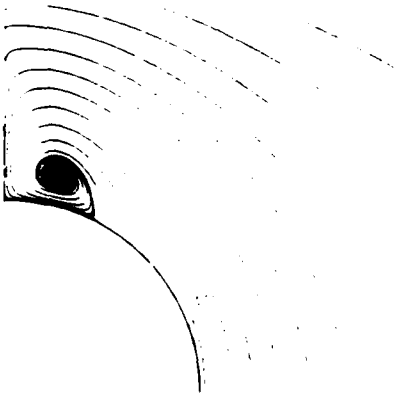

Fig. 1 Crossflow streamlines on the 5 deg circular cone ($M_\infty = 4.25$, $\alpha = 12.35$ deg) separation due to shock vorticity alone at $\theta = 151.3$ deg.

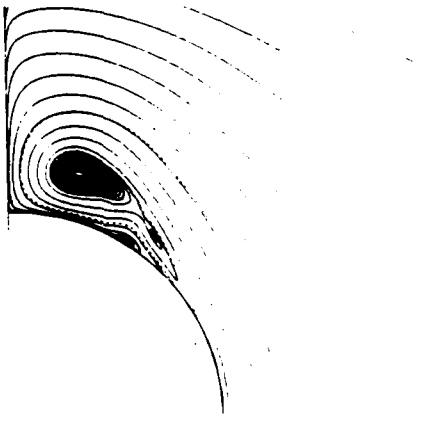

Fig. 3 Crossflow streamlines on the 5 deg circular cone ($M_\infty = 4.25$, $\alpha = 12.35$ deg) separation forced at $\theta = 115$ deg.

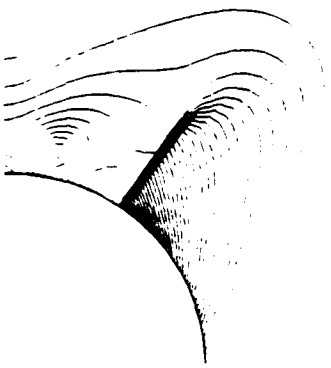

Fig. 2 Isobars on the 5 deg circular cone ($M_\infty = 4.25$, $\alpha = 12.35$ deg) separation due to shock vorticity alone at $\theta = 151.3$ deg.

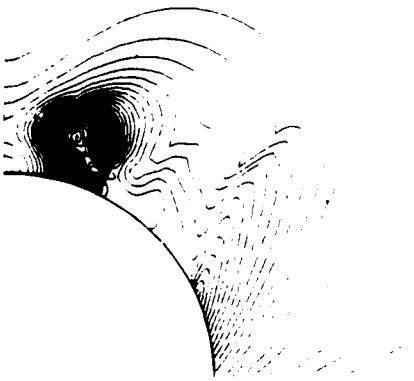

Fig. 4 Isobars on the 5 deg circular cone ($M_\infty = 4.25$, $\alpha = 12.35$ deg) separation for [illegible] at $\theta = 115$ deg.

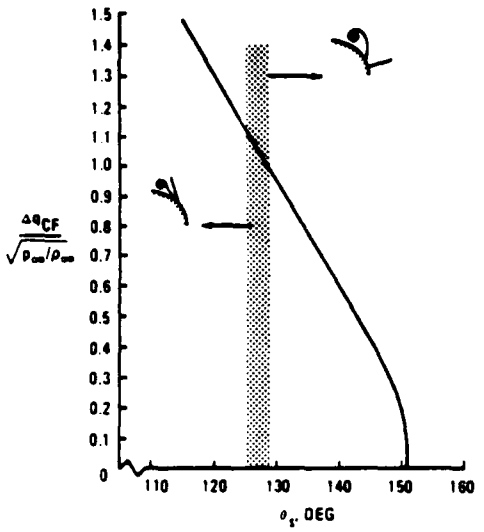

Fig. 5 Vorticity shed into the flowfield as a function of separation point location.

data of Ref. 5 indicate primary separation at 120 deg and secondary separation at 160 deg for this case. The shock configuration transition from an oblique crossflow shock to a detached normal crossflow shock occurs at about $\theta_s \approx 128$ deg (indicated by the shaded area in Fig. 5). It should be pointed out that the jump in velocity at the separation point in the oblique shock cases was computed by subtracting the oblique shock velocity jump from the numerical results. Thus, the jumps in velocity in Fig. 5 represent the jumps across the vortex sheet at separation. The figure shows that this velocity jump goes to zero smoothly as the separation point location due to shock vorticity alone is approached ($\theta_s = 151.3$ deg).

Conclusion

The results of this analysis indicate that there is a relationship between separation produced by shock vorticity and shed vorticity and that both sources of vorticity may be important. The relationship is inferred because the jump in velocity (i.e., vorticity shed) smoothly goes to zero as the shock vorticity separation point location is approached. In fact, it would seem that separation due to shock vorticity alone can be considered a limiting solution of the set of solutions in which vorticity is shed from the surface. In this limiting solution the vorticity shed is zero.

Acknowledgment

This work was supported by the Air Force Office of Scientific Research under Contract F49620-84-C0056.

References

[1]Marconi, F., "Supersonic Conical Separation Due to Shock Vorticity," *AIAA Journal*, Vol. 22, Aug. 1984, pp. 1048–1055.

[2]Salas, M. D., "Recent Developments in Transonic Euler Flow Over a Circular Cylinder," NASA TM 83282, 1982.

[3]Smith, J. H. B., "Remarks on the Structure of Conical Flow," *Progress in Aeronautical Sciences*, Vol. 12, June 1972, pp. 241–271.

[4]Marconi, F., "The Spiral Singularity in the Supersonic Inviscid Flow Over a Cone," AIAA Paper 83-1665, 1983.

[5]Rainbird, W. J., "The External Flow Field About Yawed Circular Cones," AGARD CP30, 1968, pp. 19-1–19-18.

APPENDIX C

COMPLEX SHOCK PATTERNS AND VORTICES IN INVISCID SUPERSONIC FLOWS

Complex Shock Patterns and Vortices in Inviscid Supersonic Flows

by

F. Marconi

Grumman Corporate Research Center
Bethpage, New York 11714-3580

Abstract

This work represents an application of Prof. Moretti's computational procedures to an investigation of fluid physics. Specifically, the effects of shock vorticity on the supersonic, inviscid flow about circular, cross-sectional cones is considered. While the Euler equations are solved, so that no viscous effects are included, the shock vorticity can cause flow separation and vortex formation. In the computational results to be shown here the interaction of these vortices and shocks produces a number of interesting phenomena which will be discussed in detail.

1. INTRODUCTION

When flows with significant vorticity were investigated by Salas [1] with computational methods, the question of whether the inviscid flow separation predicted was a numerical artifice was a serious concern. After the careful shock fitting procedures proposed by Moretti [2] were applied to an investigation of this phenomenon [3], some of the doubts were dispelled. After a number of investigations in the area, it is now accepted that shock systems can produce enough vorticity to cause flow separation. While Salas [1] may have been the first researcher in modern computational fluid dynamics to investigate this phenomenon, Küchemann [4] considered the possibility of shock vorticity causing separation in 1967. In addition, Frankel [5] developed analytical solutions to the Euler equations which exhibited separation due to distributed vorticity. The current paper will show that the shock system produced by a circular cone flying at supersonic speeds and high angle of attack can generate enough distributed vorticity to cause separation and vortex formation.

Figure 1 shows a sketch of the flow field that is considered here. The geometry is a slender cone that is immersed in a high speed flow at a high angle of attack. As the angle of attack is increased past the cone half angle, the crossflow component tangent to the body (u) will become supersonic. Due to symmetry, this velocity must go to zero in the lee plane, causing a crossflow shock to develop on the lee side of the body. As the angle of attack is raised, this shock's strength increases. The strongest portion of this shock is at the cone surface, and it diminishes as it moves into the field. It goes to zero strength relatively close to the body. It is this rapid decrease in shock strength which produces enough vorticity to cause vortex formation. It was Smith [6] who showed that in order to have a vortex in conical flow a non-zero component of radial vorticity is required.

Figure 1 shows the simplest shock/vortex pattern encountered during this work. The interaction of the shock and vortex can produce complex shock patterns and multiple vortices. In addition, aside from shock vorticity, vorticity can be shed from the surface of the cone. The present author [7] applied a model to the Euler equations for shedding vorticity from the surface of smooth bodies. In Ref. [8] the relationship between shock and shed vorticity is studied. In this paper only shock vorticity will be considered. The flow about a 10° half angle cone at two Mach numbers, one intermediate 5 and the other low hypersonic 10, will be analyzed. As the angle of attack is increased from 10° to 25°, shock/vortex patterns of increasing complexity result. Before these interesting flow fields are discussed, the computational procedures used will be outlined.

2. COMPUTATIONAL PROCEDURE

The fully three-dimensional Euler's equations are solved with an explicit marching technique. The marching direction, z (Fig. 1), is an iterative coordinate for the conical flow considered here. The scheme is restricted by the fact that the axial component of velocity, W (Fig. 1), must be supersonic everywhere. The marching scheme is continued until the flow field is invariant with respect to the computational marching direction except for a scale factor. The finite difference scheme used is Moretti's characteristic based λ-scheme [9]. The bow shock and the primary crossflow shock are fit and are forced to satisfy the exact Rankine-Hugoniot jump conditions. The bow shock is fit as the outermost boundary of the flow field. On the low pressure

side of the bow shock, freestream conditions exist. The crossflow shock is fit as an internal boundary of the flow field with its low pressure side being computed as the computation proceeds [10].

The crossflow shock computation is a critical part of the overall procedure, particularly since it plays such a critical role in separation. As mentioned in the Introduction, it is the vorticity produced by the crossflow shock which is significant. Any scheme that captures the crossflow shock and introduces additional artificial viscosity to stabilize it runs the risk of distorting the separation and vortex. The bow shock also introduces vorticity into the flow field but not enough to produce separation. The low pressure side of the crossflow shock is computed with one-sided differences away from the shock. This is consistent with the fact that the crossflow is supersonic. The Rankine-Hugoniot conditions, together with the compatibility condition along a bicharacteristic reaching the shock on its high pressure side, supply enough information to compute the deviation of each shock point from a conical ray in addition to all the primitive variables on its high pressure side. The bicharacteristic used is the one in the plane containing the local normal to the shock and the marching direction. All shock points are computed with the post correction scheme proposed by Rudman [11] and independently by deNeef [12]. The shocks converge (i.e., each shock point becomes aligned with a conical ray) with the rest of the flow field. In all the computations presented here, the last crossflow shock point fit had a normal Mach number of approximately 1.05 (pressure ratio of 1.12). The finite difference scheme was able to capture weaker shock points. In addition, the finite difference scheme was used to capture all reverse crossflow shocks and oblique crossflow shocks in the flow field (to be discussed later). These shocks are usually weak and the scheme can capture them accurately.

The computational grid used here was developed from the polar coordinate system (r,θ,z) shown in Fig. 1. The grid is clustered exponentially in the radial (r) direction with a stretching of the form

$$r = -\ln[1 - (1-e^{-\beta})X]\ (C-B)/\beta+B \qquad (1)$$

where X is the computational coordinate going from 0 on the body to 1 at the bow shock. The other computational coordinate is Y, which is a linearly normalized polar angle θ. Y is normalized to go from 0 in the windward symmetry plane to 1 on the low pressure side of the crossflow shock and from 0

again on the high pressure side of the shock to 1 in the lee plane. The transformation to the computational plane is completed by $Z = z$. In the transformation, Eq (1), B and C are the polar radii of the body and bow shock, and β is a clustering parameter. The grid points are evenly spaced in each X-Y plane. The transformation clusters grid points near the body depending on the value of β used, and it approaches linear as β goes to zero. All the calculations shown here were performed with $\beta = 2.5$. The gradient in the strength of the crossflow shock is quite large, which is the reason for the large vorticity produced behind it. The clustering of grid points near the body allows for enough resolution to compute this shock decay properly. The number of points required to resolve this phenomenon without a stretching would be inordinately large. In all the calculations shown here the cross-sectional grid had 89x89 points. There were anywhere from 13 to 20 points on the lee side of the crossflow shock depending on its position; the rest of the 89 points were evenly spaced on the low pressure side of the shock.

Shock induced inviscid separation produces a contact surface emanating from the separation point (Fig. 1). It is this contact that ultimately spirals to form a vortex. The contact surface has a jump in entropy and an accompanying jump in velocity. In conical flow, entropy is constant on crossflow streamlines. Thus, one can see (Fig. 1) that the entropy on the windward side of the separating contact comes from the windward stagnation point of the cone. The streamline that wets the body passes through the base of the crossflow shock to form the high entropy side of the contact. There are a number of possibilities for the entropy on the lee side of the contact. The crossflow streamlines that wet the body are tracked in each step of the iteration, and the proper entropy is imposed on the surface including the jump in entropy at the separation point. All entropy discontinuity off the body is captured with the finite difference scheme.

The finite difference scheme used in this work is an explicit marching scheme, which is notoriously inefficient for converging to a conical or steady solution. One advantage of the explicit marching scheme is that it is totally "vectorizable." The time consuming parts of the code (i.e., interior point computation) utilized the vector architecture of the Cray XMP computer. The computations shown here typically took 45 CPU minutes on the Cray XMP. In

each case shown, the maximum residual (i.e., the derivative of pressure in the marching direction) was reduced at least six orders of magnitude.

3. COMPLEX SHOCK/VORTEX PATTERNS

In this computational investigation, a single cone is considered. The half angle is 10°, and two Mach numbers (5 and 10) were studied. At both Mach numbers the angle of attack was increased from 10° to 25° in increments of 5°. Of interest is the development of the shock/vortex pattern with increasing angle of attack.

First the low Mach number (5) will be discussed. When the angle of attack is equal to the cone angle of 10°, the cross flow does not expand enough to become supercritical. The maximum crossflow Mach number on the surface is only 0.93. Figure 2 shows the crossflow streamline pattern and the shock system (note the absent of a crossflow shock). The crossflow streamlines are traced by projecting the conical velocity components (u and v of Fig. 1) onto a plane. If the angle of attack is increased by 5° to 15°, a small region of supersonic crossflow does appear in the flow field. Figure 3 shows the sonic bubble and an accompanying crossflow shock. Figure 4 shows the crossflow streamlines for this case. Figure 4a shows the whole cross-sectional flow field while Fig. 4b shows only the region near the lee plane. In Fig. 4b a small vortex is shown very near the lee plane. The crossflow shock has a maximum normal Mach number of 1.66 at the body. This shock is strong enough to produce only a very small vortex.

When the angle of attack is increased to 20°, the shock gets significantly stronger (maximum shock Mach number of 2.46) and the resulting vortex is large. Figure 5 shows the crossflow streamlines and shock system at $\alpha = 20°$. While the shock/vortex system is significant, it is simple in the sense that there is still one vortex and one crossflow shock. Figure 6 shows the isobars for this case, and Fig. 7 shows the surface pressure distribution. The closed isobars of Fig. 6 represent a minimum in pressure at the center of the vortex. The surface pressure shows a local minimum (Fig. 7, $\theta = 170°$) directly under the vortex. The reverse crossflow expands from the lee plane to achieve it maximum velocity at the minimum in pressure at $\theta = 170°$. The flow then recompresses to go to zero crossflow velocity at the separation point $\theta = 165°$. This recompression can become a shock as will be seen at higher angle of attack when the shock pattern becomes complex.

Figure 8 shows contour lines of the radial component of vorticity:

$$\Omega_R = -(u \cos \phi + \frac{\partial u}{\partial \phi} \sin \phi - \frac{\partial v}{\partial \theta})/(R \sin \phi)$$

where u and v are the spherical crossflow velocities and R, θ, ϕ are the spherical coordinates shown in Fig. 1. Actually, Fig. 8 shows $R\Omega_R$ contours, which is the appropriate conical quantity. The figure shows that the vorticity is distributed somewhat uniformly along the lower portion of the shock. The uniform vorticity is carried downstream and swept into the vortex. This vorticity distribution can be understood more clearly by considering the entropy distribution along the shock. Figure 9 shows the entropy distributions on the low and high pressure sides of the shock. According to Crocco theorem, the vorticity is related to the gradient of entropy. The highest gradient of entropy is at the surface on the high pressure side of the shock. The entropy gradient decreases away from the surface and seems to have a constant value for $s/r > 0.3$. This ($s/r = 0.3$) is where the shock has a rapid change in slope. Figure 8 indicates that the vorticity is constant after this point. The rapid change in shock slope seems to occur at a radius equal to that at the top of the vortex. At even larger angles of attack, this slope change becomes a discontinuity and the shock system becomes complex.

At a freestream Mach number of 5, the shock system becomes complex at an angle of attack of 25°. Figure 10 shows the crossflow streamlines and Fig. 11 the isobars. The rapid change in shock slope has become a discontinuity as the shock extends over the top of the vortex. This discontinuity in shock slope is accompanied by an additional shock which extends toward the lee plane. This shock is captured but is clearly seen in the isobar plot of Fig. 11. The crossflow shock is no longer simple but has a triple point separating two portions of shock.

Around the primary vortex a "pin wheel" [13] shock pattern is formed. The crossflow shock becomes oblique to the flow just off the surface so that the cross flow behind the shock is supersonic just off the surface; see the sonic line plot of Fig. 12. The bundle of supersonic cross flow extends to the triple point. This flow must be shocked in order to meet the symmetry condition in the lee plane, and so a crossflow shock sits on top of the vortex (Fig. 11). As lee plane flow is accelerated by the vortex, it becomes supersonic so that another sonic bubble is formed attached to the lee plane

(Fig. 12). This supersonic flow must be shocked to meet the surface boundary condition. Note in Fig. 11 that the shock is normal to the lee plane just above the body. Finally, the surface flow is accelerated under the primary vortex and becomes supersonic (see the third sonic bubble in Fig. 12). This flow is shocked in order to become tangent to the inside of the separation line. This process of expanding and shocking as the flow moves around the vortex sets up a system of three shocks which the author first referred to as the pin wheel type in Ref. 13. This shock system is clearly shown in the isobars of Fig. 11.

Figure 10 shows a second small vortex just off the lee plane above the primary vortex. This is a spiral node caused, it seems, by the vorticity produced above the triple point on the main crossflow shock. A plot of entropy contours (Fig. 13) indicates that the contact surfaces at the separation point and the triple point are captured quite sharply by the finite difference scheme. Figure 13 also indicates that the captured shocks have no entropy jumps associated with them. This inaccuracy of the scheme is minimal since the normal Mach number to any of these shocks is small (i.e., maximum of 1.52). Figure 13 also shows the entropy singularity on the lee plane just above the secondary vortex. This is due to the coalescence of streamlines with vastly different entropy. For the sake of comparison the surface pressure distribution is shown in Fig. 14. This figure should be compared to Fig. 7 in which the angle of attack is 20°. The comparison indicates how much stronger the crossflow shock has become with a 5° increase in angle of attack and how the recompression under the vortex has turned into a reverse crossflow shock.

The same 10° half angle cone was investigated in the low hypersonic regime. At Mach 10 the 10° angle of attack case was attached as was the $M_\infty = 5$, $\alpha = 10°$ case. Even though at Mach 10 the crossflow is supersonic, no crossflow shock was present. Figure 15 compares the crossflow Mach numbers at $M_\infty = 5$ and 10 at $\alpha = 10°$. The figure shows that the $M_\infty = 10$ case has a slightly supercritical bubble (maximum level Mach number of 1.15) but not high enough to form a shock or a vortex. As the angle of attack is increased by 5° to 15°, a crossflow shock and vortex do form. Figure 16 shows the crossflow streamlines and the shock. In this case the shock is significant (maximum normal Mach number of 2), but the resulting vortex is small.

Complex shock patterns occur at $\alpha = 20°$ for $M_\infty = 10$ instead of $\alpha = 25°$ at $M_\infty = 5$. Figures 17 and 18 show the crossflow streamlines and isobars, respectively, for the $M_\infty = 10$ and $\alpha = 20°$ case. Figure 18 shows the pin wheel type shock pattern discussed previously in addition to the triple point in the crossflow shock. It should be noted that there is no secondary vortex in this case; instead, there is a simple node in the lee plane above the primary vortex.

The last case considered is $M_\infty = 10$ and $\alpha = 25°$. Figure 19 shows the streamlines and Fig. 20 the isobars. Again the pin wheel shock pattern is quite evident in addition to the triple point. The primary crossflow shock has a maximum normal Mach number of 3.8 at the surface and is quite strong. The captured reverse crossflow shock has a normal Mach number of 1.8. This has a secondary vortex above the main vortex in addition to a simple node in the lee plane halfway between the body and the bow shock (not shown in the figure). The secondary spiral node above the main vortex is seen more clearly in the expanded view of its region shown in Fig. 21. Figure 21 is an expanded view of the dashed box in Fig. 19. It can be seen that the node does not form a large vortex as does the primary vortex but it does seem to spiral at the node.

ACKNOWLEDGEMENT

The author wishes to express his gratitude to Prof. Gino Moretti for his many years of tutelage and friendship without which this work would not be possible.

REFERENCES

1. M.D. Salas, Recent developments in transonic Euler flow over a circular cylinder, NASA TM83282 (1982).

2. G. Moretti, Three-dimensional, supersonic, steady flows with any number of imbedded shocks, AIAA Paper No. 74-10 (1974).

3. F. Marconi, Supersonic conical separation due to shock vorticity, AIAA J., 22, 1048-1055 (1984).

4. D. Küchemann, Inviscid shear flow near the trailing edge of an aerofoil, R.A.E. TR 67068 (1967).

5. L.E. Frankel, On corner eddies in plane inviscid shear flow, J. Fluid Mechanics, 10, 400-406 (1961).

6. J.H.B. Smith, Remarks on the structures of conical flow, Progress in Aeronautical Sciences, 12, 241-271 (1972).

7. F. Marconi, The spiral singularity in the supersonic inviscid flow over a cone, AIAA Paper 83-1665 (1983).

8. F. Marconi, Conical, separated flows with shock and shed vorticity, AIAA J., 25, 173-175 (1987).

9. G. Moretti, The λ-scheme, Computers and Fluids, 7, 191-205 (1979).

10. F. Marconi, M.D. Salas, and L. Yaeger, Development of a computer code for calculating the steady supersonic/hypersonic inviscid flow around real configurations, NASA CR-2675 (1976).

11. S. Rudman, Multinozzle plume flow fields - structure and numerical calculations, AIAA Paper 77-710 (1977).

12. T. deNeef and G. Moretti, Shock fitting for everybody, Computers and Fluids, 8, 327-334 (1980).

13. F. Marconi, Fully three-dimensional separated flows computed with the Euler equations, AIAA Paper 87-0451 (1987).

FIGURE LEGENDS

1. Sketch of flow field and coordinate systems.
2. Crossflow streamlines and shocks 10° cone, $M_\infty = 5$, $\alpha = 10°$.
3. Crossflow sonic line and shock 10° cone, $M_\infty = 5$, $\alpha = 15°$.
4. Crossflow streamlines and shocks.
   a. entire cross section
   b. region near lee plane
5. Crossflow streamlines and shock 10° cone, $M_\infty = 5$, $\alpha = 20°$.
6. Cross sectional isobars and shock 10° cone, $M_\infty = 5$, $\alpha = 20°$.
7. Surface pressure distribution 10° cone, $M_\infty = 5$, $\alpha = 20°$.
8. Cross sectional vorticity contours 10° cone, $M_\infty = 5$, $\alpha = 20°$.
9. Entropy distribution along the crossflow shock 10° cone, $M_\infty = 5$, $\alpha = 20°$ (s in the arch length above the shock, r is the cone radius).
10. Crossflow streamlines and shock 10° cone, $M_\infty = 5$, $\alpha = 25°$.
11. Isobars and shocks 10° cone, $M_\infty = 5$, $\alpha = 25°$.
12. Crossflow sonic lines and shock 10° cone, $M_\infty = 5$, $\alpha = 25°$.
13. Cross sectional entropy contours and shock 10° cone, $M_\infty = 5$, $\alpha = 25°$.
14. Surface pressure distribution 10° cone, $M_\infty = 5$, $\alpha = 25°$.
15. Surface Mach number comparison 10° cone, $\alpha = 10°$, $M_\infty = 5$ and $= 10$.
16. Crossflow streamlines and shocks 10° cone, $M_\infty = 10$, $\alpha = 15°$.
17. Crossflow streamlines and shock 10° cone, $M_\infty = 10$, $\alpha = 20°$.
18. Isobars and shocks 10° cone, $M_\infty = 10$, $\alpha = 20°$.
19. Crossflow streamlines and shocks 10° cone, $M_\infty = 10$, $\alpha = 25°$.
20. Isobars and shocks 10° cone, $M_\infty = 10$, $\alpha = 25°$.
21. Expanded view of crossflow streamline 10° cone, $M_\infty = 10$, $\alpha = 25°$.

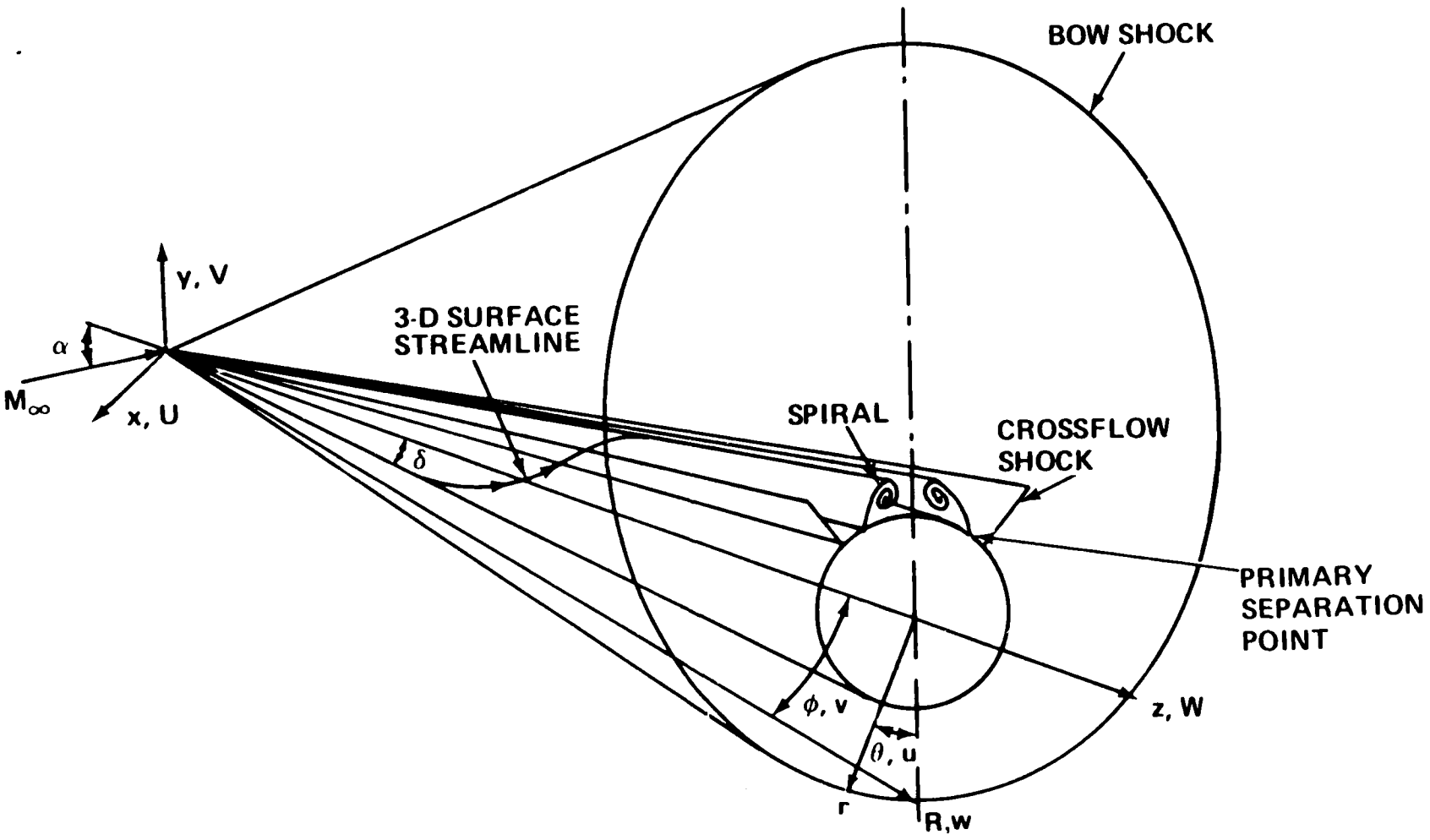
BOW SHOCK
y, V
α
M∞
x, U
3-D SURFACE
STREAMLINE
δ
SPIRAL
CROSSFLOW
SHOCK
PRIMARY
SEPARATION
POINT
z, W
φ, v
θ, u
r
R,w

Fig. 1

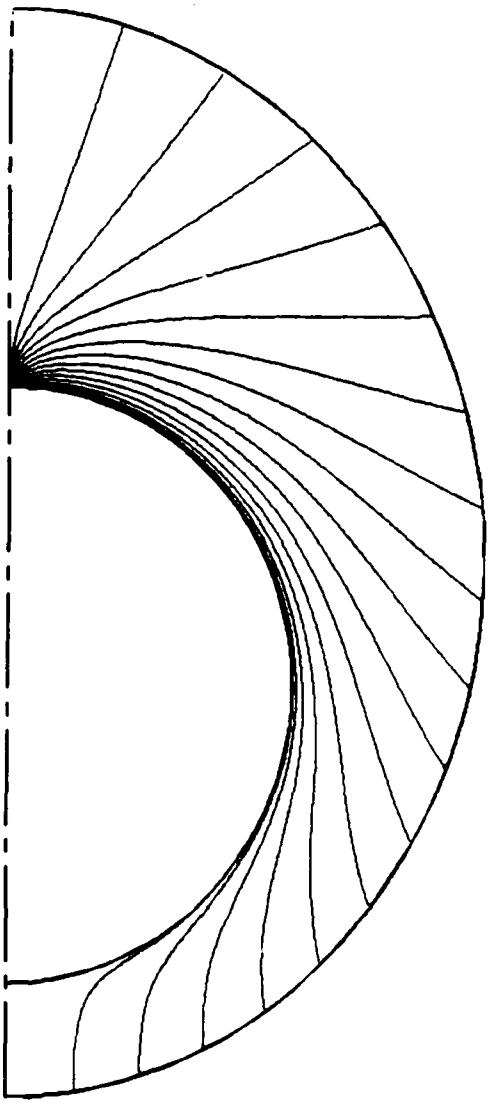

Fig. 2

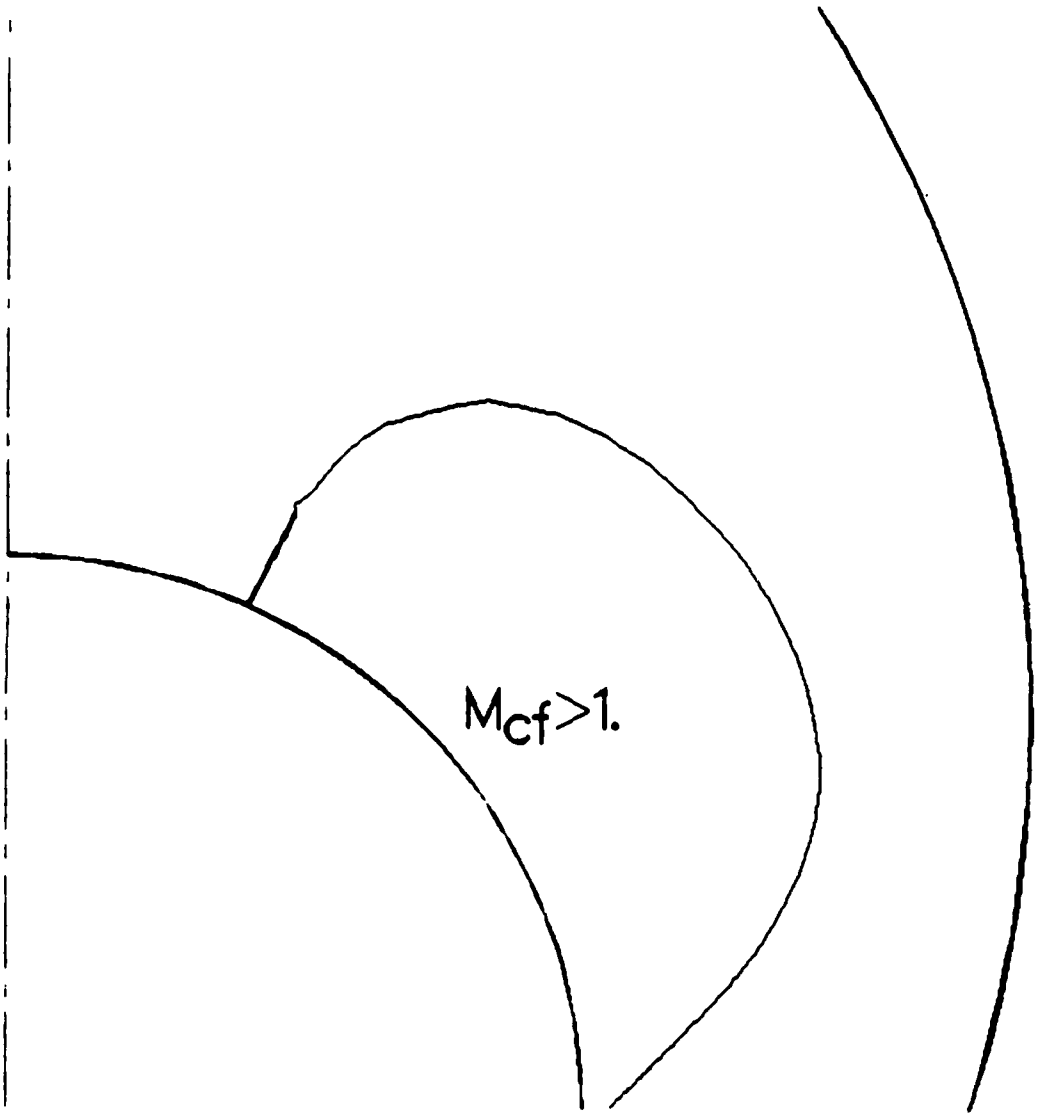

Fig. 3

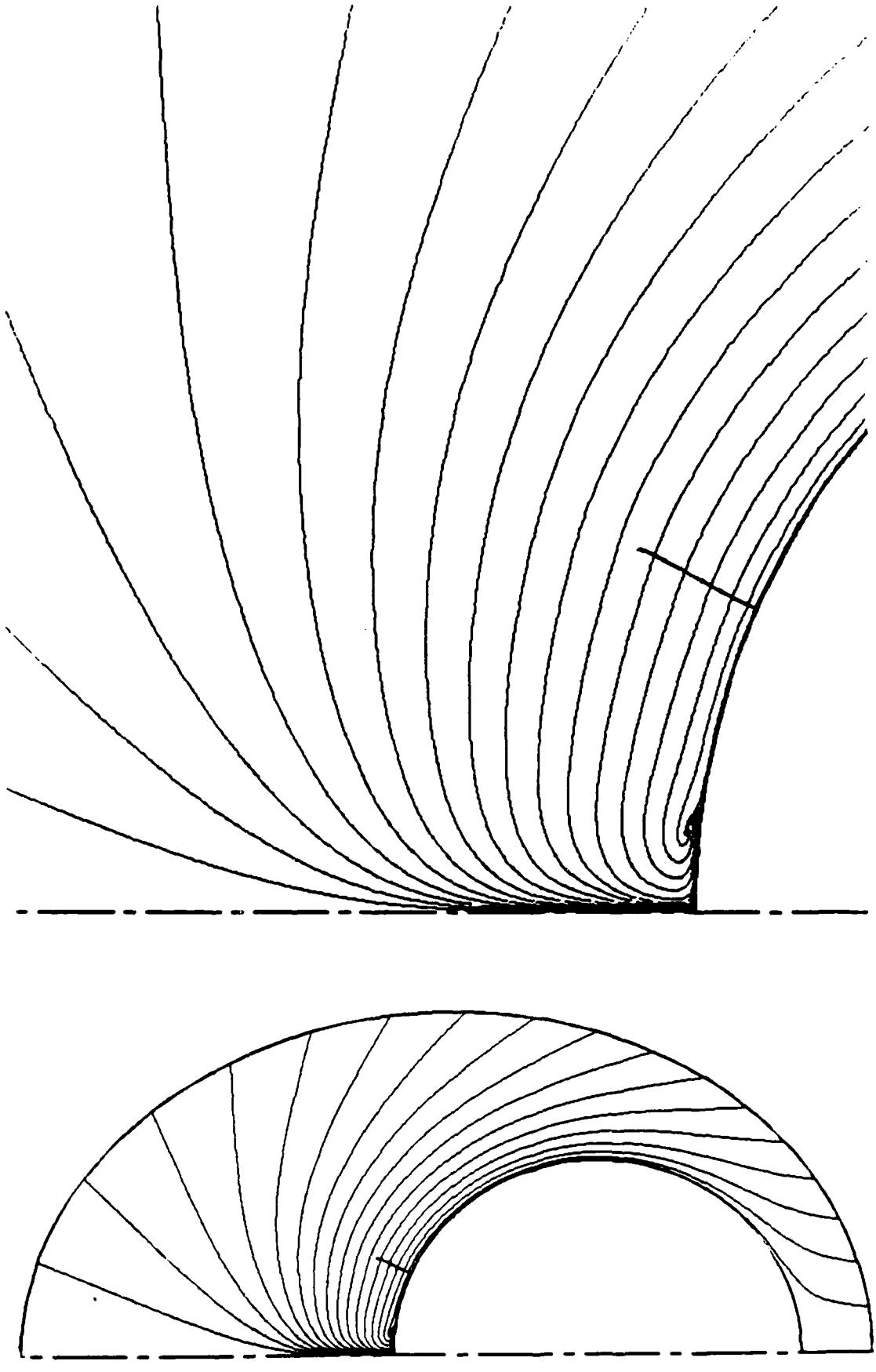

Fig. 4

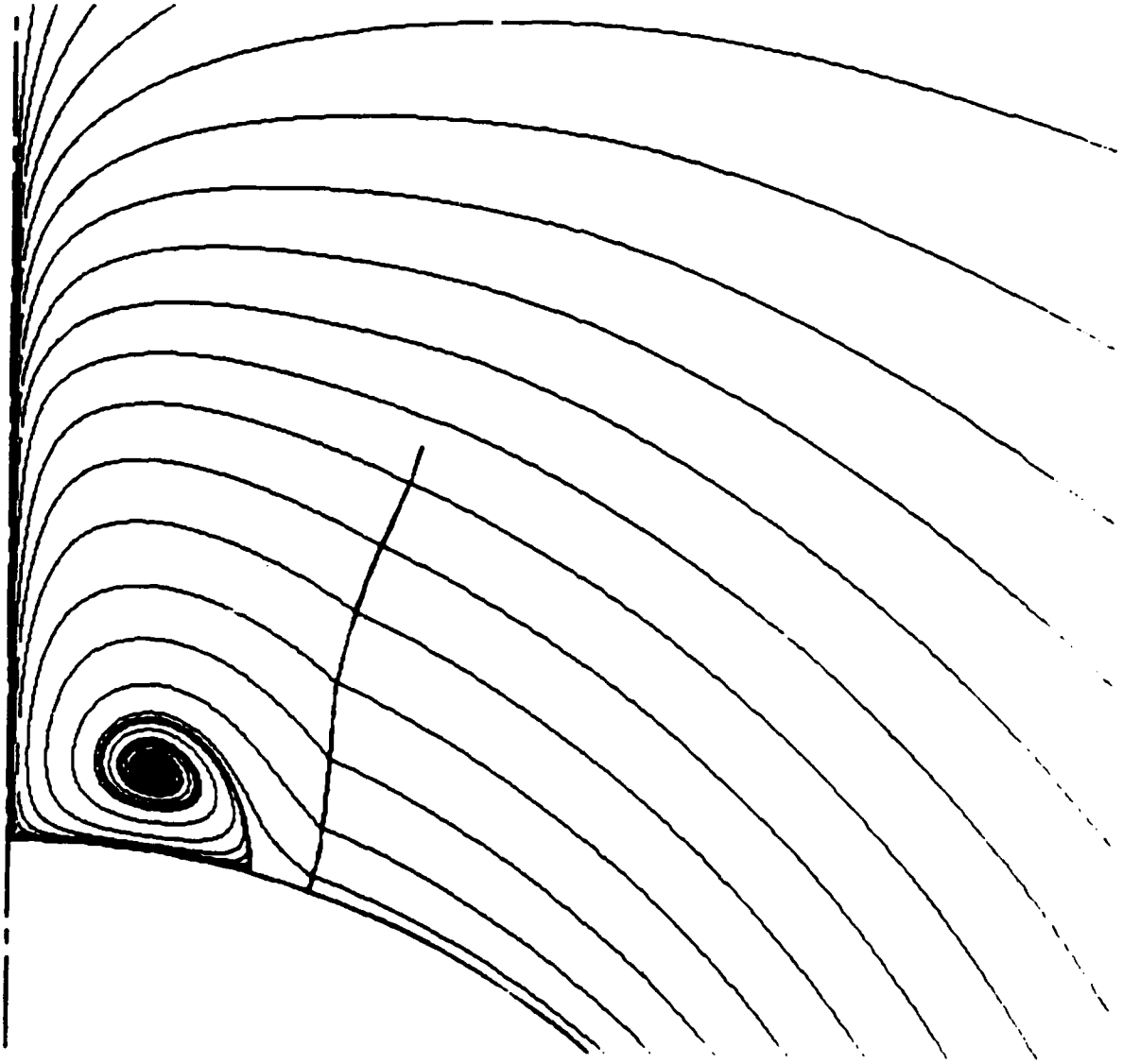

Fig. 5

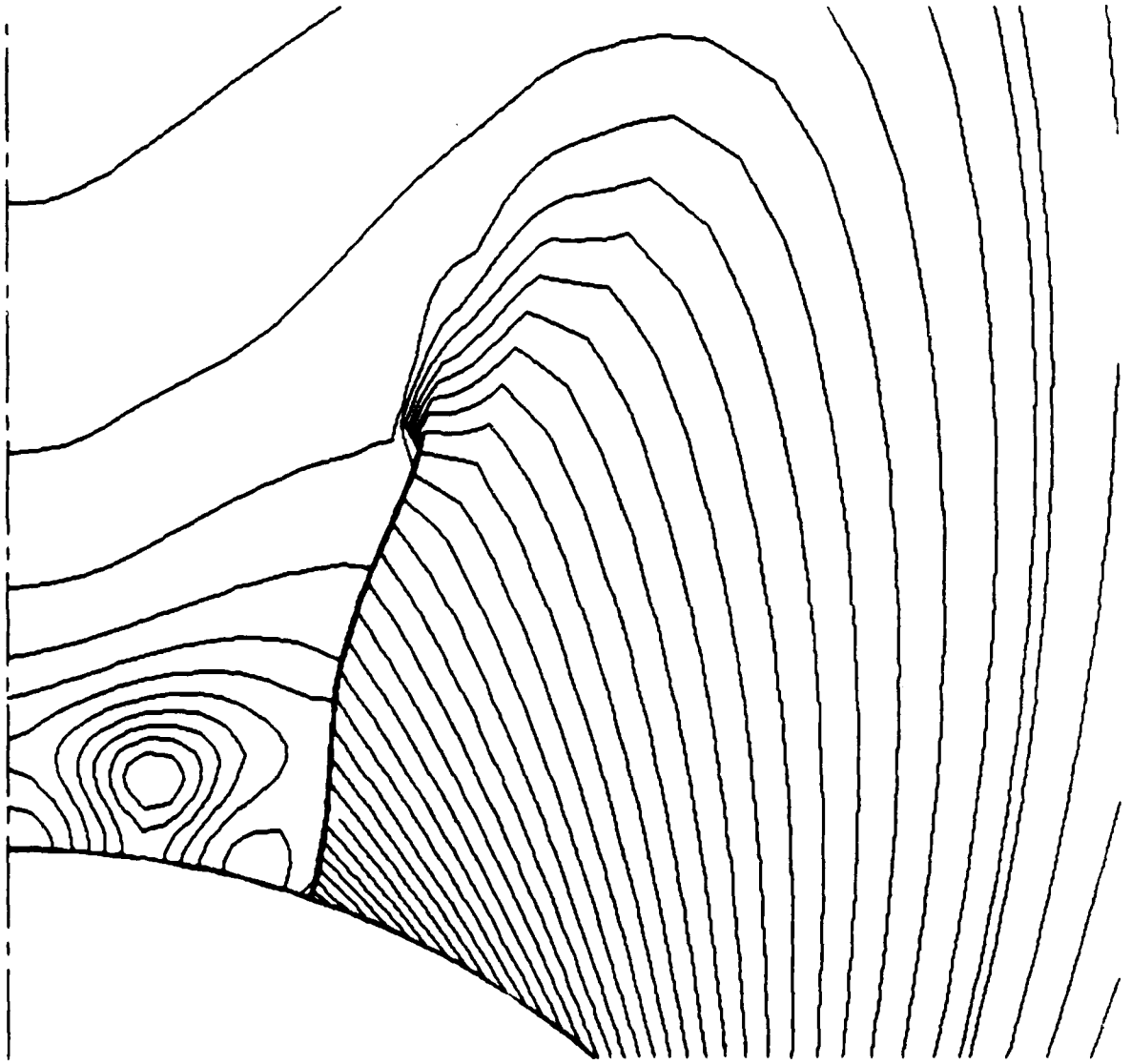

Fig. 6

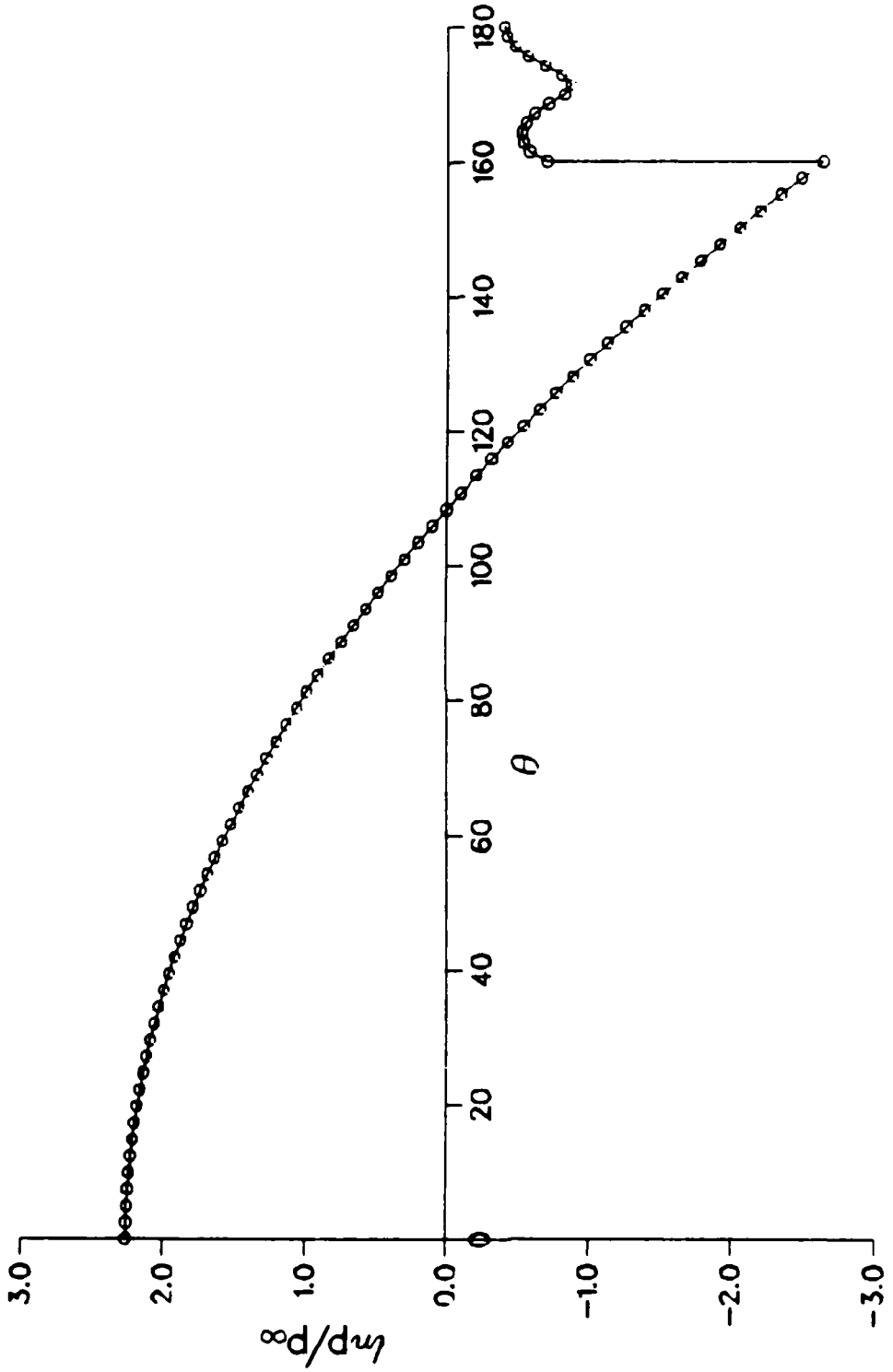
3.0
2.0
1.0
0.0
-1.0
-2.0
-3.0
$\Delta p/p_\infty$
0
20
40
60
80
100
120
140
160
180
θ

Fig. 7

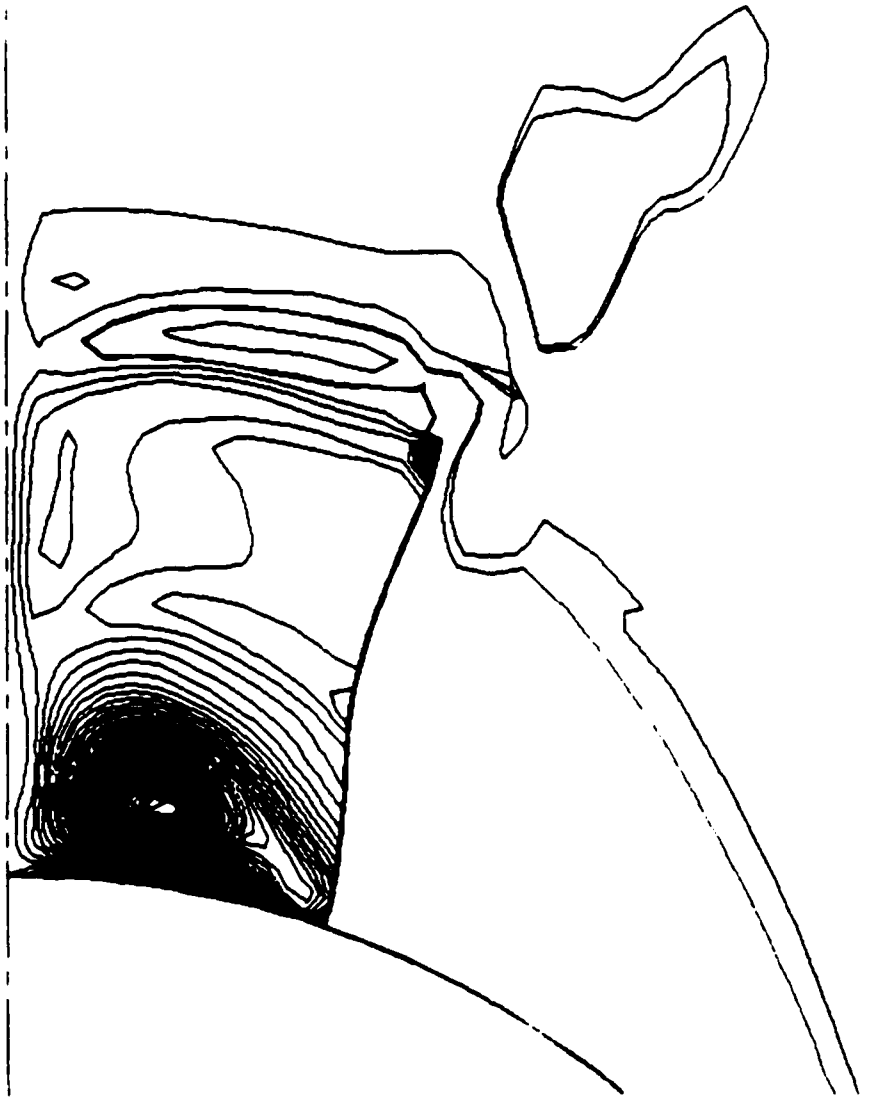

Fig. 8

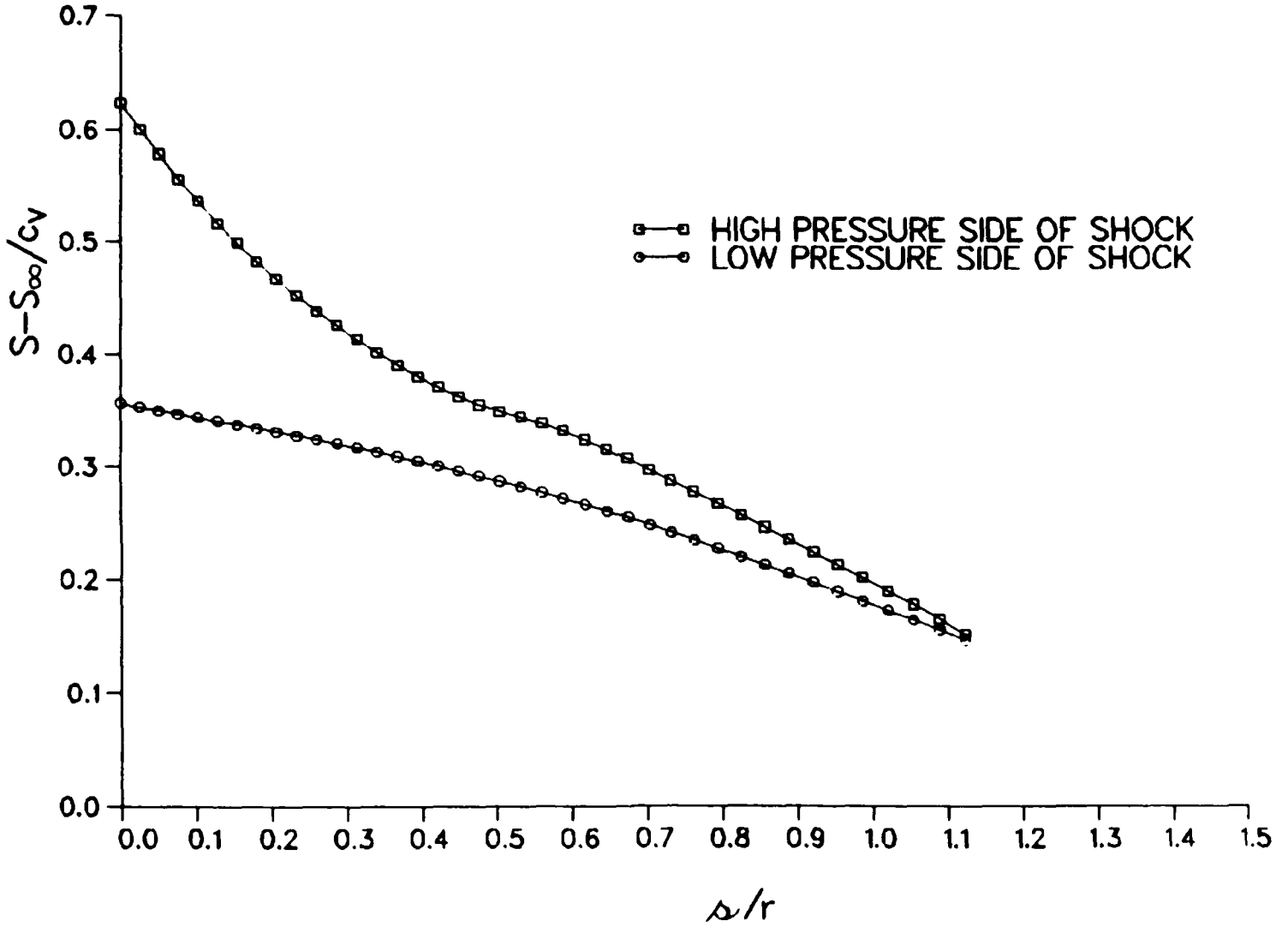
0.7
0.6
0.5
0.4
0.3
0.2
0.1
0.0
S−S∞/cv
HIGH PRESSURE SIDE OF SHOCK
LOW PRESSURE SIDE OF SHOCK
0.0 0.1 0.2 0.3 0.4 0.5 0.6 0.7 0.8 0.9 1.0 1.1 1.2 1.3 1.4 1.5
s/r

Fig. 9

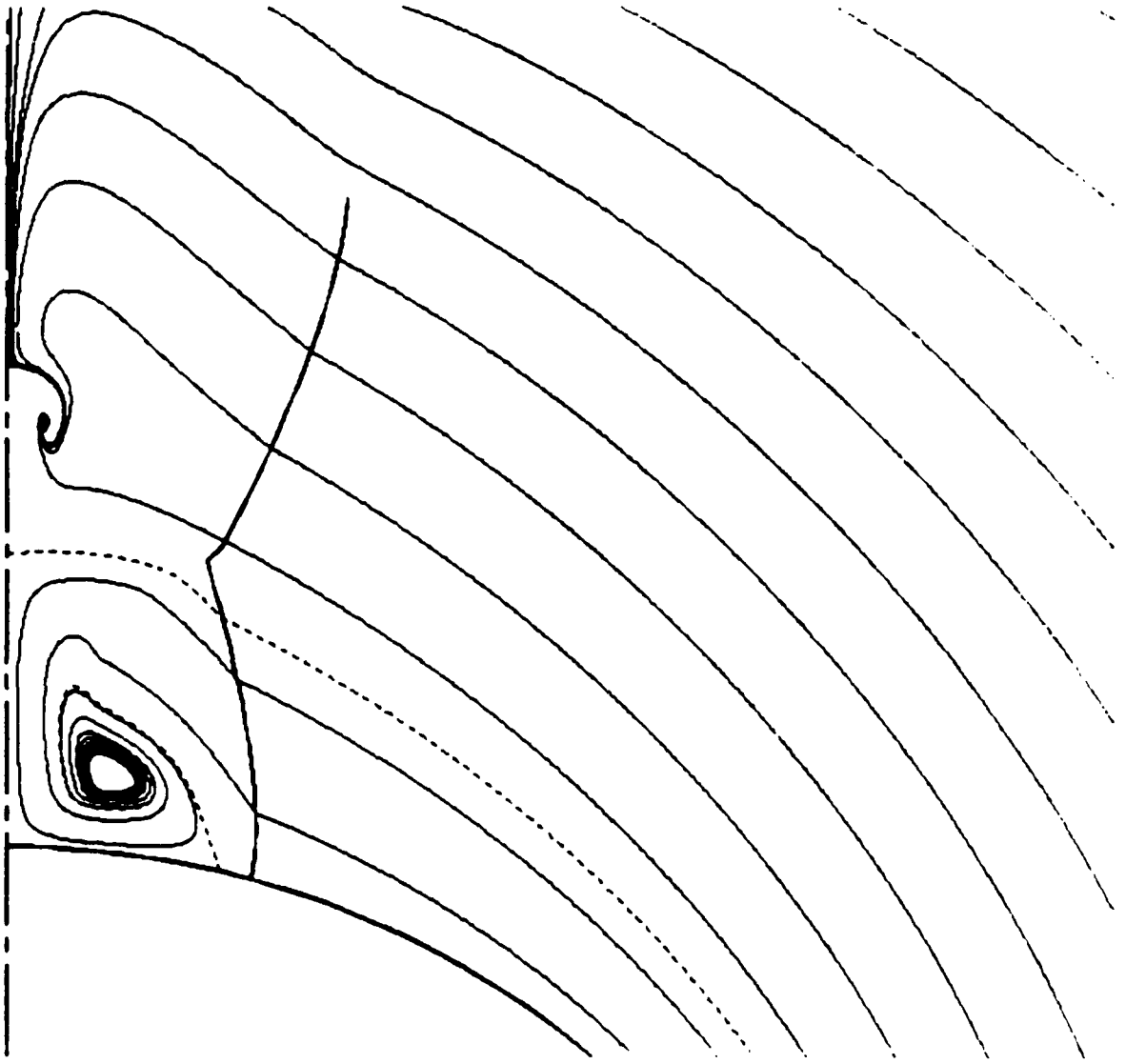

Fig. 10

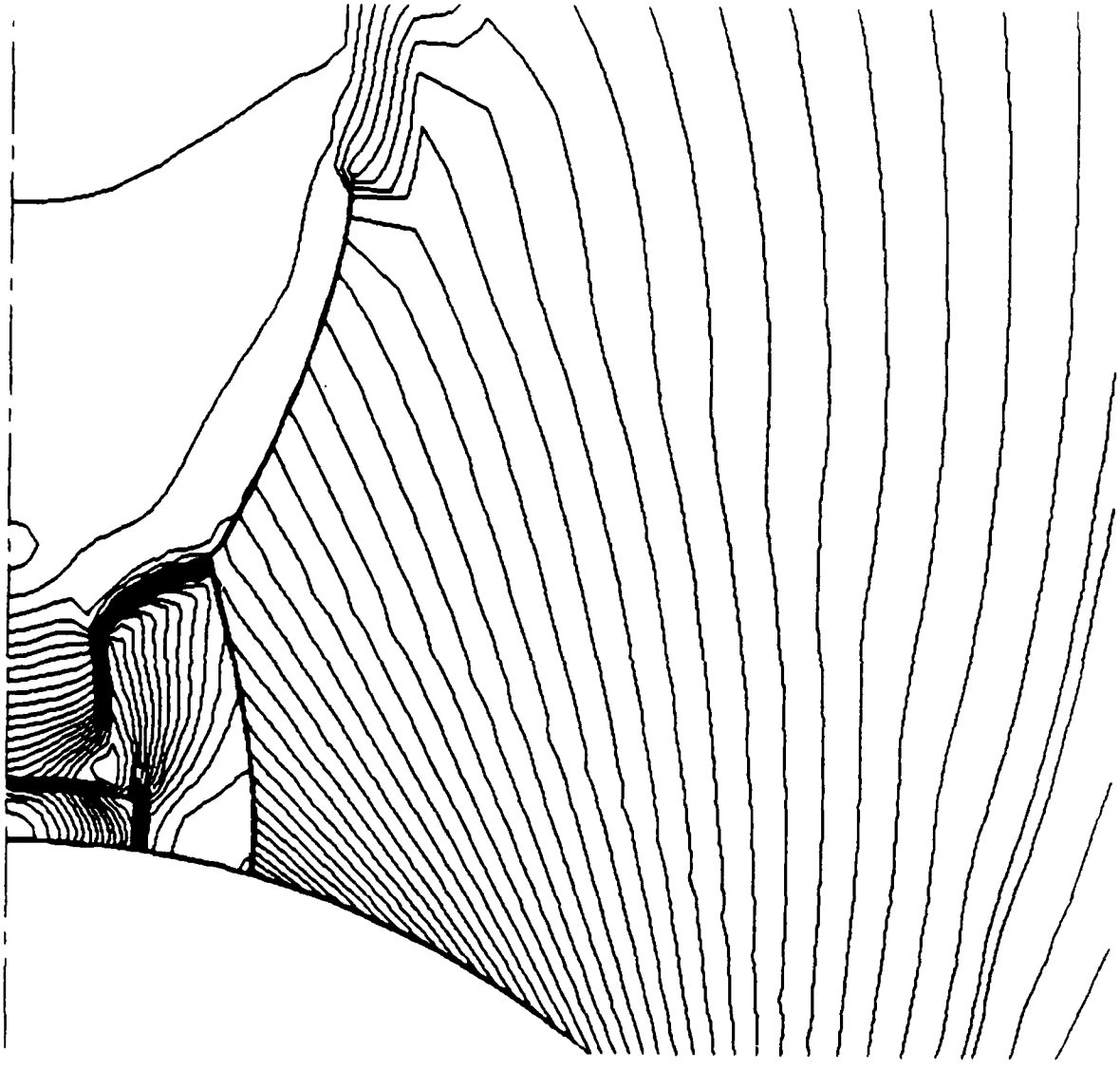

Fig. 11

Fig. 12

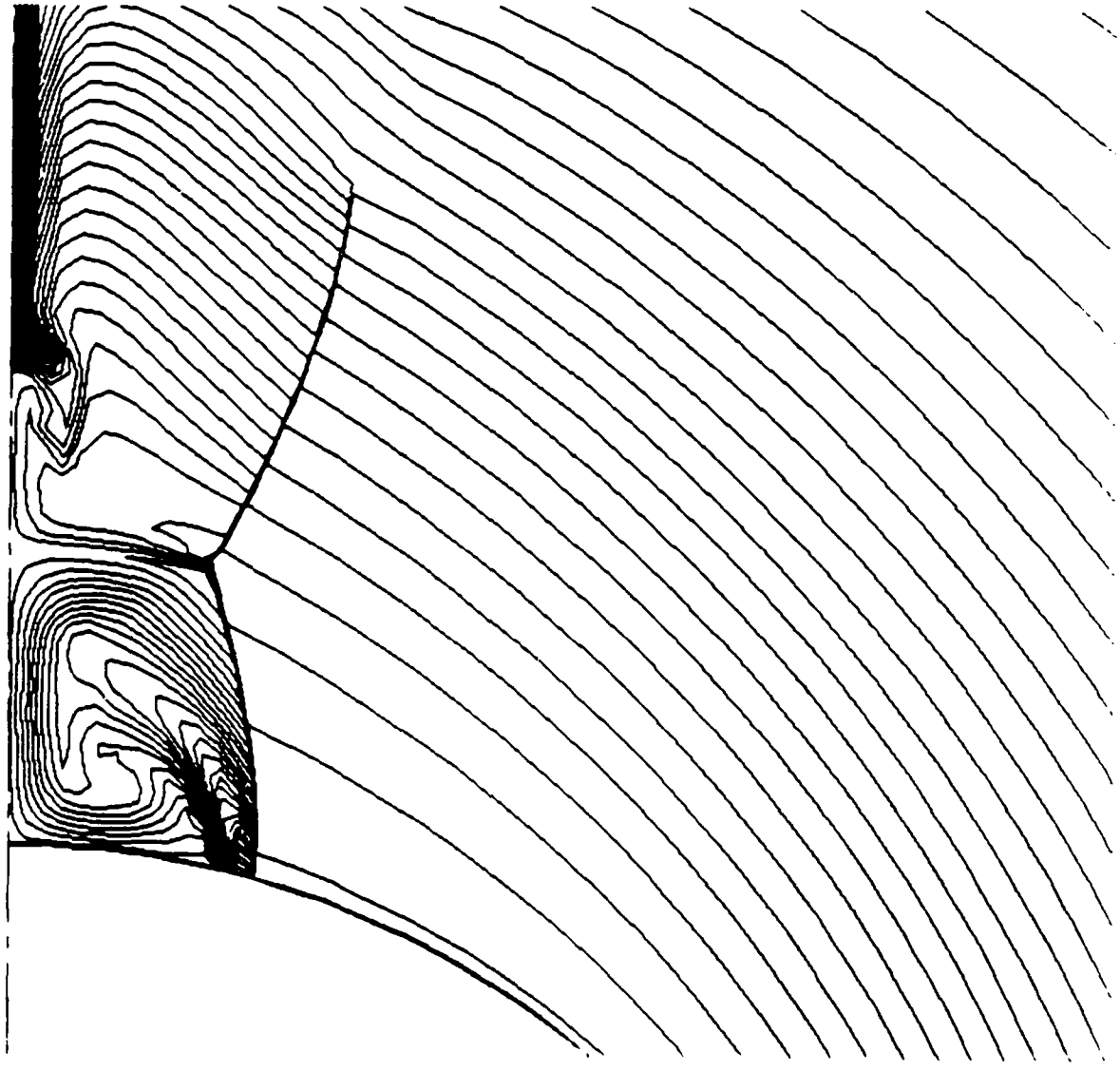

Fig. 13

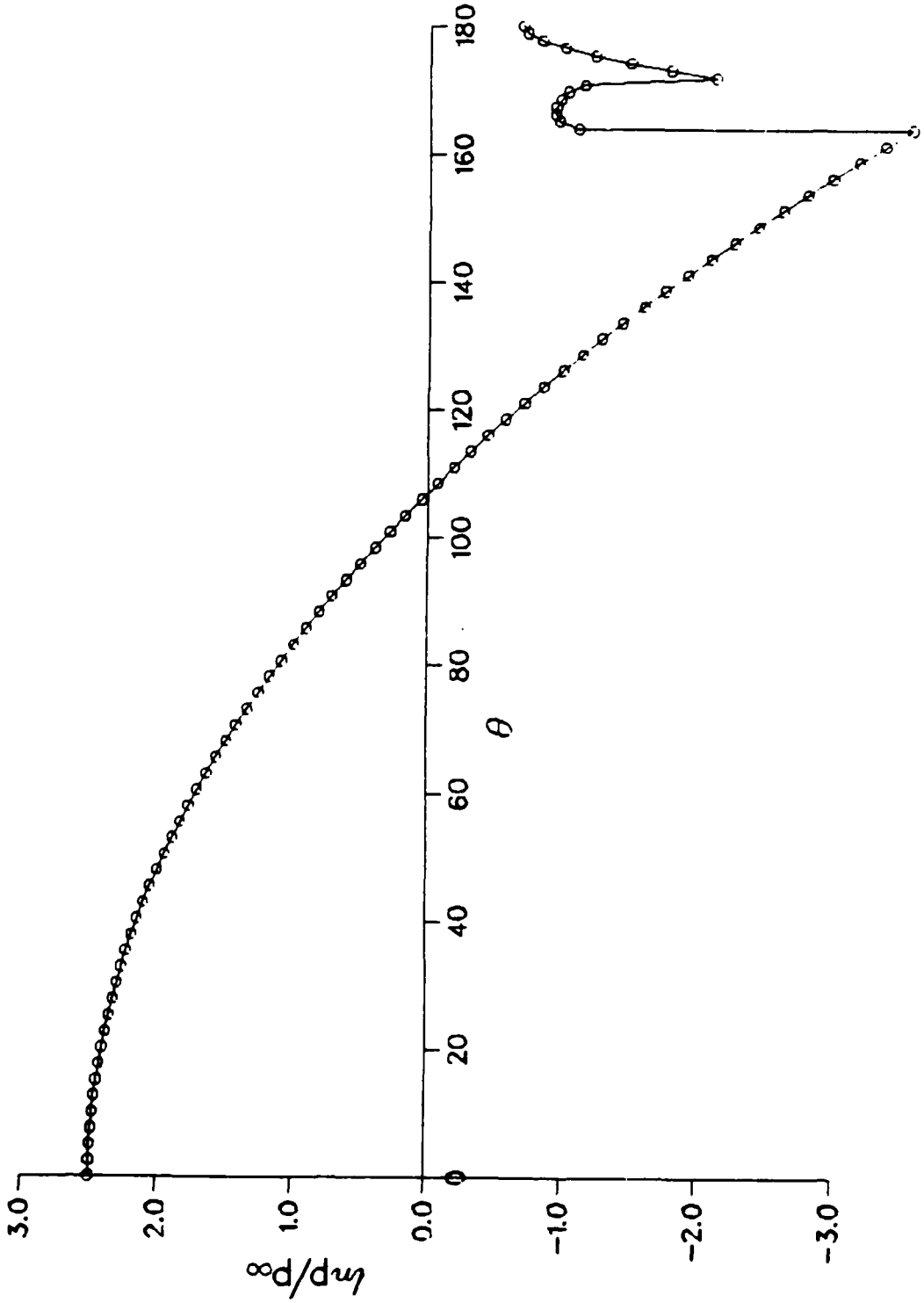

Fig. 14

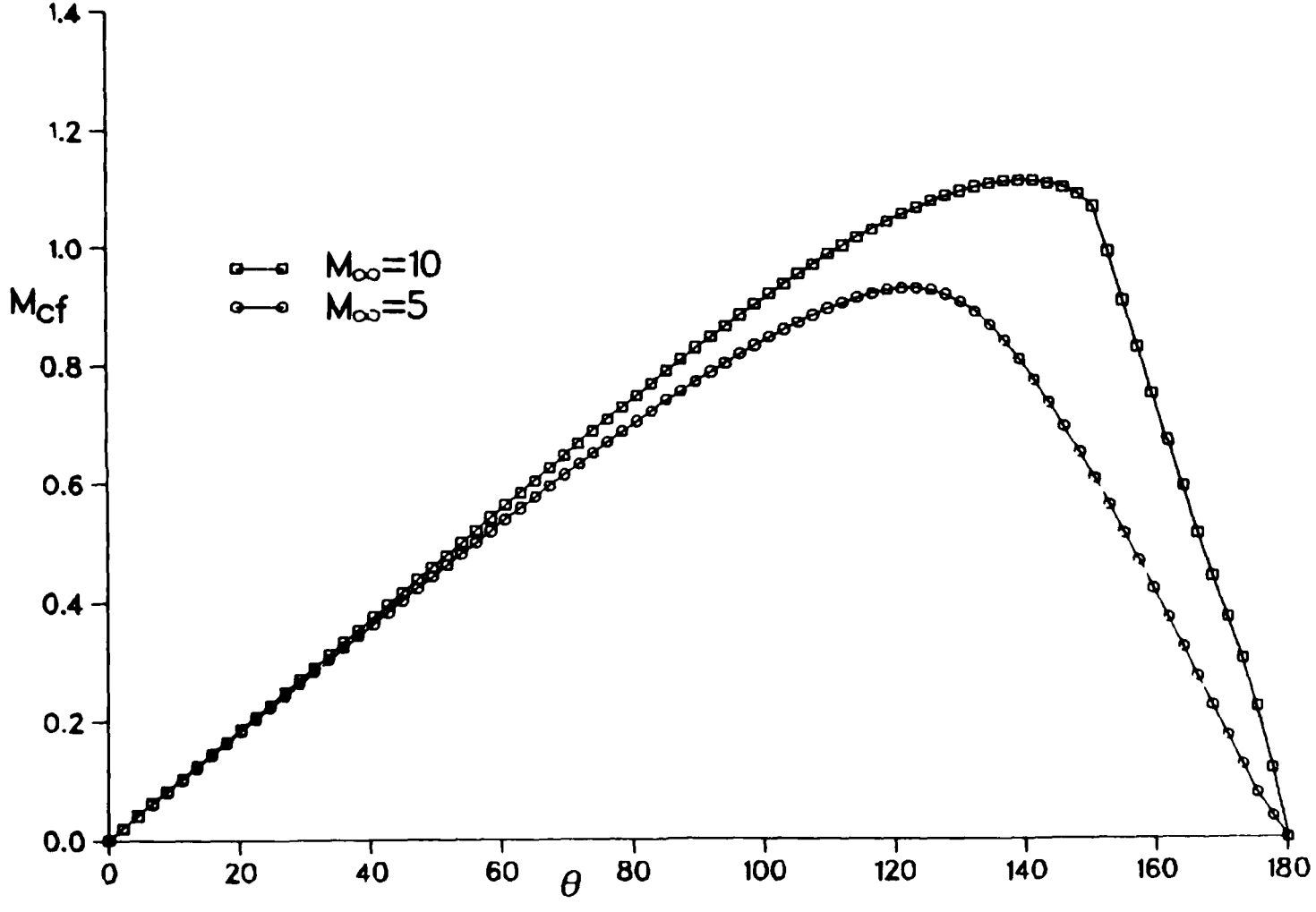
1.4
1.2
1.0
0.8
0.6
0.4
0.2
0.0
M_{cf}
M_∞=10
M_∞=5
0
20
40
60
80
100
120
140
160
180
θ

Fig. 15

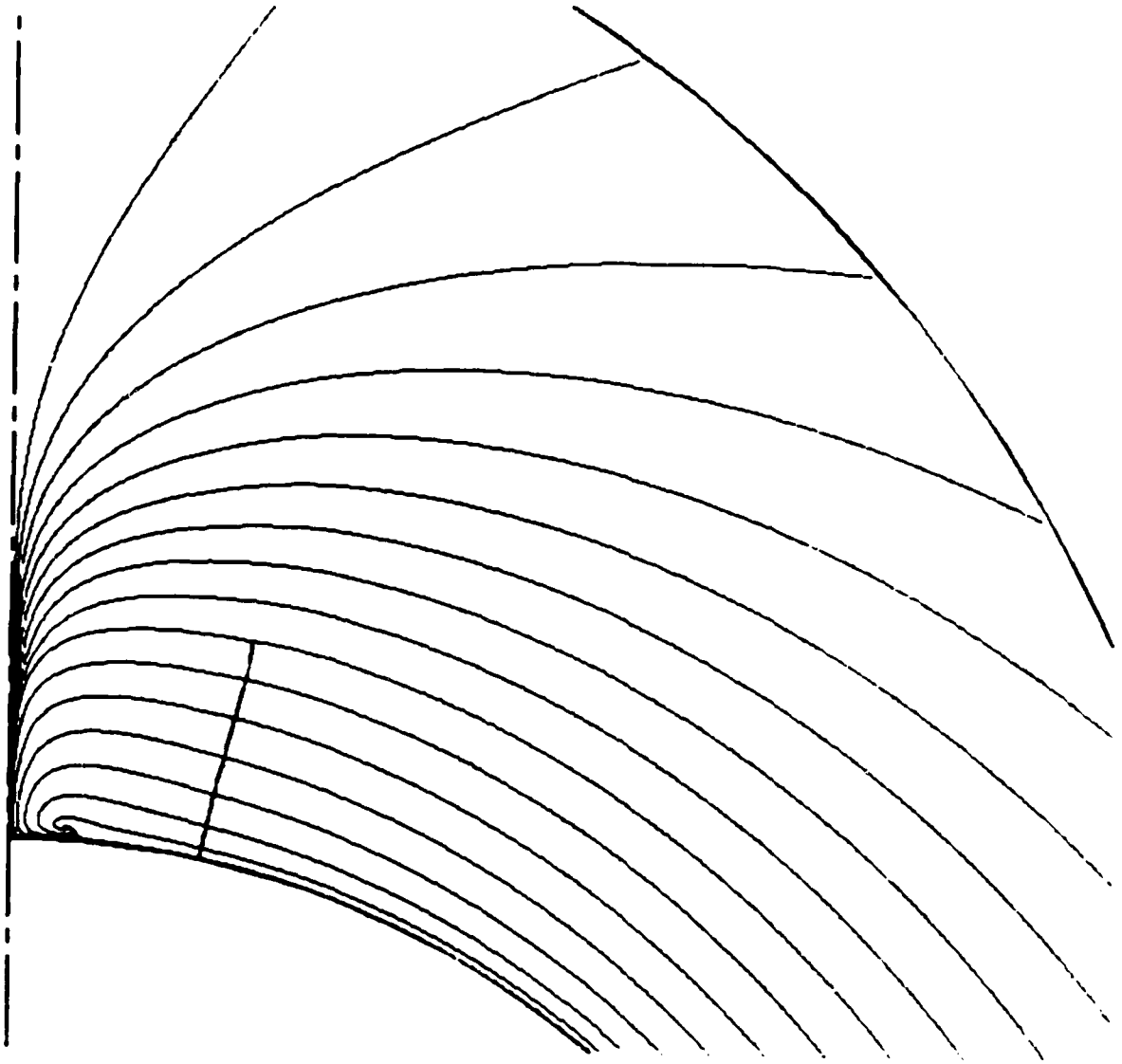

Fig. 16

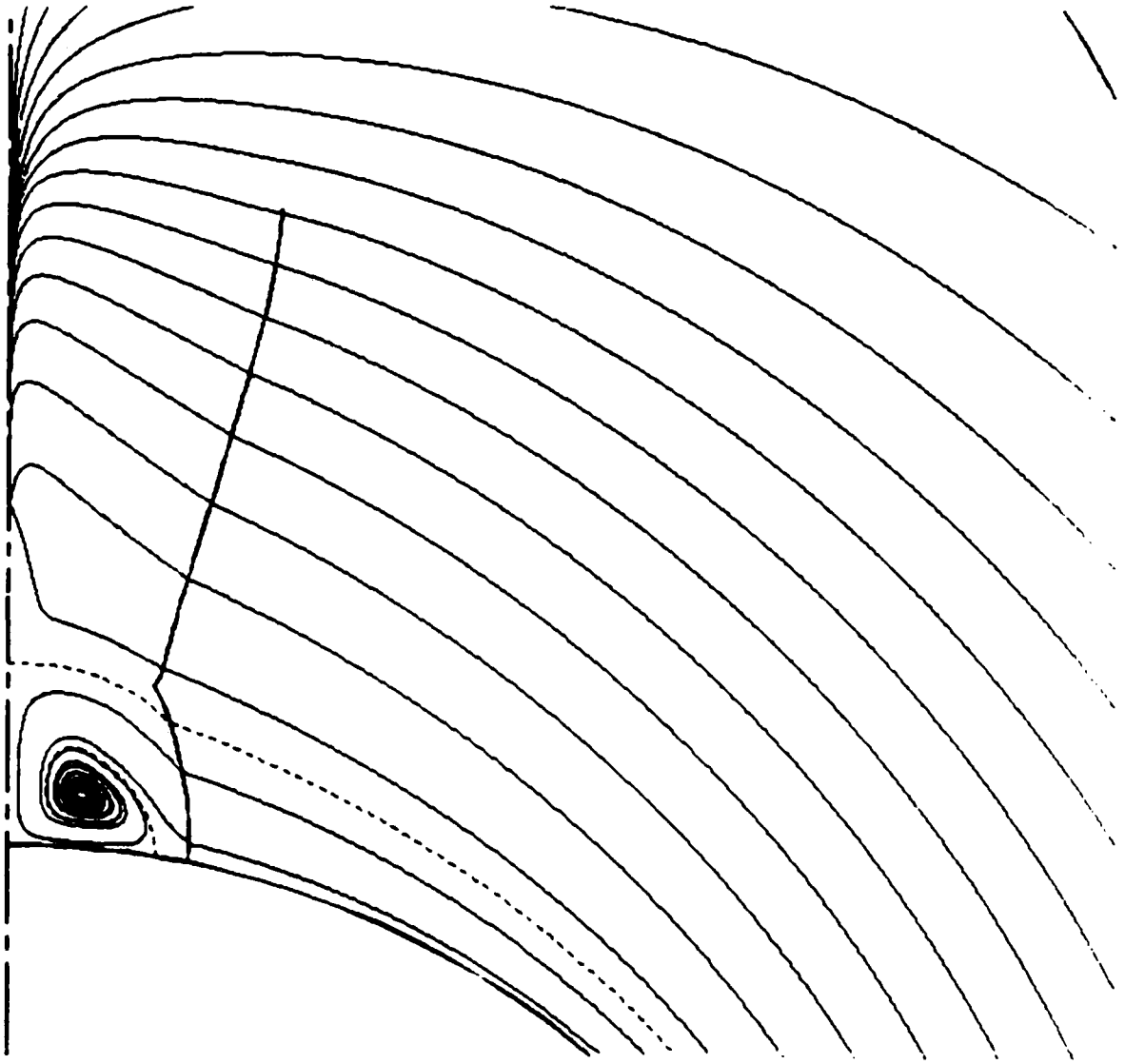

Fig. 17

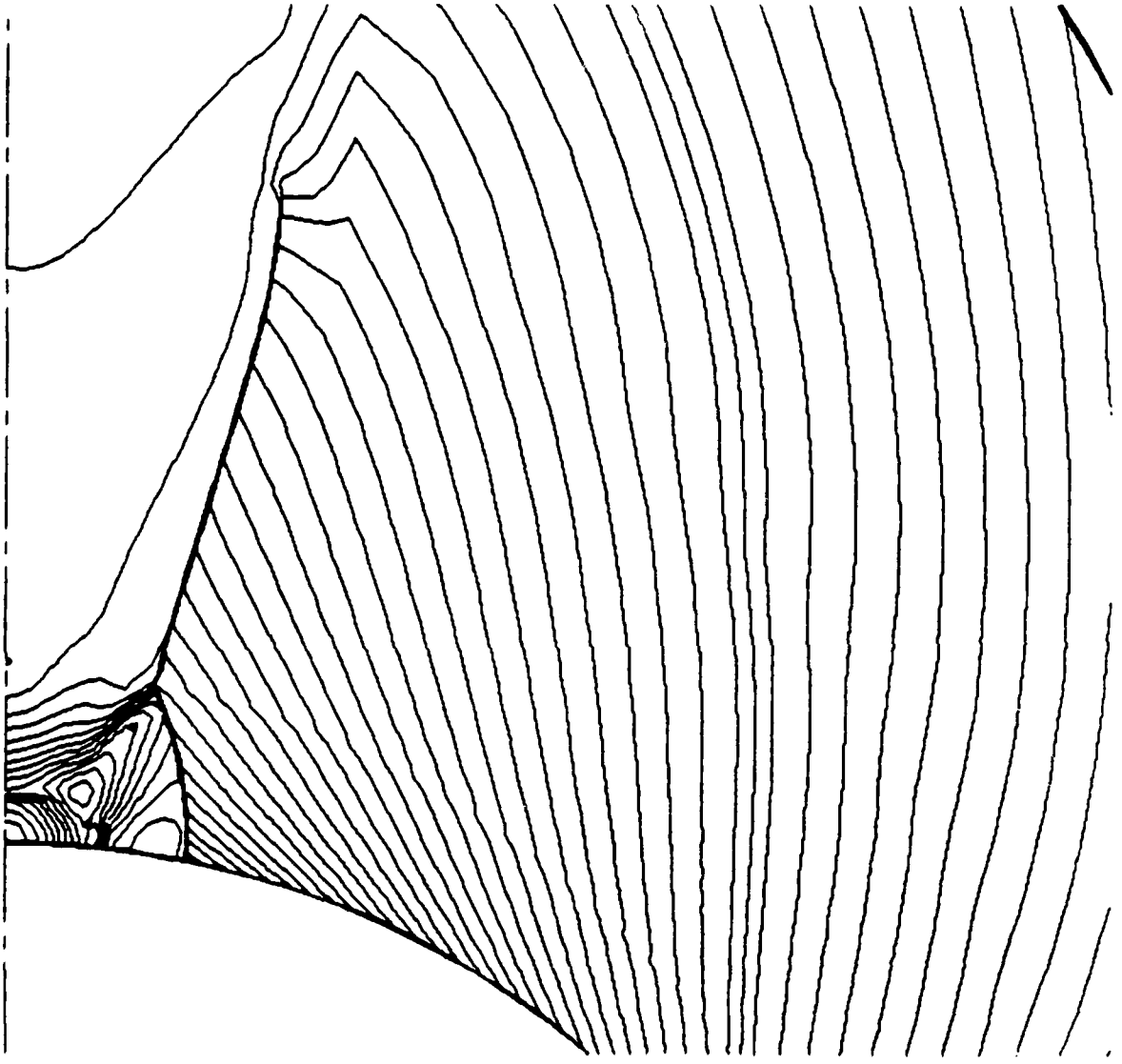

Fig. 18

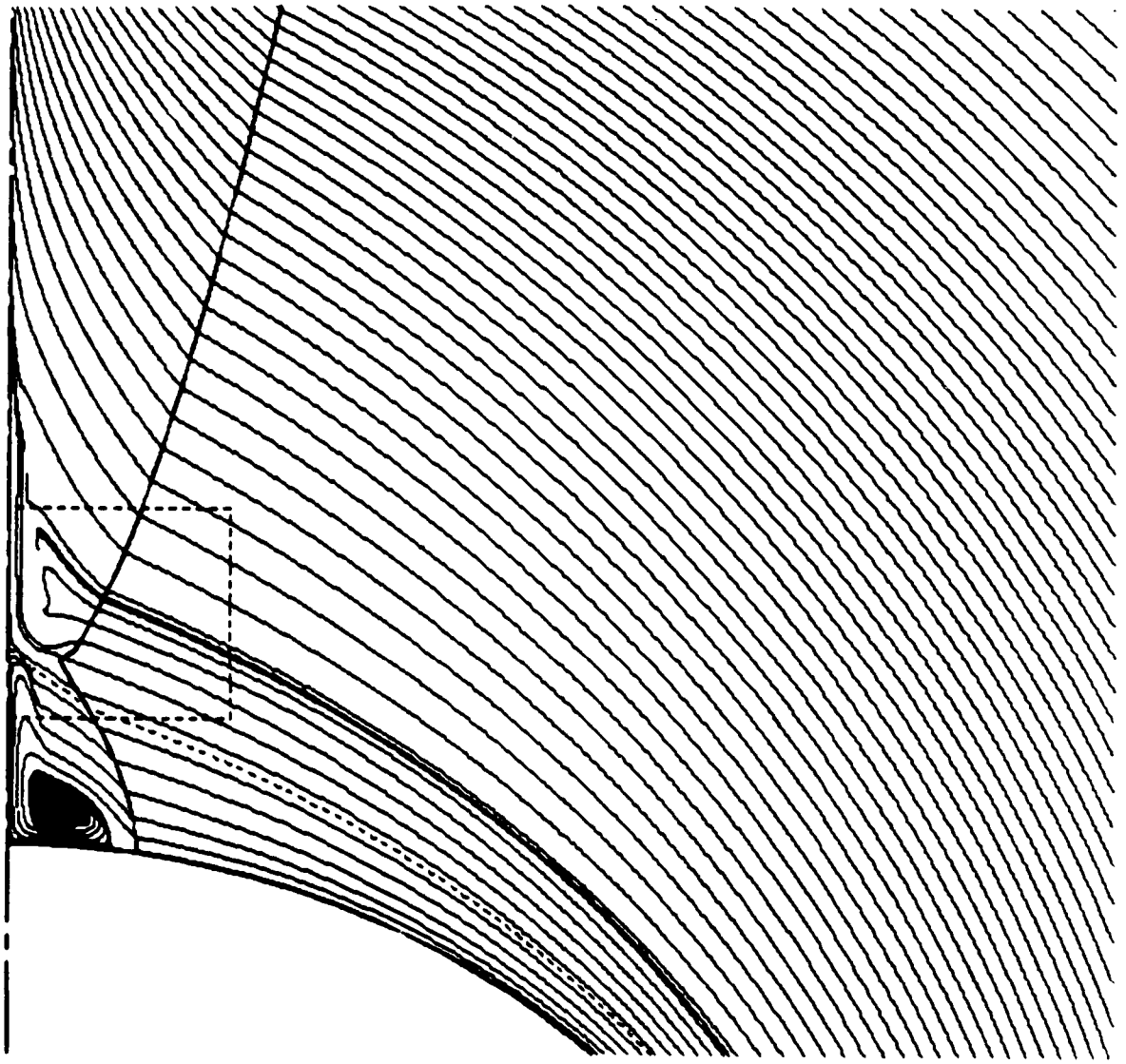

Fig. 19

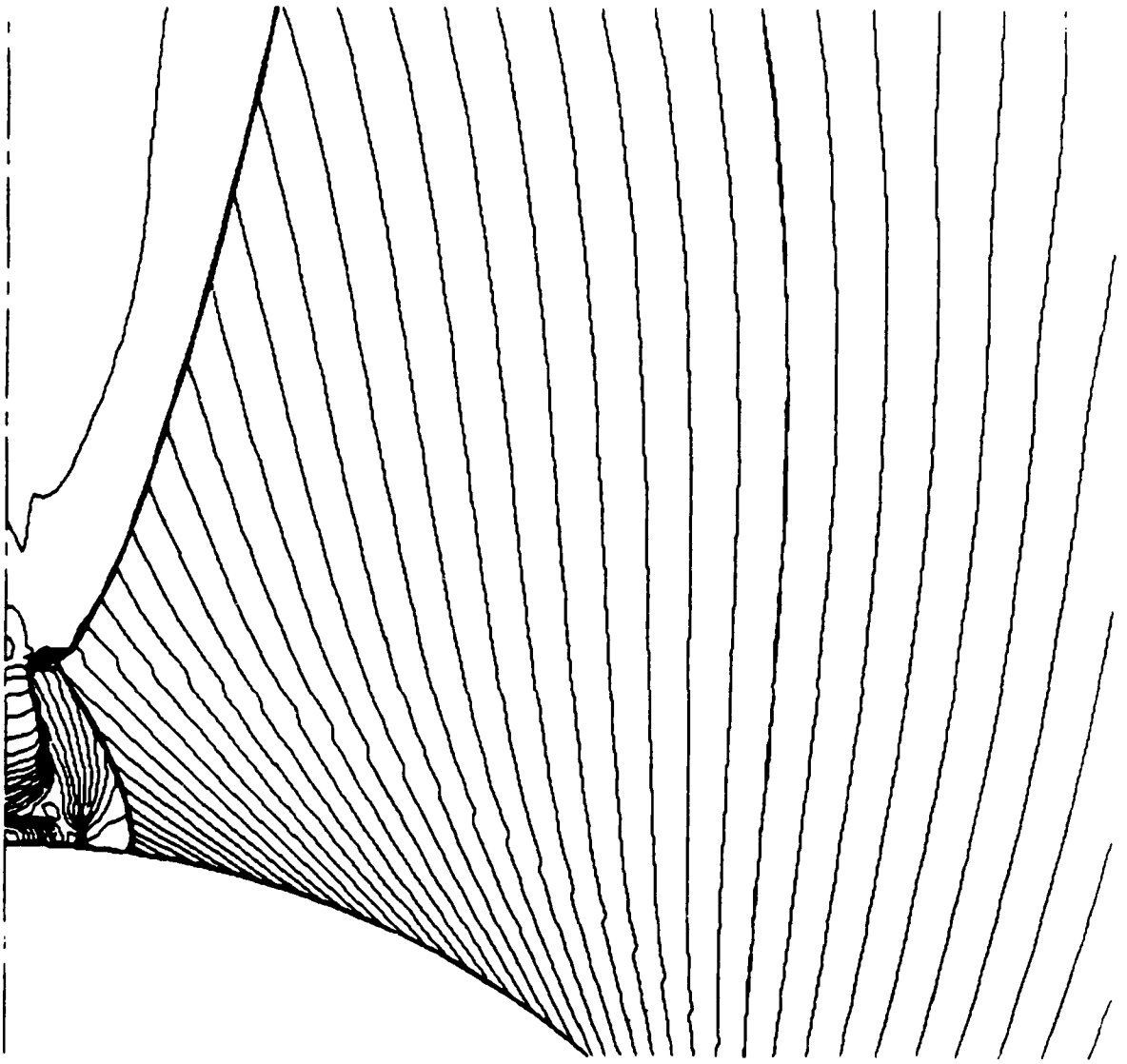

Fig. 20

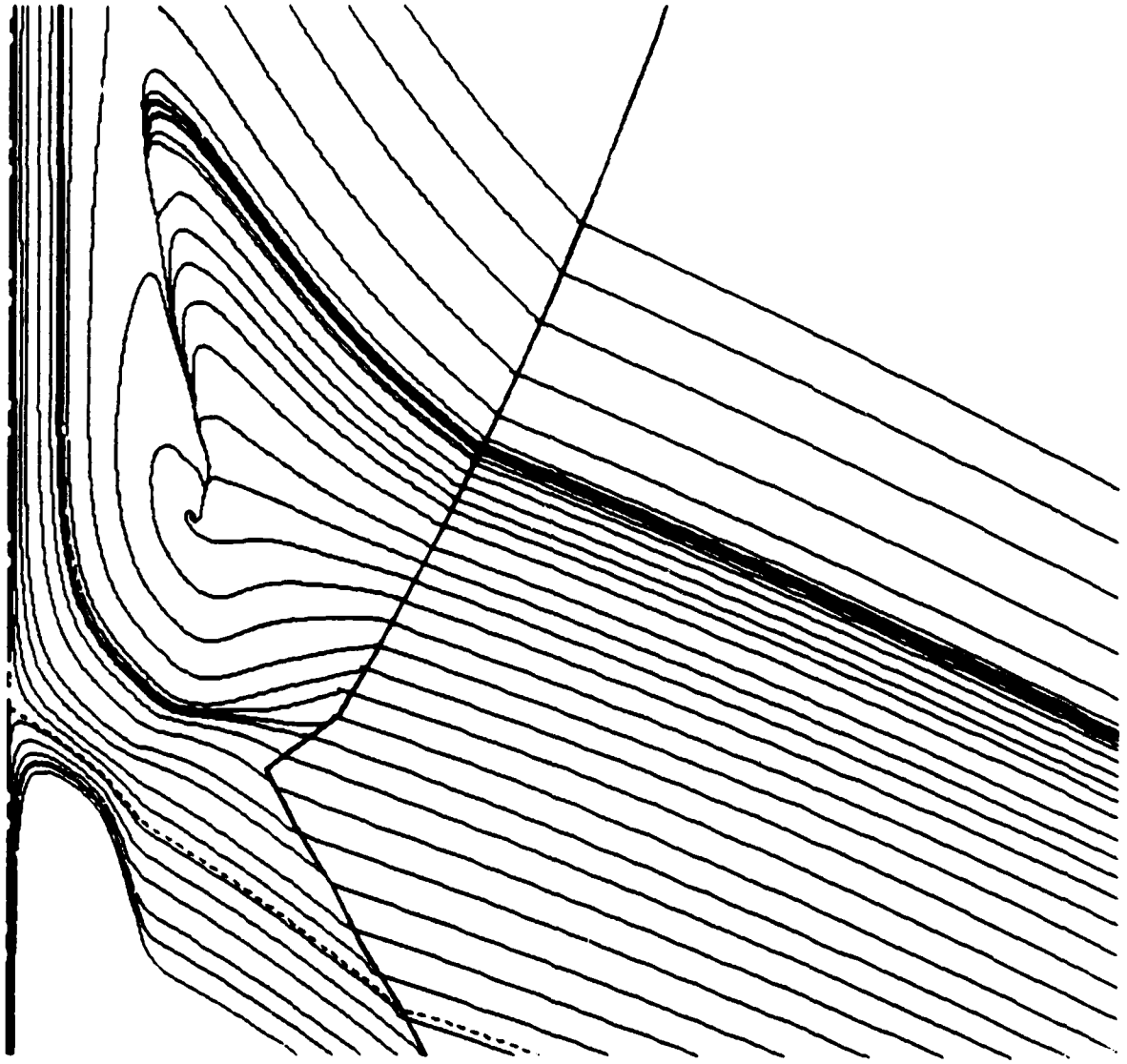

Fig. 21

END
DATE
FILMED
4-88
DTIC